

CHEMICAL METHOD AND DEVICE TO DETECT UNDERWATER TRACE  
EXPLOSIVES VIA PHOTO-LUMINESCENCE

by

Tye A. Langston

A Thesis Submitted to the Faculty of  
The College of Engineering and Computer Science  
in Partial Fulfillment of the Requirements for the Degree of  
Master of Science

Florida Atlantic University

Dania Beach, Florida 33304

December, 2006

**CHEMICAL METHOD AND DEVICE TO DETECT UNDERWATER TRACE  
EXPLOSIVES VIA PHOTO-LUMINESCENCE**

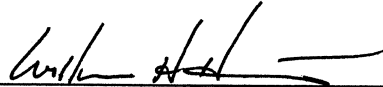
by  
Tye A. Langston

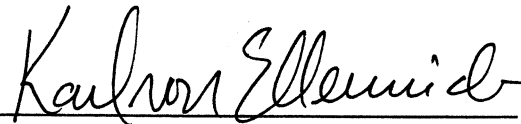
This thesis was prepared under the direction of the candidate's thesis advisor, Prof. Richard Granata, Department of Ocean Engineering, and has been approved by the members of his supervisory committee. It was submitted to the faculty of the College of Engineering and Computer Science and was accepted in partial fulfillment of the requirements for the degree of Master of Science.

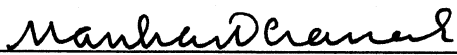
SUPERVISORY COMMITTEE:



Thesis Advisor



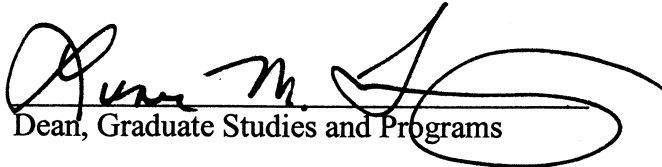




Chairman, Department of Ocean Engineering



Dean, College of Engineering and Computer Science



Dean, Graduate Studies and Programs

12.12.06

Date

## **ACKNOWLEDGEMENTS**

I wish to thank Prof. Richard Granata for the guidance, support and time he has contributed to this work. Through this project, I have been afforded an opportunity to expand my engineering knowledge and improve myself as an engineer. I consider it a great pleasure and opportunity to work with a talented scientist with a willingness to teach.

To Dr. William Hartt and Dr. Karl von Ellenrieder, thank you for your time and assistance in overseeing my work. Your perspectives are valued.

Thanks to Joel of the FAU pharmacy for aiding me in the acquisition of the materials needed for this research.

I would like to thank the U.S. Office of Naval Research, Center for Coastline Security Technology, for the financial support provided under Contract/PR No. N00014-05-C-0031.

## ABSTRACT

Author: Tye A. Langston  
Title: Chemical Method and Device to Detect Underwater Trace Explosives via Photo-Luminescence  
Institution: Florida Atlantic University  
Thesis Advisor: Dr. Richard Granata  
Degree: Master of Science  
Year: 2006

This research tests the use of sensitized lanthanide ions to determine if they can detect water-borne explosive traces and produces two designs for a field-deployable underwater explosive trace detector. 1,10-phenanthroline and thenoyltrifluoroacetone are evaluated as sensitizing ligands to absorb energy and initiate the fluorescence process in europium ions. Different compounds obtained via ligand choice and mixing order are evaluated for their ability to produce a large fluorescence differential between explosive-laden and explosive-absent solutions. Optimal excitation and emission wavelengths for several different compounds are determined, as well as practical wavelengths to be applied in the field. The effect of methanol as a solvent to deliver the reagents is evaluated and rough solubility limits are determined. The effects of seawater constituents on detection are investigated and explosive detection limits are determined. It was found that this method and device are viable for underwater explosive trace detection. A field-deployable device is designed, characterized, and proven.

## TABLE OF CONTENTS

<b>LIST OF TABLES.....</b>	<b>viii</b>
<b>LIST OF FIGURES.....</b>	<b>ix</b>
<b>CHAPTER 1 INTRODUCTION.....</b>	<b>1</b>
<b>CHAPTER 2 THEORY AND LITERATURE REVIEW.....</b>	<b>3</b>
<b>CHAPTER 3 RESEARCH GOALS.....</b>	<b>16</b>
<b>CHAPTER 4 RESEARCH APPROACH.....</b>	<b>18</b>
4.1    Primary Test Materials.....	18
4.2    Primary Test Equipment and Configurations.....	21
4.3    Feasibility Investigations.....	38
4.4    Experimental Techniques and Procedures.....	47
<b>CHAPTER 5 RESULTS AND DISCUSSION.....</b>	<b>64</b>
5.1    Solubility Limit Results.....	64
5.2    Luminescence Spectrometer Results.....	65
5.3    Field-Deployable Detector Results.....	91
5.4    Proof of Design.....	99
<b>CHAPTER 6 CONCLUSIONS AND PROPOSED DESIGN CONFIGURATIONS.....</b>	<b>101</b>
<b>CHAPTER 7 FURTHER RESEARCH.....</b>	<b>108</b>
<b>REFERENCES.....</b>	<b>110</b>
<b>APPENDICES.....</b>	<b>115</b>
A1    Additional Luminescence Spectrometer Data.....	115
A1-1  Europium Complex Comparisons.....	115

A1-2	Ideal Excitation of Eu/TTA.....	124
A1-3	Methanol Effect.....	128
A1-4	Nitroglycerin Detection Limit.....	133
A1-5	Fresh Water Testing.....	143
A1-6	Acid and Metal Ion Tests.....	150
A2	Nitroglycerin Sublingual Tablets Information Sheet.....	152
A3	Wet Labs Inc. WETStar Chlorophyll Fluorometer.....	155
A4	Convection - Diffusion Equation Derivation and Calculations.....	157
A4-1	Forward Direction Diffusion – Convection Solution.....	157
A4-2	Matlab Code for Forward Direction Diffusion-Convection Calculation.....	170
A4-3	Matlab Code for Cross-Channel Diffusion Calculation.....	172

## LIST OF TABLES

Table 1 – Europium compound solubility limits in methanol.....	65
--	----

## LIST OF FIGURES

Figure 1 – Description of the fluorescence process.....	5
Figure 2 – Internal conversion and fluorescence from an excited state.....	
Figure 3 – Fluorescence Resonance Energy Transfer (FRET) from a sensitizing ligand to a lanthanide ion.....	8
Figure 4 – Spectral overlap of donor emission range and the acceptor excitation range during Fluorescence Resonance Energy Transfer (FRET).....	9
Figure 5 – Water molecule vibration modes.....	11
Figure 6 – RDX explosive structure with nitrites.....	14
Figure 7 – Nitroglycerin explosive structure with nitrites.....	14
Figure 8 – Handheld ultraviolet LED.....	22
Figure 9 – Luminescence spectrometer and setup.....	23
Figure 10 – Luminescence spectrometer cuvette.....	24
Figure 11 – WETStar chlorophyll fluorometer.....	25
Figure 12 – Emission transmission profile of filter chosen for the customized (WETStar) fluorometer.....	26
Figure 13 – Calculated downstream concentration as a function of time.....	29
Figure 14 – Calculated cross-channel diffusion behavior.....	31
Figure 15 – Static mixer mixing process.....	32



Figure 16 – Static mixer flow paths around elements.....	33
Figure 17 – Deployable detector characterization test setup schematic.....	34
Figure 18 – Deployable detector characterization test setup.....	34
Figure 19 – Deployable detector test setup schematic.....	36
Figure 20 – Deployable detector proof of design test setup.....	37
Figure 21 – Absorption coefficient vs. electromagnetic wavelength for liquid water.....	39
Figure 22 – HPLC result for distilled water.....	42
Figure 23 – HPLC result for distilled water and nitroglycerin tablets.....	42
Figure 24 – HPLC result for seawater.....	43
Figure 25 – HPLC result for seawater and nitroglycerin tablets.....	43
Figure 26 – Kamyshny et al. Results – Detectability of explosives after soaking in tap water, based on the material to which the explosive was adhered (SF – Seat Fabric, Al – Aluminum, Gls – Glass, PE – Polyethylene).....	46
Figure 27 – Kamyshny et al. Results – Detectability of explosives after soaking in seawater, based on the material to which the explosive was adhered (SF – Seat Fabric, Al – Aluminum, Gls – Glass, PE – Polyethylene).....	46
Figure 28 – Turbidity measurement locations.....	61
Figure 29 – Turbidity measurement results.....	61
Figure 30 – Eu/TTA peak excitation when scanning for 613 nm emission, with and without nitroglycerin.....	66
Figure 31 – Eu/TTA excitation when scanning for 613 nm emission, with and without nitroglycerin.....	67

Figure 32 – Eu/TTA/OP excitation when scanning for 613 nm emission, with and without nitroglycerin.....	68
Figure 33 – Eu/OP/TTA excitation when scanning for 613 nm emission, with and without nitroglycerin.....	68
Figure 34 – Eu/TTA emission in seawater, excited at 370 nm.....	70
Figure 35 – Eu/TTA/OP emission in seawater, excited at 370 nm.....	70
Figure 36 – Eu/OP/TTA emission in seawater, excited at 370 nm.....	71
Figure 37 – Luminescence spectrometer cuvette emission, excited at 370 nm.....	72
Figure 38 – Distilled water emission, excited at 370 nm.....	72
Figure 39 – Methanol emission, excited at 370 nm.....	73
Figure 40 – Seawater emission, excited at 370 nm.....	73
Figure 41 – 5% methanol / seawater solution emission, excited at 370 nm.....	74
Figure 42 – Nitroglycerin and seawater emission, excited at 370 nm.....	74
Figure 43 – 5% methanol / $1 \times 10^{-3}$ M nitroglycerin / seawater solution emission, excited at 370 nm.....	75
Figure 44 – Response of all three europium compounds in seawater, with and without nitroglycerin, excited at 370 nm.....	76
Figure 45 – Difference in intensity between nitroglycerin-laden and nitroglycerin-absent solutions for each europium compound. Excited at 370 nm.....	77
Figure 46 – Eu/TTA emission, excited at 370 nm, with and without nitroglycerin .....	79
Figure 47 – Eu/TTA Emission, excited at 382 nm, with and without nitroglycerin .....	79
Figure 48 – 613 nm fluorescence intensity as a function of solution methanol percentage.....	81

Figure 49 – Solution clarities with varying amounts of methanol .....	82
Figure 50 – 613 nm intensity as a function of nitroglycerin concentration .....	85
Figure 51 – Eu/TTA 613 nm emission, 370 nm excitation, with and without nitroglycerin.....	86
Figure 52 – Eu/TTA 613 nm emission, 382 nm excitation, with and without nitroglycerin .....	87
Figure 53 – Eu/TTA 613 nm emission, 370 nm and 382 nm excitation, with and without nitroglycerin.....	87
Figure 54 – Fresh water Eu/TTA 613 nm emission, 370 nm excitation, with and without nitroglycerin .....	88
Figure 55 – Fresh water and seawater Eu/TTA 613 nm emission, 370 nm excitation, with and without nitroglycerin .....	89
Figure 56 – Eu/TTA emission in the presence of sodium, calcium and hydrogen ions, 370 nm excitation, with nitroglycerin .....	91
Figure 57 – Strong visible fluorescence with nitroglycerin ( $10^{-3}$ M) at Eu/TTA ( $8 \times 10^{-4}$ M in Methanol) .....	93
Figure 58 – Weak visible fluorescence without nitroglycerin at Eu/TTA ( $8 \times 10^{-4}$ M in Methanol).....	93
Figure 59 – Deployable detector static test with $5 \times 10^{-5}$ M (Me) europium concentration .....	94
Figure 60 – Deployable detector static test with $1 \times 10^{-4}$ M (Me) europium concentration .....	95

Figure 61 – Deployable detector static test with $2 \times 10^{-4}$ M (Me) europium concentration .....	95
Figure 62 – Deployable detector static test with $4 \times 10^{-4}$ M (Me) europium concentration .....	96
Figure 63 – Deployable detector static test with $8 \times 10^{-4}$ M (Me) europium concentration .....	96
Figure 64 – Deployable detector static test with $1.25 \times 10^{-3}$ M (Me) europium concentration .....	97
Figure 65 – Filtration effects on the deployable detector performance.....	98
Figure 66 – Flow-through detector results from the proof of design tests.....	100
Figure 67 – Proposed design schematic no. 1.....	107
Figure 68 – Proposed design schematic no. 2.....	107
Figure 69 – Eu/TTA $1 \times 10^{-4}$ M Emission in Seawater Under 370 nm Excitation, With and Without Nitroglycerin, 5% Methanol.....	115
Figure 70 – Eu/TTA $7.94 \times 10^{-5}$ M Emission in Seawater Under 370 nm Excitation, With and Without Nitroglycerin, 5% Methanol.....	115
Figure 71 – Eu/TTA $6.3 \times 10^{-5}$ M Emission in Seawater Under 370 nm Excitation, With and Without Nitroglycerin, 5% Methanol.....	116
Figure 72 – Eu/TTA $5 \times 10^{-5}$ M Emission in Seawater Under 370 nm Excitation, With and Without Nitroglycerin, 5% Methanol.....	116
Figure 73 – Eu/TTA $3.97 \times 10^{-5}$ M Emission in Seawater Under 370 nm Excitation, With and Without Nitroglycerin, 5% Methanol.....	117
Figure 74 – Eu/TTA $3.15 \times 10^{-5}$ M Emission in Seawater Under 370 nm	

Excitation, With and Without Nitroglycerin, 5% Methanol.....	117
Figure 75 – Eu/TTA $2.5 \times 10^{-5}$ M Emission in Seawater Under 370 nm	
Excitation, With and Without Nitroglycerin, 5% Methanol.....	118
Figure 76 – Eu/TTA/OP $1 \times 10^{-4}$ M Emission in Seawater Under 370 nm	
Excitation, With and Without Nitroglycerin, 5% Methanol.....	118
Figure 77 – Eu/TTA/OP $5 \times 10^{-5}$ M Emission in Seawater Under 370 nm	
Excitation, With and Without Nitroglycerin, 5% Methanol.....	119
Figure 78 – Eu/TTA/OP $3.15 \times 10^{-5}$ M Emission in Seawater Under 370 nm	
Excitation, With and Without Nitroglycerin, 5% Methanol.....	119
Figure 79 – Eu/TTA/OP $2.5 \times 10^{-5}$ M Emission in Seawater Under 370 nm	
Excitation, With and Without Nitroglycerin, 5% Methanol.....	120
Figure 80 – Eu/TTA/OP $1.98 \times 10^{-5}$ M Emission in Seawater Under 370 nm	
Excitation, With and Without Nitroglycerin, 5% Methanol.....	120
Figure 81 – Eu/TTA/OP $1.25 \times 10^{-5}$ M Emission in Seawater Under 370 nm	
Excitation, With and Without Nitroglycerin, 5% Methanol.....	121
Figure 82 – Eu/OP/TTA $1 \times 10^{-4}$ M Emission in Seawater Under 370 nm	
Excitation, With and Without Nitroglycerin, 5% Methanol.....	121
Figure 83 – Eu/OP/TTA $5 \times 10^{-5}$ M Emission in Seawater Under 370 nm	
Excitation, With and Without Nitroglycerin, 5% Methanol.....	122
Figure 84 – Eu/OP/TTA $3.97 \times 10^{-5}$ M Emission in Seawater Under 370 nm	
Excitation, With and Without Nitroglycerin, 5% Methanol.....	122
Figure 85 – Eu/OP/TTA $3.15 \times 10^{-5}$ M Emission in Seawater Under 370 nm	
Excitation, With and Without Nitroglycerin, 5% Methanol.....	123

Figure 86 – Eu/OP/TTA $2.5 \times 10^{-5}$ M Emission in Seawater Under 370 nm Excitation, With and Without Nitroglycerin, 5% Methanol.....	123
Figure 87 – Eu/TTA $1 \times 10^{-4}$ M Emission in Seawater Under 382 nm Excitation, With and Without Nitroglycerin, 5% Methanol.....	124
Figure 88 – Eu/TTA $7.94 \times 10^{-5}$ M Emission in Seawater Under 382 nm Excitation, With and Without Nitroglycerin, 5% Methanol.....	124
Figure 89 – Eu/TTA $6.3 \times 10^{-5}$ M Emission in Seawater Under 382 nm Excitation, With and Without Nitroglycerin, 5% Methanol.....	125
Figure 90 – Eu/TTA $5 \times 10^{-5}$ M Emission in Seawater Under 382 nm Excitation, With and Without Nitroglycerin, 5% Methanol.....	125
Figure 91 – Eu/TTA $3.97 \times 10^{-5}$ M Emission in Seawater Under 382 nm Excitation, With and Without Nitroglycerin, 5% Methanol.....	126
Figure 92 – Eu/TTA $3.15 \times 10^{-5}$ M Emission in Seawater Under 382 nm Excitation, With and Without Nitroglycerin, 5% Methanol.....	126
Figure 93 – Eu/TTA $2.15 \times 10^{-5}$ M Emission in Seawater Under 382 nm Excitation, With and Without Nitroglycerin, 5% Methanol.....	127
Figure 94 – Eu/TTA $7.94 \times 10^{-5}$ M Emission in Seawater Under 370 nm Excitation, With and Without Nitroglycerin, 1.15% Methanol.....	128
Figure 95 – Eu/TTA $7.94 \times 10^{-5}$ M Emission in Seawater Under 370 nm Excitation, With and Without Nitroglycerin, 2.5% Methanol.....	128
Figure 96 – Eu/TTA $7.94 \times 10^{-5}$ M Emission in Seawater Under 370 nm Excitation, With and Without Nitroglycerin, 5% Methanol.....	129
Figure 97 – Eu/TTA $7.94 \times 10^{-5}$ M Emission in Seawater Under 370 nm Excitation,	

With and Without Nitroglycerin, 10% Methanol.....	129
Figure 98 – Eu/TTA $7.94 \times 10^{-5}$ M Emission in Seawater Under 370 nm Excitation,	
With and Without Nitroglycerin, 15% Methanol.....	130
Figure 99 – Eu/TTA $7.94 \times 10^{-5}$ M Emission in Seawater Under 370 nm Excitation,	
With and Without Nitroglycerin, 20% Methanol.....	130
Figure 100 – Eu/TTA $7.94 \times 10^{-5}$ M Emission in Seawater Under 370 nm Excitation,	
With and Without Nitroglycerin, 25% Methanol.....	131
Figure 101 – Eu/TTA $7.94 \times 10^{-5}$ M Emission in Seawater Under 370 nm Excitation,	
With and Without Nitroglycerin, 30% Methanol.....	131
Figure 102 – Eu/TTA $7.94 \times 10^{-5}$ M Emission in Seawater Under 370 nm Excitation,	
With and Without Nitroglycerin, 35% Methanol.....	132
Figure 103 – Eu/TTA $1 \times 10^{-4}$ M Emission in Seawater Under 370 nm Excitation, 5%	
Methanol, No Nitroglycerin.....	133
Figure 104 – Eu/TTA $1 \times 10^{-4}$ M Emission in Seawater Under 370 nm Excitation, 5%	
Methanol, $1 \times 10^{-3}$ M Nitroglycerin.....	133
Figure 105 – Eu/TTA $1 \times 10^{-4}$ M Emission in Seawater Under 370 nm Excitation, 5%	
Methanol, $5 \times 10^{-4}$ M Nitroglycerin.....	134
Figure 106 – Eu/TTA $1 \times 10^{-4}$ M Emission in Seawater Under 370 nm Excitation, 5%	
Methanol, $2.5 \times 10^{-4}$ M Nitroglycerin.....	134
Figure 107 – Eu/TTA $1 \times 10^{-4}$ M Emission in Seawater Under 370 nm Excitation, 5%	
Methanol, $1.25 \times 10^{-4}$ M Nitroglycerin.....	135
Figure 108 – Eu/TTA $1 \times 10^{-4}$ M Emission in Seawater Under 370 nm Excitation, 5%	
Methanol, $6.25 \times 10^{-5}$ M Nitroglycerin.....	135

Figure 109 – Eu/TTA $1 \times 10^{-4}$ M Emission in Seawater Under 370 nm Excitation, 5%	
Methanol, $3.13 \times 10^{-5}$ M Nitroglycerin.....	136
Figure 110 – Eu/TTA $1 \times 10^{-4}$ M Emission in Seawater Under 370 nm Excitation, 5%	
Methanol, $1.56 \times 10^{-5}$ M Nitroglycerin.....	136
Figure 111 – Eu/TTA $1 \times 10^{-4}$ M Emission in Seawater Under 370 nm Excitation, 5%	
Methanol, $7.81 \times 10^{-6}$ M Nitroglycerin.....	137
Figure 112 – Eu/TTA $1 \times 10^{-4}$ M Emission in Seawater Under 370 nm Excitation, 5%	
Methanol, $3.91 \times 10^{-6}$ M Nitroglycerin.....	137
Figure 113 – Eu/TTA $1 \times 10^{-4}$ M Emission in Seawater Under 370 nm Excitation, 5%	
Methanol, $1.95 \times 10^{-6}$ M Nitroglycerin.....	138
Figure 114 – Eu/TTA $1 \times 10^{-4}$ M Emission in Seawater Under 370 nm Excitation, 5%	
Methanol, $9.77 \times 10^{-7}$ M Nitroglycerin.....	138
Figure 115 – Eu/TTA $1 \times 10^{-4}$ M Emission in Seawater Under 370 nm Excitation, 5%	
Methanol, $4.88 \times 10^{-7}$ M Nitroglycerin.....	139
Figure 116 – Eu/TTA $1 \times 10^{-4}$ M Emission in Seawater Under 370 nm Excitation, 5%	
Methanol, $2.44 \times 10^{-7}$ M Nitroglycerin.....	139
Figure 117 – Eu/TTA $1 \times 10^{-4}$ M Emission in Seawater Under 370 nm Excitation, 5%	
Methanol, $1.22 \times 10^{-7}$ M Nitroglycerin.....	140
Figure 118 – Eu/TTA $1 \times 10^{-4}$ M Emission in Seawater Under 370 nm Excitation, 5%	
Methanol, $6.1 \times 10^{-8}$ M Nitroglycerin.....	140
Figure 119 – Eu/TTA $1 \times 10^{-4}$ M Emission in Seawater Under 370 nm Excitation, 5%	
Methanol, $3.05 \times 10^{-8}$ M Nitroglycerin.....	141
Figure 120 – Eu/TTA $1 \times 10^{-4}$ M Emission in Seawater Under 370 nm Excitation, 5%	



Methanol, $1.53 \times 10^{-8}$ M Nitroglycerin.....	141
Figure 121 – Eu/TTA $1 \times 10^{-4}$ M Emission in Seawater Under 370 nm Excitation, 5%	
Methanol, $7.63 \times 10^{-9}$ M Nitroglycerin.....	142
Figure 122 – Eu/TTA $1 \times 10^{-4}$ M Emission in Fresh Water Under 370 nm Excitation,	
5% Methanol, With and Without Nitroglycerin.....	143
Figure 123 – Eu/TTA $7.94 \times 10^{-5}$ M Emission in Fresh Water Under 370 nm	
Excitation, 5% Methanol, With and Without Nitroglycerin.....	143
Figure 124 – Eu/TTA $6.3 \times 10^{-5}$ M Emission in Fresh Water Under 370 nm	
Excitation, 5% Methanol, With and Without Nitroglycerin.....	144
Figure 125 – Eu/TTA $5 \times 10^{-5}$ M Emission in Fresh Water Under 370 nm Excitation,	
5% Methanol, With and Without Nitroglycerin.....	144
Figure 126 – Eu/TTA $3.97 \times 10^{-5}$ M Emission in Fresh Water Under 370 nm	
Excitation, 5% Methanol, With and Without Nitroglycerin.....	145
Figure 127 – Eu/TTA $3.15 \times 10^{-5}$ M Emission in Fresh Water Under 370 nm	
Excitation, 5% Methanol, With and Without Nitroglycerin.....	145
Figure 128 – Eu/TTA $2.5 \times 10^{-5}$ M Emission in Fresh Water Under 370 nm	
Excitation, 5% Methanol, With and Without Nitroglycerin.....	146
Figure 129 – Eu/TTA $1.98 \times 10^{-5}$ M Emission in Fresh Water Under 370 nm	
Excitation, 5% Methanol, With and Without Nitroglycerin.....	146
Figure 130 – Eu/TTA $1.57 \times 10^{-5}$ M Emission in Fresh Water Under 370 nm	
Excitation, 5% Methanol, With and Without Nitroglycerin.....	147
Figure 131 – Eu/TTA $1.25 \times 10^{-5}$ M Emission in Fresh Water Under 370 nm	
Excitation, 5% Methanol, With and Without Nitroglycerin.....	147

Figure 132 – Eu/TTA $9.9 \times 10^{-6}$ M Emission in Fresh Water Under 370 nm	
Excitation, 5% Methanol, With and Without Nitroglycerin.....	148
Figure 133 – Eu/TTA $7.86 \times 10^{-6}$ M Emission in Fresh Water Under 370 nm	
Excitation, 5% Methanol, With and Without Nitroglycerin.....	148
Figure 134 – Eu/TTA $6.24 \times 10^{-6}$ M Emission in Fresh Water Under 370 nm	
Excitation, 5% Methanol, With and Without Nitroglycerin.....	149
Figure 135 – Eu/TTA $4.95 \times 10^{-6}$ M Emission in Fresh Water Under 370 nm	
Excitation, 5% Methanol, With and Without Nitroglycerin.....	149
Figure 136 – Eu/TTA $1 \times 10^{-4}$ M Emission in 0.55 M NaCl Solution Under 370 nm	
Excitation, 5% Methanol, $1 \times 10^{-3}$ M Nitroglycerin.....	150
Figure 137 – Eu/TTA $1 \times 10^{-4}$ M Emission in 0.27 M CaCl <sub>2</sub> Solution Under 370 nm	
Excitation, 5% Methanol, $1 \times 10^{-3}$ M Nitroglycerin.....	150
Figure 138 – Eu/TTA $1 \times 10^{-4}$ M Emission in 0.55 M HCl Solution Under 370 nm	
Excitation, 5% Methanol, $1 \times 10^{-3}$ M Nitroglycerin.....	151

## CHAPTER 1

### INTRODUCTION

Due to the increasing terrorism threat to the United States and other countries, there is a demand to research and design anti-terrorism tactics and equipment. One area that requires attention is that of coastline security. Not only can terrorism attacks originate from airports and land borders, but there is also the potential that they can come from our coastal boundaries. This danger has not escaped the attention of the Center of Coastline Security Technology (CCST), and they have funded an effort to design an unmanned underwater vehicle (UUV) capable of countering this threat. The ultimate purpose of this UUV component is to detect underwater dissolved explosives and provide a signal so that action can be taken. This process breaks down to three basic steps: (1) Obtain an underwater sample for testing (2) Analyze the obtained sample for explosives and (3) Provide feedback of the results so that appropriate action can be taken. The success of the project in whole ultimately depends on the fruition of step (2), the ability to analyze a sample and discern existent explosive traces from their seawater background.

Several methods exist to analyze a water sample for explosive traces<sup>1</sup>, but practicality in UUV application dictates several limitations, such as size, cost, autonomy and processing speed. Consequently, these limitations in conjunction with the unique

seawater environment eliminate most existing explosive detection methods. The research contained herein focuses on the formulation and testing of a detection method based on fluorescent tagging and the development of a field-deployable device to detect waterborne explosive traces with this method. Attention has been given to UUV parameters such as size, cost, power consumption, autonomy, analysis speed and sensitivity.

## CHAPTER 2

### THEORY AND LITERATURE REVIEW

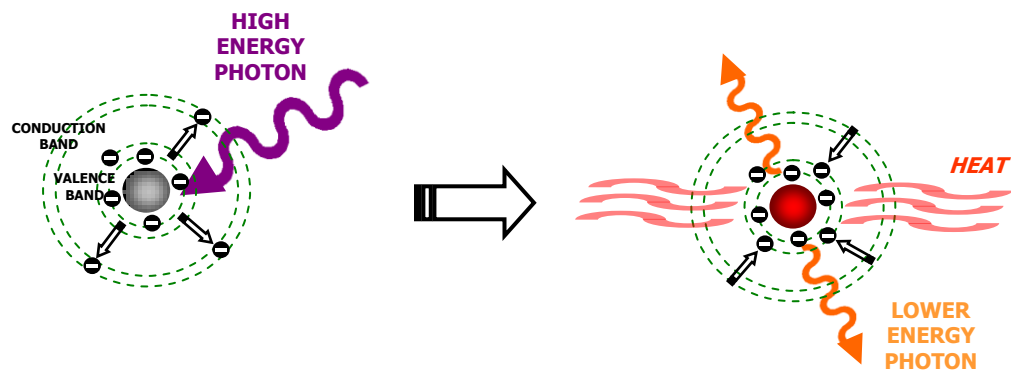
Trace explosive detection is practiced frequently through a variety of methods, including, but not limited to, chromatography, mass spectrometry, colorimetry and x-ray analysis.

Several different forms of chromatography have been applied to trace explosive analysis. In most cases, it involves passing the analyte in a mobile phase through a stationary phase. The stationary phase hinders the passing of the different components of the sample, some more than others. As the components traverse the stationary phase at different rates, they become separated and can be subsequently identified individually. Among the types of chromatography that have been applied to trace explosive analysis are thin-layer, gas, high-performance liquid, supercritical fluid, and ion chromatography<sup>1</sup>. Chromatography methods present obstacles to use in an UUV environment. A sample must be converted to a gas for gas chromatography and converted to a supercritical state (above critical temperature and pressure) for supercritical fluid chromatography analysis. The conditions required for these state conversions are too harsh to assure the integrity of many types of explosive traces.

Colorimetric methods do not require the complicated equipment that chromatography, mass spectrometry and x-ray analysis do, and are used in field applications to identify explosive traces by chemically analyzing a dry sample<sup>2</sup>. Such is the case with the Israel Police. If explosives are present on the sample paper, there is a visible color change when the test chemicals are applied.

Colorimetric methods, however, yield poor sensitivity in comparison to photoluminescent methods<sup>2,3</sup>. Sensitivity may prove very important in a situation where lower detection limits are beneficial. In a related study, explosive traces were tagged with a highly fluorescent lanthanide element, imparting strong fluorescence to the trace explosive compound in a dry environment. Most lanthanide elements are unable to fluoresce in the presence of water. The lanthanide series comprises the 14 rare earth elements from cerium to lutetium on the periodic table, with atomic numbers 58 through 71. Some lanthanide elements, particularly europium and terbium, luminesce with high quantum efficiency<sup>2,4</sup>. They also have long luminescence lifetimes<sup>2</sup>. In a seawater environment, europium is preferred over terbium, because its characteristic fluorescence is in the red-orange range (approximately 613 nm), while terbium's falls in the green range (550 nm)<sup>4</sup>. The red-orange color of europium should be more discernable from background chlorophyll fluorescence than terbium's green. Other advantages of europium over terbium will be introduced later. In addition to europium's use in trace explosive detection, it has been utilized in other applications such as in fluorescent glass and phosphorescent paints, some of which can glow for days after a few minutes of light exposure<sup>5</sup>.

Europium fluorescence (and fluorescence in general) is the emission of electromagnetic radiation (especially visible light) by an atom when it is stimulated by the absorption of incident radiation. In the fluorescence process, the first step is the excitation of an atom with a photon. The photon excites an orbital electron to jump to a higher energy level, from a valence band to the conduction band<sup>6</sup>. After cessation of the excitation, the electron will fall back to the original energy level, re-emitting energy as the atom returns to its original energy state. Some of the energy is lost to heat and some is released as another photon. In the case of fluorescence, the emitted photon is of a lower energy, corresponding to a longer wavelength and lower frequency than the one that first excited the molecule. If this radiation falls within the visible range of the electromagnetic spectrum, it will appear as a different color than the excitation radiation<sup>7,8</sup>.



Step 1: A high-energy photon excites the electrons in the valence band of the fluorescent atom to jump to the conduction band.

Step 2: After the excitation ceases, the atom returns to the original state, releasing energy in the forms of heat and lower energy photons.

Figure 1 – Description of the fluorescence process

In returning to the ground state from the excited state, a molecule may undergo other processes, in addition to fluorescence. The absorption of a photon occurs due to an interaction of the oscillating electric field vector of the light wave with the charges (electrons) of the molecule. Following photon absorption, an excited fluorophore will quickly undergo relaxation to the lowest vibrational energy level of the first excited state. This process is known as internal conversion or vibrational relaxation, and describes loss of energy in the absence of light emission. The excess vibrational energy is converted into heat. A result of internal conversion is that all subsequent relaxation pathways (such as fluorescence or quenching) proceed from the lowest vibrational level of the first excited state. Internal conversion means that emission spectra do not strictly depend on the excitation wavelength. The Jablonski energy diagram shown below in Figure 2 illustrates the sequential processes of internal conversion and fluorescence from an excited state to a ground state.<sup>42</sup>

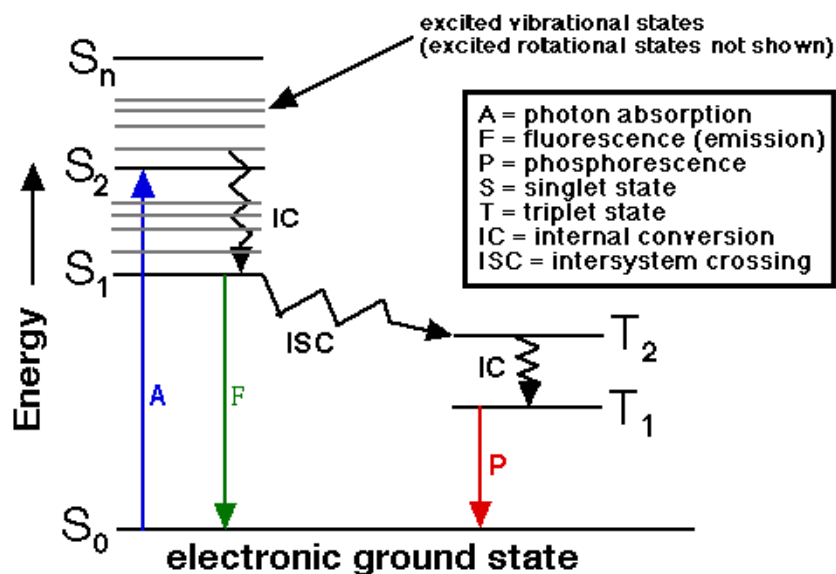
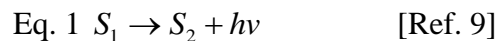


Figure 2 – Internal conversion and fluorescence from an excited state<sup>43</sup>



The equation for fluorescence is as follows:



$S_1 = \text{State 1}$

$S_2 = \text{State 2}$

$h = \text{Planck's Constant}$

$\nu = \text{Frequency of fluorescing light}$

Lanthanide elements in particular are highly fluorescent with a large stoke's shift, but they do not absorb photons (energy) well. Low levels of energy in means low levels out. To capture their fluorescence ability, they must be sensitized to better absorb incoming radiation. This sensitization can be accomplished by binding the lanthanide ion to photon-absorbent ligands. Once combined, these sensitizing ligands act as antennae for the resulting compound, collecting photons and transferring the energy to the lanthanide element<sup>10,11,12</sup>. During this process, a photon is not emitted from the donor. This energy transfer is referred to as Fluorescence Resonance Energy Transfer (FRET). FRET is the radiationless transmission of energy from a donor molecule (sensitizer) to an acceptor molecule. This interaction occurs over greater than interatomic distances, without conversion to thermal energy and without molecular collision<sup>7</sup>.

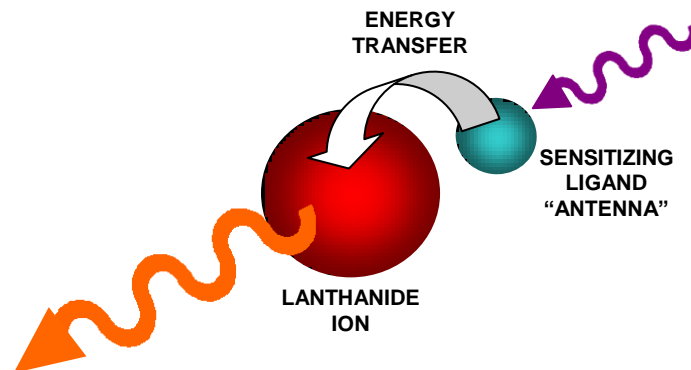


Figure 3 – Fluorescence Resonance Energy Transfer (FRET) from a sensitizing ligand to a lanthanide ion

FRET is governed by several factors, but most important are the proximity of the donor and acceptor molecules and the spectral overlap of the donor's emission range and the acceptor's excitation range. Typically, the donor and acceptor molecules are within 10-100 Å of each other. The donor's emission range must overlap the acceptor's excitation range for energy transfer to occur. Refer to Figure 4 for an illustration of the spectral overlap integral ( $J$ )<sup>7</sup>.

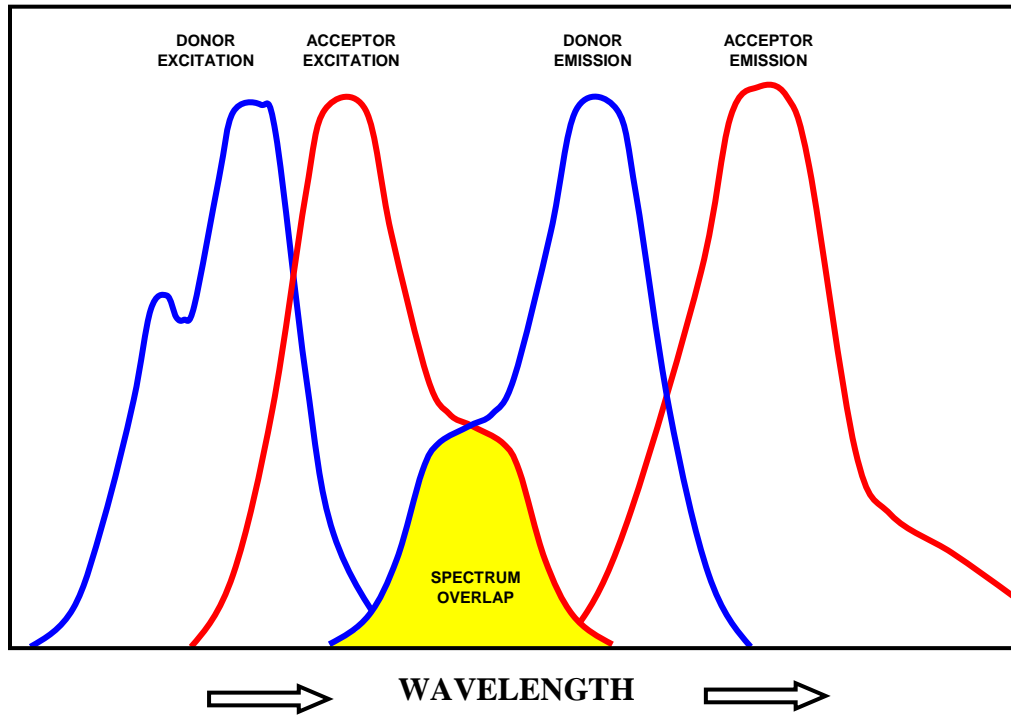


Figure 4 – Spectral overlap of donor emission range and the acceptor excitation range during Fluorescence Resonance Energy Transfer (FRET)

Förster has shown that the efficiency ( $E$ ) of the FRET process depends on the inverse sixth-distance between the donor and acceptor, as shown in equation 2.

$$\text{Eq. 2 } E = \frac{Ro^6}{(Ro^6 + r^6)} \quad [\text{Ref. 8}]$$

$E$  = Fluorescence Resonance Energy Transfer Efficiency

$Ro$  = Förster Distance

$r$  = Actual Distance Between Donor and Acceptor

The Förster distance,  $R_o$ , is the distance at which energy transfer is 50 percent efficient<sup>8</sup>. The Förster distance is dependent on several factors, including the fluorescence quantum yield of the donor in the absence of acceptor ( $fd$ ), the refractive index of the solution ( $n$ ), the dipole angular orientation of each molecule ( $k^2$ ), and the spectral overlap integral of the donor and acceptor ( $J$ ). Equation 3 defines the Förster distance.

$$\text{Eq. 3} \quad R_o = 9.78(10^3) \cdot (n^{-4} \cdot fd \cdot k^2 \cdot J)^{\frac{1}{6}} \text{ \AA} \quad [\text{Ref. 8}]$$

*R<sub>o</sub> = Förster Distance*

*n = Refractive Index of Solution*

*fd = Fluorescence Quantum Yield of Donor without Acceptor*

*k<sup>2</sup> = Dipole Angular Orientation of Molecules*

*J = Spectral Overlap Integral of the Donor and Acceptor*

Thenoyltrifluoroacetone (TTA) and ortho-phenanthroline (OP) have been used as donor molecules to lanthanide ions in past studies, including purposes such as latent fingerprint detection by photoluminescent analysis. TTA and OP are both bidentate sensitizing ligands, meaning that each donor ligand occupies two available bonding sites on an acceptor compound<sup>2,3</sup>. In the case of a europium ion, bidentate ligands can occupy 8 of the 9 available bonding sites<sup>2,4</sup>. The last, lone site is left unoccupied. This leaves one site open to accept something else, such as a water molecule or an explosive trace<sup>2,3,4</sup>.

While europium compounds fluoresce well after donor-acceptor sensitization, their luminescent properties are vulnerable to water<sup>2,4</sup>. Positively charged europium ions ( $\text{Eu}^{+3}$ ) are attracted to the dipolar nature of water. Since the oxygen end of a water

molecule is more negative than the hydrogen end, water bonds to a positively charged lanthanide ion through its oxygen<sup>13,14</sup>. The bonding of water to the lanthanide ion is neither ionic nor purely covalent; rather it is an “attraction” between a charged ion and an electric dipole. When europium forms a compound with water, its photoluminescence is quenched via coupling of the O-H vibrational overtones<sup>2,4,15</sup>. Interestingly, this is not true of all lanthanide compounds, as terbium does not exhibit this strong water-quenching<sup>4</sup>. This identifies another advantage of europium over terbium in this application, as quenching plays a vital role in the explosive detection method outlined in this thesis. Quenching arises from a competing process that acts to induce non-radiative relaxation of electrons to the ground state. This can come about through collision with another non-fluorescent molecule in solution, resulting in deactivation and return to the ground state. Usually, neither molecule is chemically altered through quenching.<sup>42</sup>

Water molecules may vibrate in several ways. The main vibrations include combinations of symmetric stretch, asymmetric stretch, bending, and rotation around the three primary axes<sup>13</sup>. These types of vibrations are shown below in Figure 5.

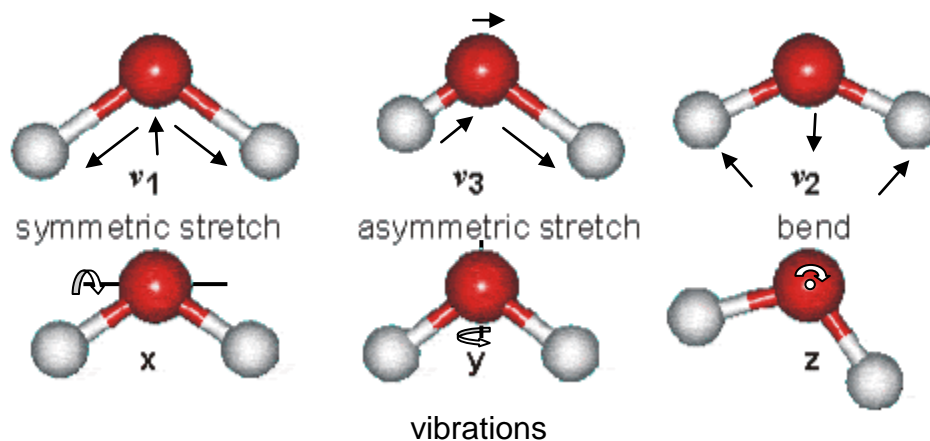


Figure 5 – Water molecule vibration modes<sup>13</sup>

Water vibrations depend strongly on hydrogen bonding, which is influenced by temperature and pressure. Hydrogen bonding occurs when an atom of hydrogen is strongly attracted to two atoms, instead of one. In the case of water, this often means that a hydrogen atom is covalently attached to an oxygen atom, but has an additional attraction to a neighboring oxygen atom of another water molecule. Chaplin<sup>13</sup> sites the covalent bond strength as about  $492 \text{ kJ mol}^{-1}$  and the additional attraction strength as about  $23.3 \text{ KJ mol}^{-1}$ . It is this attraction to more than one atom that causes the vibrations noted. In a sense, the hydrogen atoms are torn between two attractions, and the cooperative/anticooperative effects hydrogen bonding has on water molecules further complicate this process. Every hydrogen bond formed increases the hydrogen bond status of two water molecules and every hydrogen bond broken reduces the hydrogen bond status of two water molecules. When a hydrogen bond forms between two water molecules, the redistribution of electrons changes the ability for further bonding. The water molecule donating the hydrogen atom has increased electron density in its lone pair region, which encourages hydrogen bond acceptance, and the accepting water molecule has reduced electron density centered on its hydrogen atoms and its remaining lone pair region, which encourages further donation but discourages further acceptance of hydrogen bonds<sup>16</sup>. While hydrogen bonds likely occur most frequently between hydrogen and oxygen atoms in water, it can occur in other forms, such as between hydrogen and chloride ions<sup>13</sup>, adding another possible dimension to seawater. The hydrogen bond is part (about 90%) electrostatic and part (about 10% covalent)<sup>17</sup>. The

hydrogen bond strength depends almost linearly on its length, which in turn varies with temperature and pressure. Short length gives stronger hydrogen bonding and vice-versa<sup>13</sup>.

Even if the water isn't attached to a bonding site of a europium compound, it may disrupt the fluorescence by just being in the vicinity<sup>18,19</sup>. Binding of an explosive to the available bonding site of the europium ion precludes the bonding of water to prevent fluorescence quenching. In addition to simply disallowing a water molecule into the available bonding site, the attachment of the explosive may further create a hydrophobic environment around the europium ion by blocking the surrounding water molecules from interfering<sup>18,19</sup>. Regardless of the mode of action, sensitized lanthanide fluorescence persists in the presence of water when an explosive trace is first attached to the compound. If the bonding of the explosive traces and the europium can be accomplished in an aqueous environment, a beneficial side effect of the water environment is that the unbonded europium compounds are quenched to eliminate non-explosive competing fluorescence.

It is possible to bond the lanthanide elements to the explosive traces, due to the oxygen part of the nitrites included with many explosive types (See Figures 6 and 7). These Nitrites likely exhibit the same bipolar charge phenomena as water (due to their geometric structure), but in addition to this, one of the oxygen atoms carries another negative charge. It is likely that this negatively charged oxygen moiety is more strongly attracted to the lanthanide ion than the dipolar charge of the surrounding water molecules.

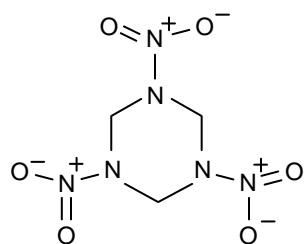


Figure 6 – RDX explosive structure with nitrites

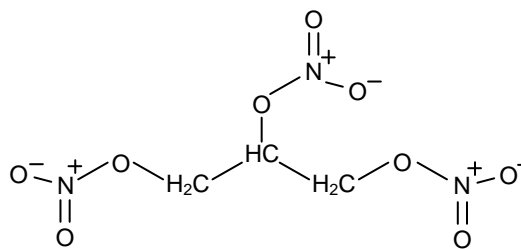


Figure 7 – Nitroglycerin explosive structure with nitrites

In addition to being susceptible to water, lanthanide fluorescence is also affected by pH and surrounding metal ions. Low pH decreases the stability of the compound (chelate) by compromising the bond between the ligand (chelating agent) and lanthanide (metal) ion. In low pH, the exchange reactions of the ligand become more rapid and competing chelating agents that may be in the solution are more likely to affect the compound. Low pH is also believed to affect the energy transfer from ligand to lanthanide ion<sup>20</sup>. pH susceptibility has been reported to begin at pH levels of 4 or 5<sup>12,20,21</sup>. Fortunately, seawater pH is limited to the range of 7.5 – 8.4<sup>22</sup>.

Surrounding metal ions can affect lanthanide fluorescence through metal-exchange reactions. When a lanthanide chelate is exposed to other metal ions that have a strong affinity for the lanthanide's ligands, the lanthanide ion may be replaced by the foreign metal ion. Lanthanide complex metal-exchange behavior has been observed with alkaline earth ions, specifically calcium<sup>12,15</sup>. Once a lanthanide ion loses ligands to another metal ion, it becomes more prone to quenching by water molecules.



It has been shown that europium – explosive compound complexes can be created without the presence of water in a controlled environment, which will then prevent water quenching and enable fluorescence. But is the europium-explosive attraction strong enough to displace existing water molecules and allow fluorescence in an aqueous environment?

## CHAPTER 3

### RESEARCH GOALS

1. Identify a potential method for detecting underwater explosive traces (photoluminescent detection).
2. Choose appropriate chemical components (europium, thenoyltrifluoroacetone, and ortho-phenanthroline) and evaluate the feasibility of developing this method for detecting underwater explosive traces.
3. Evaluate the hypothesis that the chemical complexes will preferentially bond with explosive compounds over water molecules in an aqueous environments, including water and seawater. This is a crucial step in the research, as water is known to quench the fluorescence of europium.
4. Optimize the detection method by examining different formulations of the chosen chemicals (europium, thenoyltrifluoroacetone and ortho-phenanthroline) and solvents, looking for optimal combinations to achieve both fluorescent loss in seawater (quenching) and maintained fluorescence in response to explosive

compounds. Different combinations, concentrations and mixing orders of the chemicals are evaluated. Other factors that influence the performance of the compounds are also evaluated, such as the amount of reagent solvent (methanol) used to deliver the chemicals into the solution.

5. Characterize the excitation and emission properties of the sensitized europium compounds, evaluated in Research Goal 2.
6. Characterize the explosive-detecting ability of the sensitized europium compounds.
7. Identify and explain important effects of seawater constituents on the detection method.
8. Evaluate expected port turbidity conditions and the need for sample filtering.
9. Design, purchase and characterize a prototype field-deployable detector for underwater trace explosive detection.
10. Create a realistic laboratory system to imitate field conditions and prove the field-deployable design concept.

## CHAPTER 4

### RESEARCH APPROACH

#### 4.1 Primary Test Materials

##### 4.1.1 Explosive Sample

Nitroglycerin ( $C_3H_5N_3O_9$ ) has been chosen as the explosive material to analyze, because of its chemical structure and availability. Nitroglycerin bears nitrites, which are common to many important types of explosives, and serve as the identifiable moiety of these compounds with this detection method. Based on this nitrite similarity, the identification of nitroglycerin strongly suggests the detectability of a large family of nitrite-bearing explosive compounds. This family is often classified as “Group B” explosives and includes important types such as RDX, Semtex, HMX, PETN, EGDN, Nitro Cellulose, Teteryl, and Smokeless Powder<sup>23</sup>. This list includes very strong explosives, commonly used in weapon and military applications such as dynamite, plastic explosives, ammunition and detonators.

Nitroglycerin is widely available, due to its common use in the medical field to relax vascular smooth muscle. Vascular muscle relaxation results in the dilation of both arterial and venous vessels, acting to lower blood pressure (Appendix A2). In particular, this study employs 0.4 mg nitroglycerin Sublingual Tablets. These tablets are designed to dissolve under the tongue and release nitroglycerin into the blood stream, where it interacts further with the body, but nitroglycerin may also be derived from them through dissolution in water. Refer to Appendix A2 for more information on the mechanism of action of these specific tablets.

#### 4.1.2 Fluorescent Material

The lanthanide series of elements comprises the 14 rare earth elements from cerium to lutetium on the periodic table, with atomic numbers 58 through 71. Europium, a lanthanide element, is characteristically fluorescent<sup>5</sup> and is the core of the fluorescent body that is designed to attach to trace explosives in this analysis. Europium has been proven in previous studies involving fluorescent analysis, and has been shown to lose its fluorescence in the presence of water<sup>2,3</sup>. These characteristics make europium a choice element for this experiment.

The europium ion was derived from europium(III) chloride hexahydrate ( $\text{EuCl}_3 \cdot 6\text{H}_2\text{O}$ ), which is available in a crystalline form. Refer to material data safety sheet CAS # 13759-92-7 for more information.

#### 4.1.3 Sensitizer (Near UV Absorber)

Thenoyltrifluoroacetone (TTA) has been utilized as a sensitizing ligand for the europium ion. Since europium cannot absorb energy well alone, the TTA serves to collect UV radiation and transfer it to the europium ion to initiate the europium fluorescence process. The TTA primary electromagnetic radiation absorption range is in the near UV portion of the spectrum (300nm – 400nm)<sup>18</sup>. The TTA also acts to preclude water molecules from bonding to the europium ion and negatively affecting the europium fluorescence<sup>2,3</sup>.

Thenoyltrifluoroacetone was obtained in crystalline form (C<sub>8</sub>H<sub>5</sub>F<sub>3</sub>O<sub>2</sub>S). Refer to material safety data sheet CAS # 326-91-0 for more information.

#### 4.1.4 Sensitizer (Far UV Absorber)

Ortho-phenanthroline (OP) serves as an absorber of UV radiation, similar to TTA, but absorbs primarily in the far UV range (less than 300nm). With respect to electromagnetic radiation absorption, OP is less desirable than TTA for this experiment, because the excitation wavelength used is in the near UV. In general, near UV radiation is more easily achieved, especially through the use of LED's. The purported advantage of OP is that it has been reported to allow better water quenching of connected, fluorescent ions than TTA<sup>3</sup>.

Ortho-phenanthroline was obtained from 1,10-phenanthroline monohydrate ( $C_{12}H_8N_2 \bullet H_2O$ ), which is available in crystalline form. Refer to material safety data sheet CAS # 66-71-7 for more information.

## **4.2 Primary Test Equipment and Configurations**

### **4.2.1 Handheld UV Light**

To qualitatively evaluate the fluorescence of a given solution, before extensive luminescence spectrometer experimentation, a handheld UV light was used for excitation. If the solution in question was absorbent to UV light of the appropriate wavelength and fluorescent, fluorescence could be visually observed. This allowed a preliminary screening of mixtures that either didn't absorb the UV radiation or didn't fluoresce.

The handheld UV light used was the Photon Micro-Light, made by Amberica West. This light operates at a wavelength of 370 nm, which is remarkably appropriate for the excitation wavelength required by the TTA ligand, and representative of the lowest wavelength that LED's can currently produce<sup>3,24,25</sup>. Figure 8 shows the Photon Micro-Light.



Figure 8 – Handheld ultraviolet LED<sup>24</sup>

#### 4.2.2 Luminescence Spectrometer

A luminescence spectrometer, Perkin-Elmer model LS50B, was used for laboratory fluorescence analysis. This particular model is capable of excitation and emission reading through a range of 200 to 800nm. It uses a windows-based program, called FL WinLab for operation. Refer to Figures 9 and 10, respectively, for pictures of the luminescence spectrometer and 4ml analysis cuvette used.

The luminescence spectrometer provides the following experimental abilities:

- (1) Identify the best excitation wavelength for each specific compound. This is done by incrementally applying a range of excitation wavelengths to the sample and identifying the excitation wavelength that results in the largest



intensity of the desired emission wavelength. The maximum intensity of the target emission wavelength identifies the best wavelength for excitation. The target emission wavelength for this study was chosen to be 613 nm, based on the emission characteristics of europium<sup>4</sup>.

- (2) Measure the emission fluorescence intensity and wavelength from a particular sample when subjected to excitation radiation of a specified wavelength.

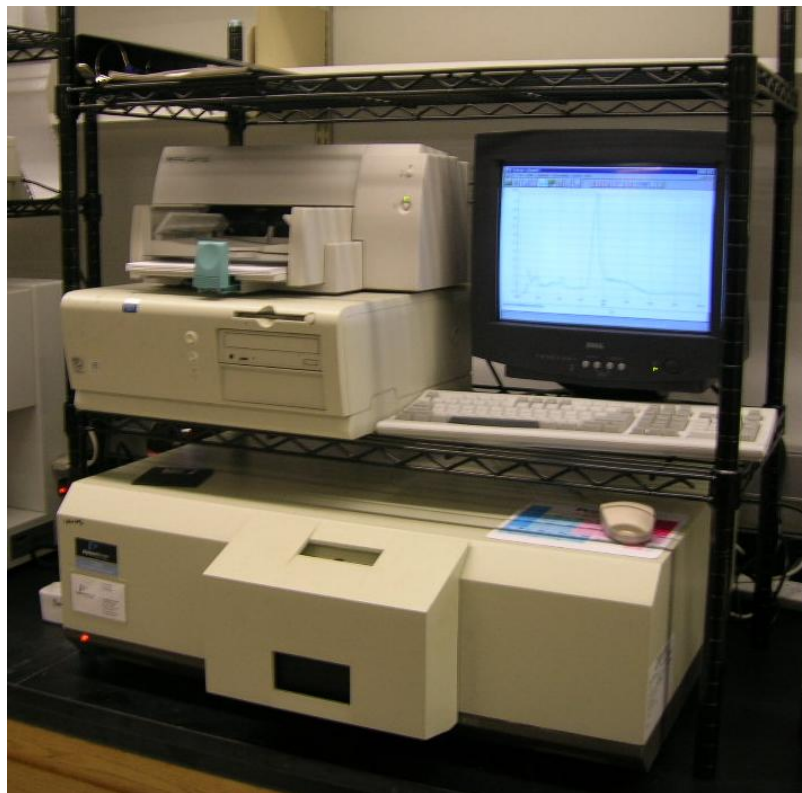


Figure 9 – Luminescence spectrometer and setup

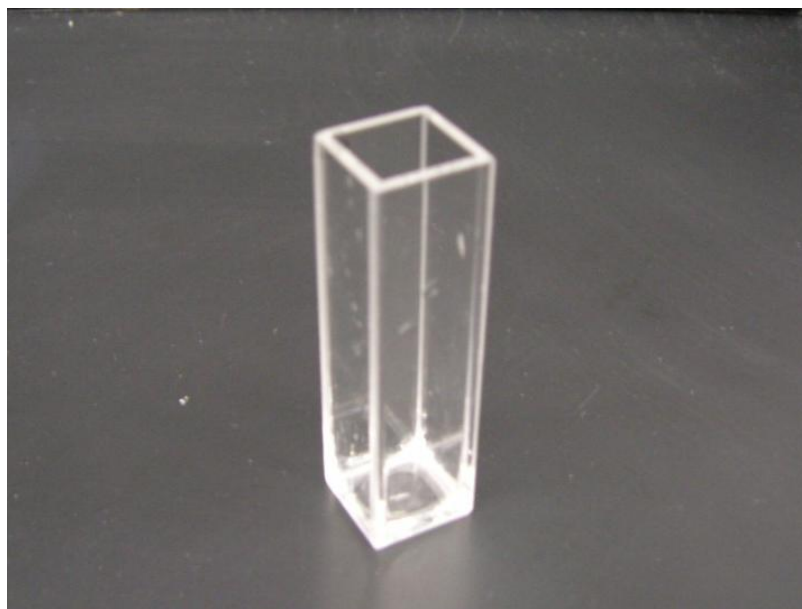


Figure 10 – Luminescence spectrometer cuvette

Use of the luminescence spectrometer requires several settings to be adjusted. In addition to the excitation and emission wavelengths, the scan speed must be specified. For this study, a relatively slow scan speed of 200 nm/sec was chosen. A slower scan speed translates directly into better resolution. A faster scan speed is warranted when scanning phosphorescent compounds that are susceptible to photo-bleaching from longer exposure to the excitation light<sup>26</sup>, which is not the case for this experiment. Emission and excitation slit widths must also be specified. Reference 26 provided guidance for setting the excitation and emission slit widths. For the experiments contained herein, relatively narrow slit widths of 5nm were chosen for both the excitation and emission wavelengths to achieve precision.

### 4.2.3 Deployable Fluorometer

A flow-through chlorophyll fluorometer was modified to use as a potential explosive trace detection field unit. The fluorometer used was the WETStar model, made by Wet Labs, Inc. The WETStar was modified with custom LED's and an optical filter to provide the excitation wavelength and monitor the emission wavelength that was determined to be appropriate in the luminescence spectrometer testing. Based on the research contained herein, the excitation wavelength was chosen to be centered at 370 nm, and the emission filter was chosen to be a narrow-band filter, designed to allow emitted light around 613 nm. The WETStar can be seen in Figure 11, the chosen emission filter profile is shown in Figure 12, and the specifications for the original commercial chlorophyll model can be found in Appendix A3.



Figure 11 – WETStar chlorophyll fluorometer

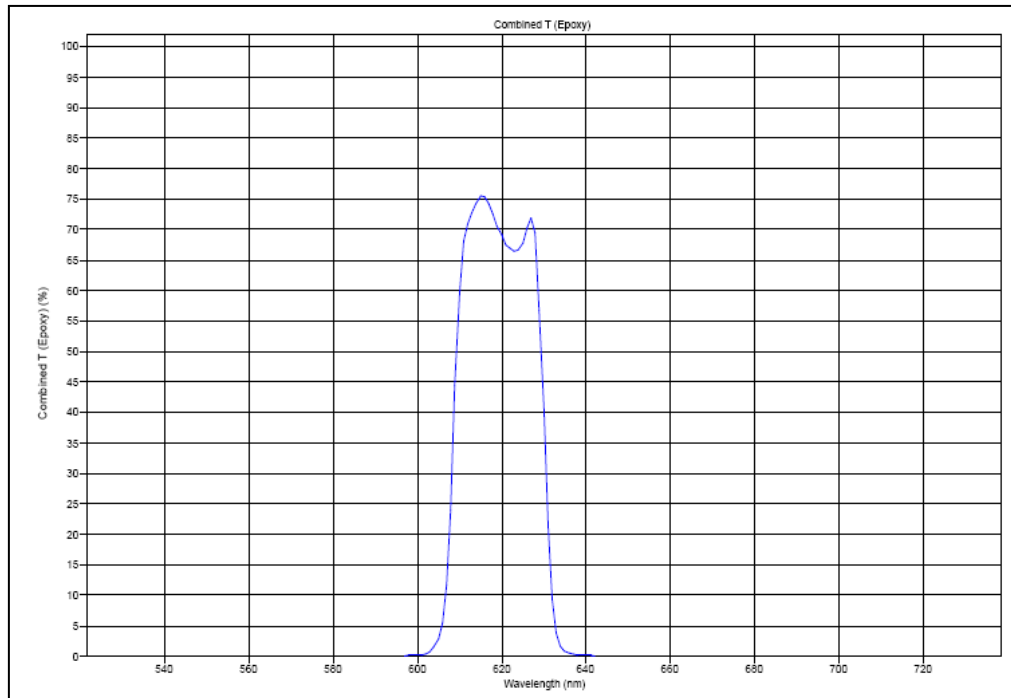


Figure 12 – Profile of emission filter chosen for the customized (WETStar) fluorometer

#### 4.2.4 Static Fluid Mixer

Due to the low flowrate of the fluid passing through the deployable fluorometer, it was calculated that the flow would be laminar. The fluorometer used in the experiments contained herein has an inside diameter of  $\frac{1}{4}$ ". Pipe flow becomes turbulent when the Reynolds number is greater than approximately  $4000^{27}$ . The minimum flowrate required to maintain a Reynolds number of this magnitude with this geometry is 1403 ml/min, as determined from equation 4 below.

$$\text{Eq. 4} \quad Q = V \cdot A = \left( \frac{\text{Re} \cdot \mu}{\rho \cdot D} \right) \cdot (\pi \cdot r^2) \quad [\text{Ref. 27}]$$

$Q = \text{Flowrate}$

$V = \text{Flow Velocity}$

$A = \text{Tube Cross-sectional Area}$

$\text{Re} = \text{Reynolds Number} = 4000$

$\mu = \text{Dynamic Viscosity}$

$\rho = \text{Density}$

$D = \text{Tube Diameter}$

This high flowrate is clearly impractical in this application, and laminar flow must be expected. Unfortunately, laminar flow provides for negligible mixing and diffusion must be relied upon as the dominant mixing process. Two diffusion calculations were done to assess the need for a mixer. The first used a moving coordinate system in order to consider diffusion and convection in the flow direction. This calculation was done to determine if the diffusion process contributed significantly in the forward direction, or if the concentration was mostly dependent on convection. The equations required were not immediately available and were derived for this calculation. The derivation is shown in Appendix A4. The derivation was accomplished with the following process:

- 1) Transform the spatial and time variables of the diffusion equation into a moving coordinate system that includes a diffusion and convection term.
- 2) Transform the equation into the frequency domain by implementing a Laplace Transform with respect to time.

- 3) Solve the frequency domain equation with the following boundary and initial conditions:
- Concentration at  $x = 0$  is constant.
  - Concentration at  $x = \infty$  is zero.
  - Concentration at  $t = 0$  is zero everywhere.
- 4) Find the time solution with an Inverse Laplace Transform. A branch cut and contour integral were required to complete this integration in the complex plane.

The solution is of the form:

$$\text{Eq. 5} \quad C(x,t) = \frac{C_0}{2} \left\{ \text{erfc} \left( \frac{x-Vt}{2\sqrt{Kt}} \right) + e^{\frac{Vx}{K}} \text{erfc} \left( \frac{x+Vt}{2\sqrt{Kt}} \right) \right\}$$

$C = \text{Concentration}$

$C_0 = \text{Initial Concentration at } x = 0$

$x = \text{Spatial Distance from the Origin}$

$V = \text{Average Flow Velocity}$

$t = \text{Time}$

$K = \text{Diffusion Coefficient}$

The notation,  $\text{erfc}(x)$ , represents the compliment to the error function of statistics. Equation 5 was plotted against time, using spatial distances of 1 and 10 feet. Figure 13 provides the results and Appendix A4 contains the Matlab code used. Figure 13 indicates that there is a sudden spike in concentration at a specific time for each distance. This time corresponds to the time it takes for the concentrated fluid in the tube to travel that

distance, so it can be accepted that forward diffusion plays a negligible role in this mixing problem and the forward wave of concentration is almost entirely dependent on convection. Because an exact diffusion coefficient is not known for these specific chemicals in seawater, the diffusion coefficient found in reference 28 for methanol in water was used.

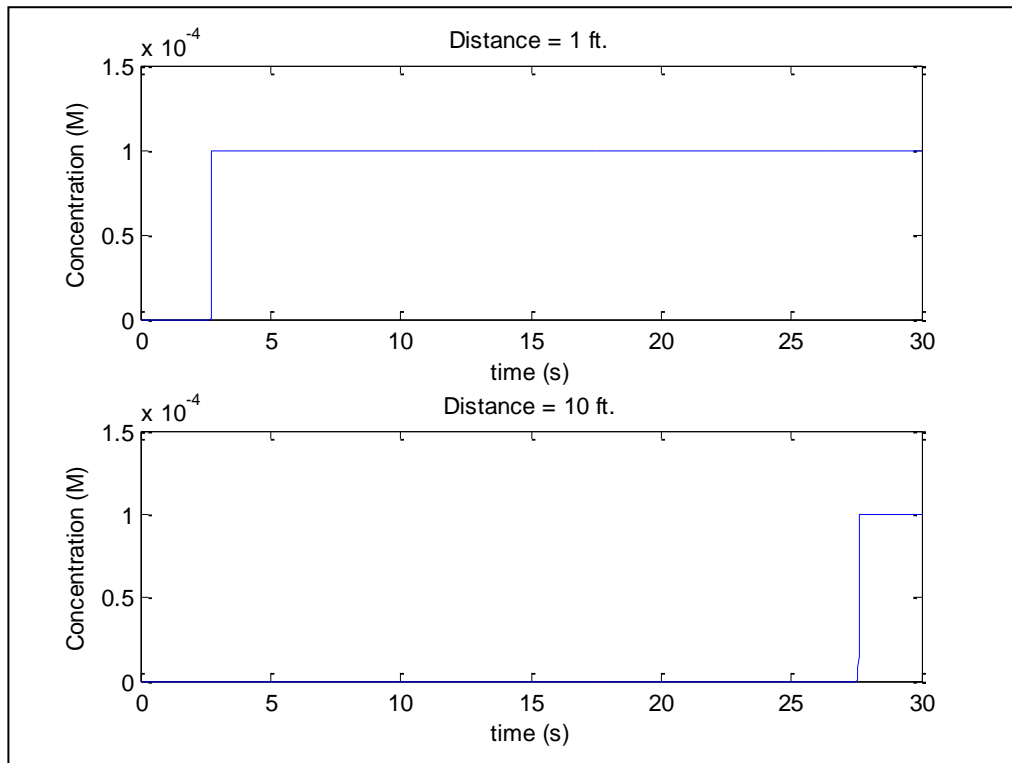


Figure 13 – Calculated downstream concentration as a function of time

The second diffusion calculation aimed at determining the ability of the reagent solution to diffuse across the flow channel. Because the reagent solution will likely be introduced into the side of the main channel, the densities of the seawater and reagent solutions differ, and the flow is laminar, it is anticipated that the reagent flow will traverse along the side of the main channel. After flow has stabilized, there will be two

main streams running alongside each other, resulting in only a two dimensional diffusion problem. To determine how quickly the reagent solution will diffuse across the channel, the two-dimensional diffusion equation was employed:

$$\text{Eq. 6} \quad \nabla^2 C - \frac{1}{K} \frac{\partial C}{\partial t} = 0 \quad [\text{Ref. 29}]$$

$C = \text{Concentration}$

$\nabla = \text{Gradient Operator}$

$t = \text{Time}$

$K = \text{Diffusion Coefficient}$

The solution to this equation is readily available and need not be derived:

$$\text{Eq. 7} \quad C(r,t) = \frac{e^{\left(\frac{-r^2}{4K \cdot t}\right)}}{4\pi K \cdot t} \quad [\text{Ref. 29}],$$

which is a normalized Gaussian function. The Gaussian probability distribution function is found by integrating over the Gaussian probability density function<sup>30</sup>. Furthermore, the error function is closely related to the Gaussian probability distribution function and is related to the normalized Gaussian function by:

$$\text{Eq. 8} \quad \int G(r) dr = \text{erf}\left(\frac{r}{\sigma\sqrt{2}}\right) \quad [\text{Ref. 31}]$$

$\sigma = \text{variance} = 2\sqrt{2Kt}$



This error function can be used to show the diffusion behavior of the reagent across the cross-section of the flow tube. The result is shown in Figure 14 below and the Matlab code is included in Appendix A4.

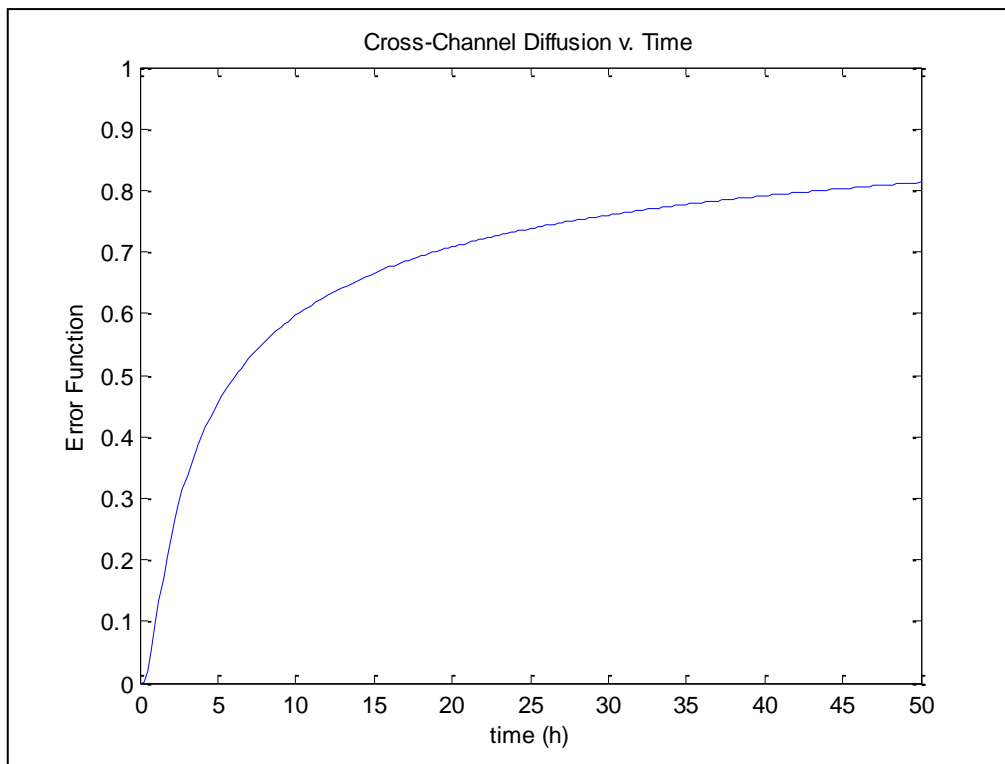


Figure 14 – Calculated cross-channel diffusion behavior

From Figure 14, it becomes apparent that diffusion of the reagent across the channel cross-section is expected to be very slow. As before, the diffusion coefficient was assumed to be that of the reagent solvent (methanol) in water<sup>28</sup>, due to the lack of availability of more detailed diffusion coefficients. It is noted that the diffusion coefficient for methanol in water is almost identical to that of the salts NaCl and CaCl<sub>2</sub>. This diffusion coefficient assumption is believed to be conservative as it is not expected

that the europium compounds will diffuse faster than their solvent (methanol), NaCl or CaCl<sub>2</sub>.

Based on the above calculations, diffusion was not expected to suffice for mixing. Therefore, to mix the fluids before passing through the fluorometer, a static mixer was employed. Static mixers use a series of elements, fixed inside a tube, to redirect and mix the fluids. The mixing process occurs as follows<sup>32</sup>:

- (1) Division of the main stream.
- (2) Streams are forced to opposite outside walls.
- (3) This causes a single-direction mixing vortex axial to the centerline of the second element.
- (4) Mixing vortex is sheared and step (1) re-occurs, with the opposite directional rotation.

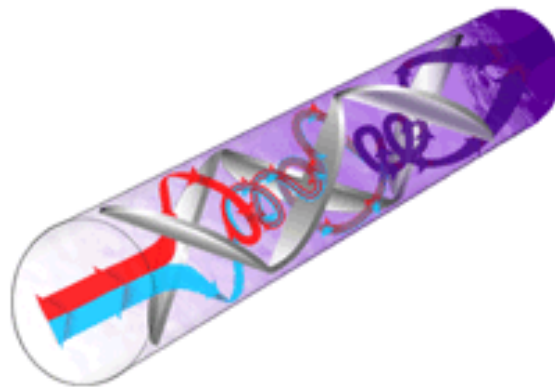


Figure 15 – Static mixer mixing process<sup>32</sup>



Figure 16 – Static mixer flow paths around elements

Based on the recommendations of the TAH Industries representative, a 24-element static mixer was used.

#### 4.2.5 Deployable Detector Characterization Setup

The chemical detection method was primarily analyzed in a laboratory luminescence spectrometer. The sensitivity of the deployable detector is different from the luminescence spectrometer and it was necessary to test the performance of the deployable detector to use it in a detection scheme. The deployable fluorometer was plugged at one end with a ball valve so that it could be filled and drained. A cover was used to prevent ambient light from affecting the fluorometer results. The fluorometer was powered with a 9-volt “battery eliminator” source and the output was measured with a digital multimeter. Figure 17 provides a schematic and Figure 18 provides a photograph of the setup.

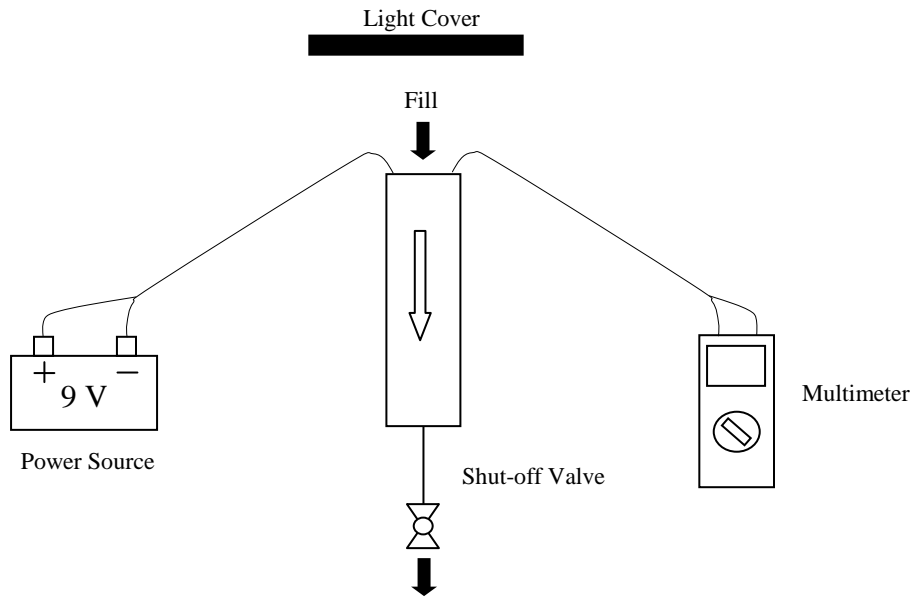


Figure 17 – Deployable detector characterization test setup schematic

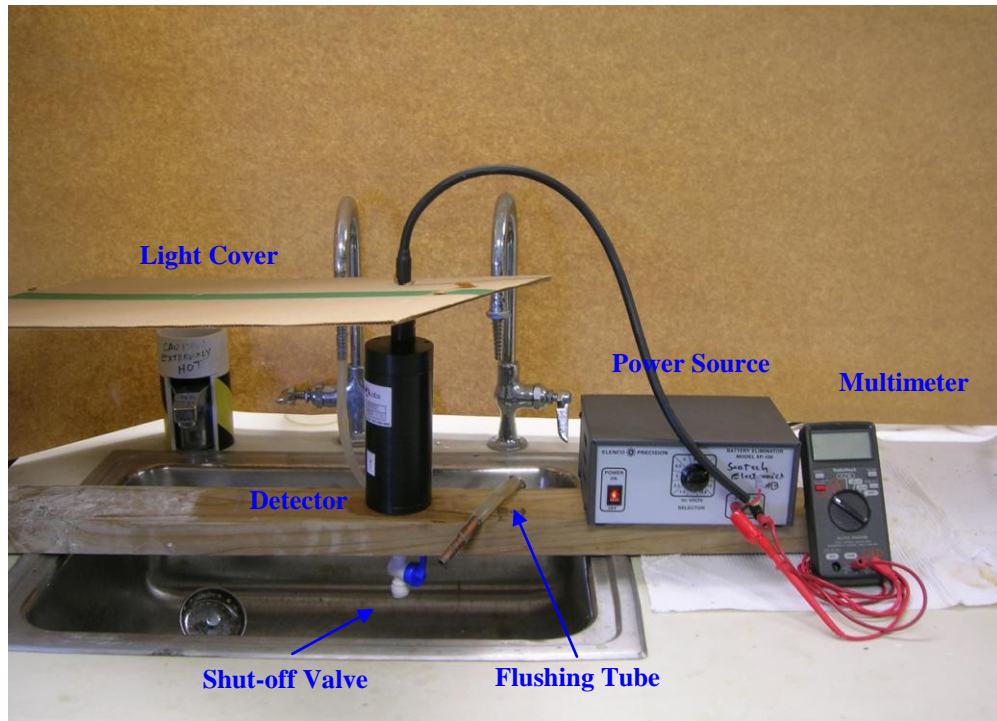


Figure 18 – Deployable detector characterization test setup

#### 4.2.6 Deployable Detector Proof of Design Test Setup

To prove the detection method overall design, a setup was required to incorporate the different design components, deliver the seawater solution and europium complex in correct proportions, and mix them together in a flowing configuration. Gravity head was used to deliver the fluids through the fluorometer, ball valves were used to control the flowrates, and an inline static mixer was used to assure proper mixing. A power source and multimeter were used in a similar way as in the deployable detector characterization tests. Figure 19 depicts a fluid schematic and Figure 20 shows a photograph of the setup. The europium solution was placed at a higher elevation than the seawater solution to assure that there was no stagnation of the europium solution flow and no backflow of the seawater solution into the europium solution line. An additional length of 8 ft. of tubing was included between the static mixer and the fluorometer to provide additional time for the reactions to take place before passing through the fluorometer.

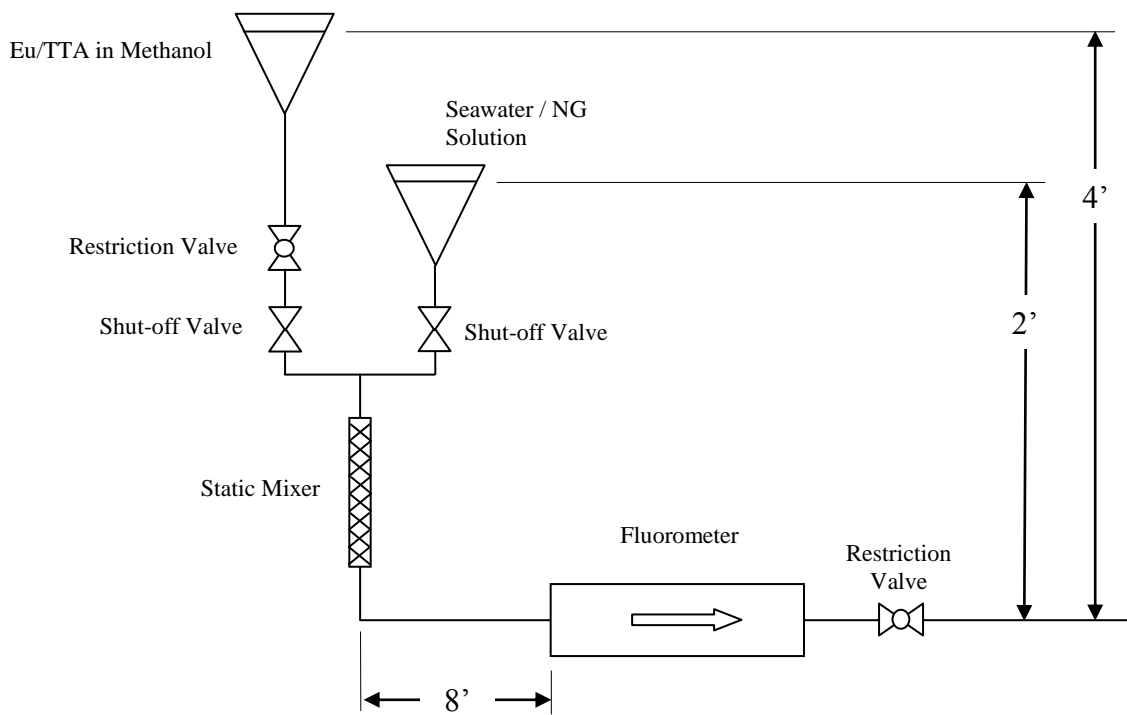


Figure 19 – Deployable detector test setup schematic

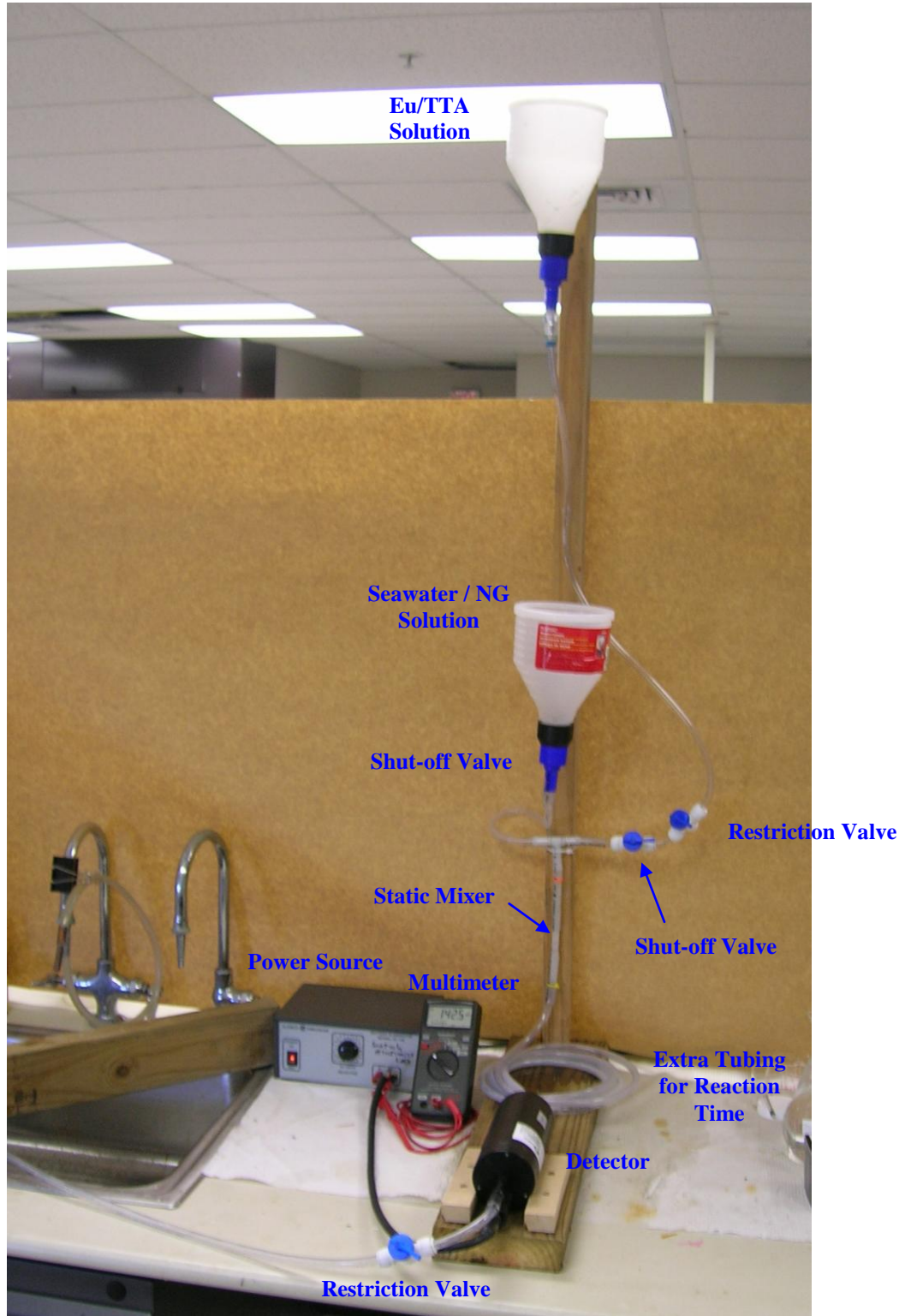


Figure 20 – Deployable detector test setup

### 4.3 Feasibility Investigations

Before embarking on extensive research into this topic, it was prudent to first examine the general feasibility of the detection and experimental methods. Three important questions to be answered before conducting research were as follows:

4.3.1 Will water allow the passage of the characteristic electromagnetic radiation excitation and emission wavelengths?

For the proposed method to be successful, it is imperative that the excitation radiation reaches the europium compound and the resulting fluorescence radiation is recovered. Water absorbs and transmits radiation differently, based on wavelength. Martin Chaplin of London South Bank University has published an absorption spectrum of liquid water<sup>13</sup>, which is shown in Figure 21. Referring to Figure 21, it becomes apparent that there is a relatively low absorption coefficient ranging from approximately 200nm through the visible light spectrum. 200nm is a sufficiently short wavelength in the UV range to serve for all fluorescence excitation purposes in this experiment and the visible spectrum will envelop the characteristic emission wavelengths to be measured.

Thus, all frequencies required in this experiment will traverse water better than or equal to long wavelength (red) visible light.



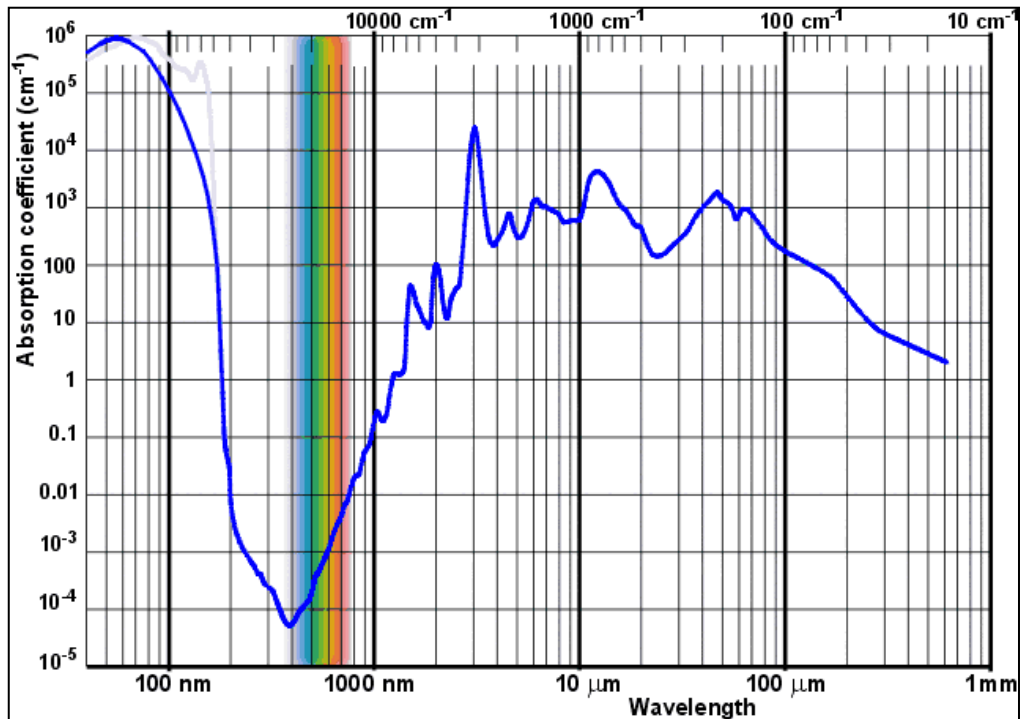


Figure 21 – Absorption coefficient vs. electromagnetic wavelength for liquid water<sup>13</sup>

4.3.2 Will the nitroglycerin source obtained (medical tablets) release nitroglycerin into the water, so that it may be in solution and detectable through the proposed experimental methods?

Before conducting fluorescence experiments and drawing conclusions from them, it must be determined if the analysis solutions actually contain nitroglycerin. The nitroglycerin source obtained is for medical use, to be dissolved in the body, and there is no guarantee that it will release nitroglycerin in only water or seawater.

To answer this question, High Performance Liquid Chromatography (HPLC) was employed. HPLC is a form of column chromatography in which the analyte is forced through a column of the stationary phase by a liquid at high pressure. Applying pressure allows the components less time to diffuse within the column, resulting in improved resolution in the resulting chromatogram. Four solutions were analyzed; distilled water, seawater, and each with nitroglycerin tablets. The number of nitroglycerin tablets was controlled to produce concentrations of  $1 \times 10^{-3}$  M. In preparation of the nitroglycerin solutions, each solvent was combined with the required number of nitroglycerin tablets, mixed, and then filtered through a  $0.45 \mu\text{m}$  filter to remove the solid matter.

Figures 22 through 25 indicate that there was a component at 13 minutes in the nitroglycerin solutions that was not present in the solvents alone. Comparison to the results of a previous identification of nitroglycerin by HPLC<sup>41</sup> indicates that the additional component found in the nitroglycerin tablet solutions is likely to be nitroglycerin, and not another ingredient from the tablet.

It should be noted that the HPLC result for distilled water alone shows some irregularity. This is mostly noticeable because of the scale. The y-scale ranges from 0 to 56.25 for this test, while it ranges from 0 to 900 for the other HPLC tests. This was also the first run performed of the four, and this could indicate that other analytes from previous experiments were still present in small quantities. Additionally, the water distiller had some unknown growth in it, which could also affect the HPLC result. The important thing to note, however, is that the nitroglycerin peak was not apparent in the distilled water run.

By this experiment, it was concluded that water / nitroglycerin and seawater / nitroglycerin solutions are attainable by the dissolution of a medical nitroglycerin sublingual tablet of the specifications listed in Appendix A2.

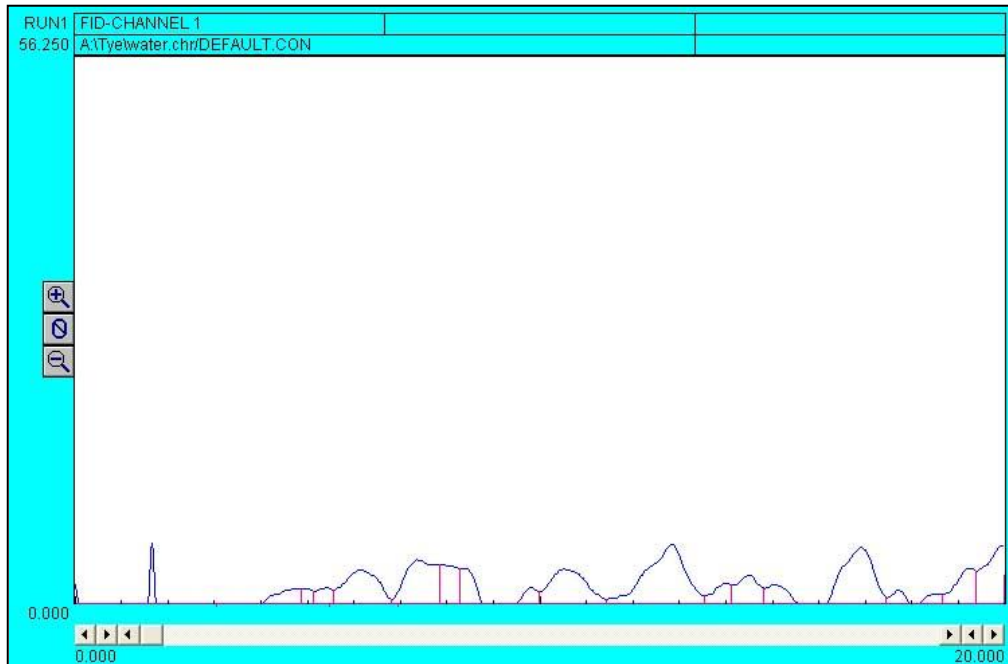


Figure 22 – HPLC result for distilled water

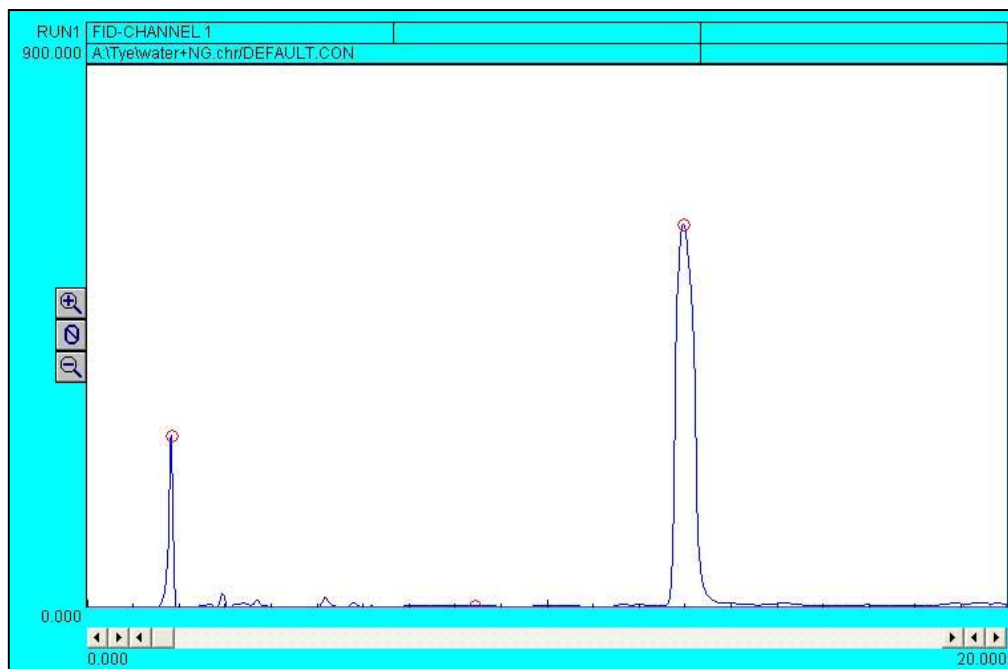


Figure 23 – HPLC result for distilled water and nitroglycerin tablets

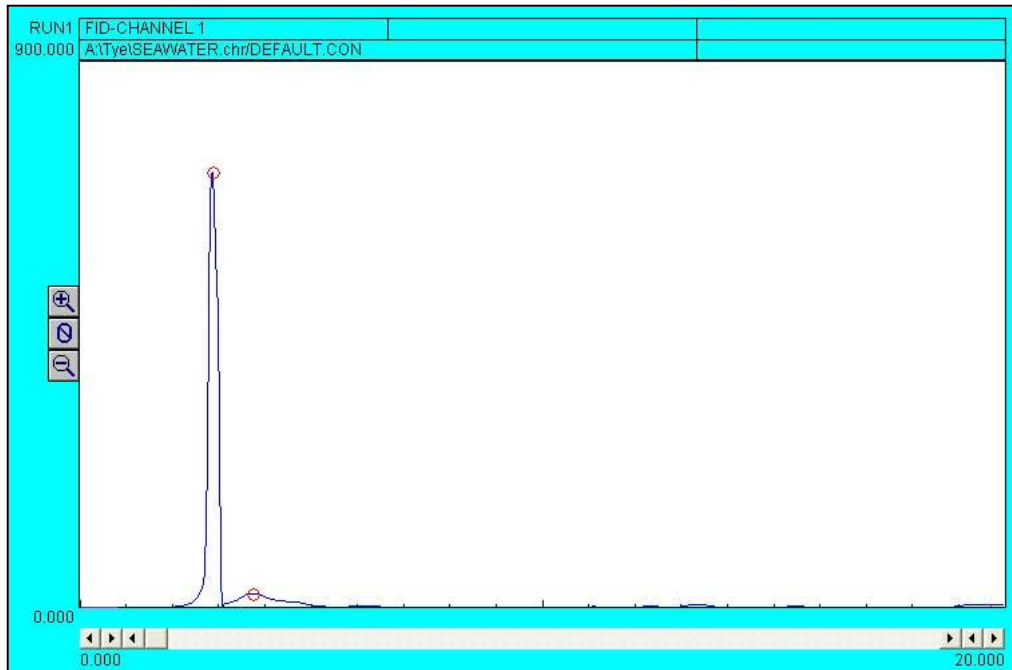


Figure 24 – HPLC result for seawater

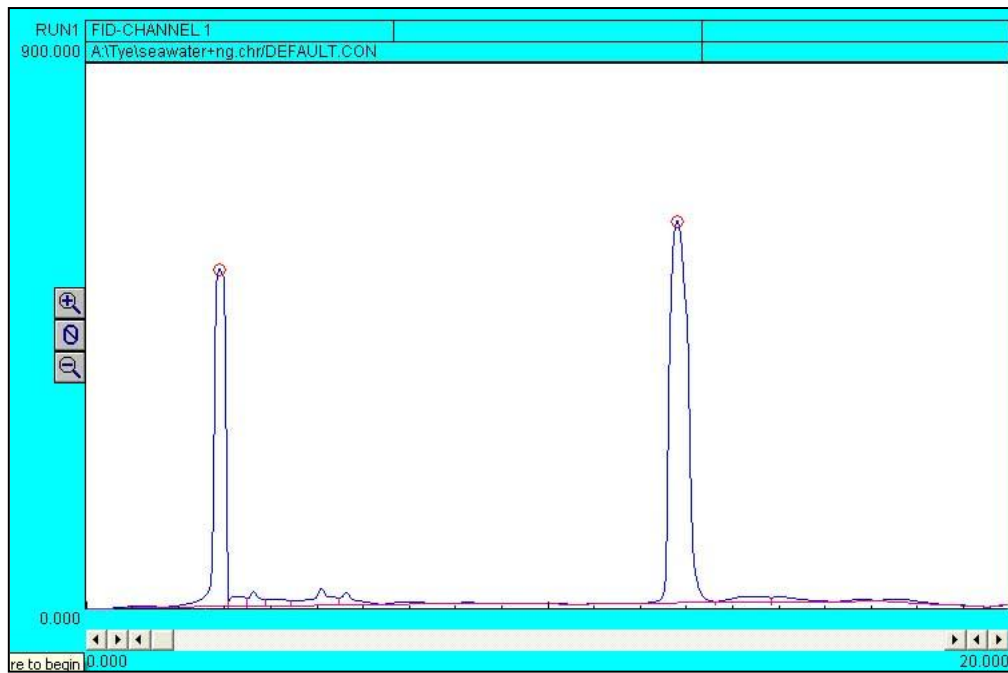


Figure 25 – HPLC result for seawater and nitroglycerin tablets

#### 4.3.3 Do explosive traces persist in seawater and freshwater?

To search for explosive traces in water and seawater solutions, it is important to know if the explosive traces survive those conditions. Explosive traces can be mechanically removed from water, consumed by microbes, modified, or decomposed by light. A study by Kamyshny et al. examined a related question<sup>33</sup>. In their study, they questioned how long explosive traces on a downed airplane would last in water and seawater. They analyzed the persistence of TNT, RDX, Semtex, and PETN traces that were adhered to typical airplane materials, including seat fabric, aluminum, glass and polyethylene. Refer to Figures 26 and 27 for the results obtained by Kamyshny et al. in tap water and seawater, respectively. It should be noted that these are “Group B” explosives, which are directly applicable to this thesis. While adhered explosive traces are not of interest for this thesis, the results do provide value by indicating that explosive traces can survive in both water and seawater solutions for significant amounts of time. It was found that adhered explosive traces were detectable through colorimetric methods up to 9 months after immersion in tap water and 5 months in seawater. The test method entailed drying the immersed material before colorimetric testing for explosive traces. The detectability duration depended on the explosive type as well as flow conditions. Since they tested for adhered traces, the shorter detectability time noted for flowing conditions most

likely indicates that the traces failed to adhere to the material, not that they broke down.

Based on the study by Kamyshny et al., it was concluded that there is significant reason to believe Group B explosive traces persist in both water and seawater. Thus, it is purposeful to develop a detection method for water-borne explosive traces.

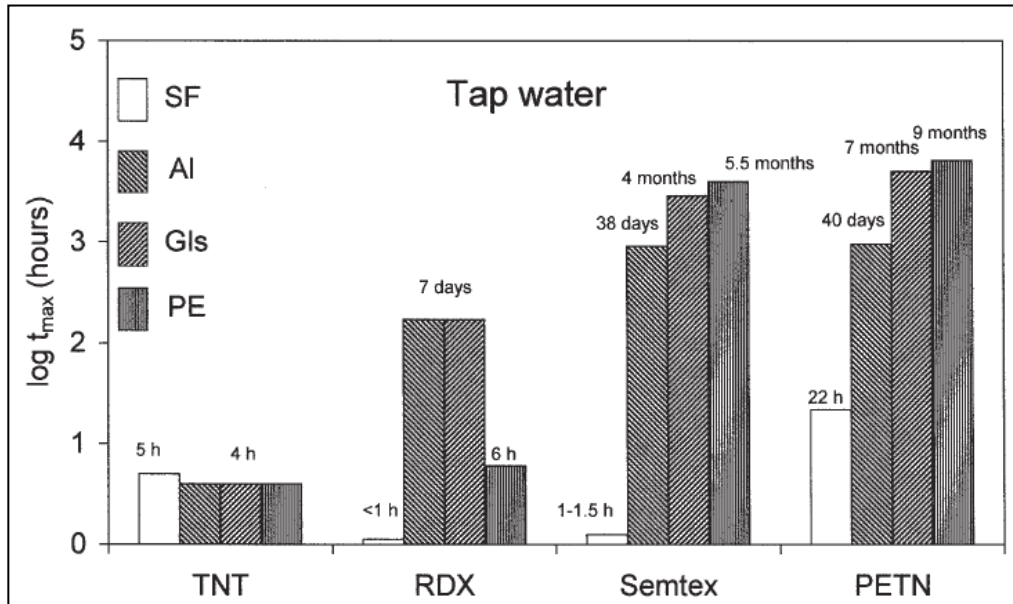


Figure 26 –Detectability of explosives after soaking in tap water, based on the material to which the explosive was adhered (SF – Seat Fabric, Al – Aluminum, Gls – Glass, PE – Polyethylene)<sup>33</sup>

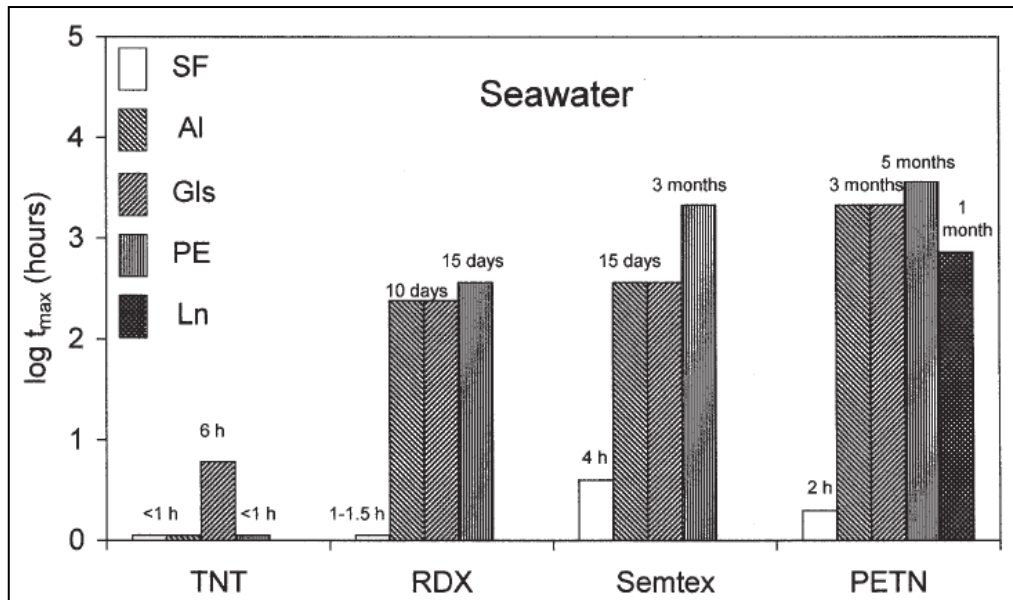


Figure 27 –Detectability of explosives after soaking in seawater, based on the material to which the explosive was adhered (SF – Seat Fabric, Al – Aluminum, Gls – Glass, PE – Polyethylene)<sup>33</sup>



## 4.4 Experimental Techniques and Procedures

### 4.4.1 Chemical Preparation

Before conducting fluorescence analysis, the nitroglycerin solution and europium complexes were prepared. The nitroglycerin solution was prepared by first dissolving the correct amount of nitroglycerin tablets in water or seawater to achieve a desired concentration. Then the nitroglycerin solution was filtered to remove the remaining solid matter from the tablet (the tablets would not completely dissolve in water). 0.45  $\mu\text{m}$  Teflon filters were used for the luminescence spectrometer tests, but 5  $\mu\text{m}$  filters were used for the field-deployable fluorometer testing. The filter size was increased because it became impractical to filter such large amounts of seawater with the fine 0.45  $\mu\text{m}$  filter. Teflon was chosen as the filter material to reduce the risk of adherence of the nitroglycerin molecules to the filter.

The fluorescent europium complexes were prepared by mixing the europium(III) chloride hexahydrate with the sensitizing ligand crystals (thenoyltrifluoroacetone and/or 1,10-phenanthroline monohydrate) in high-grade methanol. Methanol was used instead of water because methanol is an inert solvent that does not react with the europium ion to quench its fluorescence, as water will. It is important to successfully form the sensitized europium compound before the introduction of water. To create the Eu/TTA compound, TTA in methanol was added to europium in methanol. To create the Eu/TTA/OP compound, TTA in methanol was first added to europium and methanol. After

waiting for 20 minutes, OP in methanol was added to the Eu/TTA solution. The Eu/OP/TTA compound was made in the same way as the Eu/TTA/OP compound, except that the order of adding the OP and TTA solutions was reversed.

The europium ion has ninefold coordination, meaning that it tends to accept nine bonds. TTA and OP are both bidentate ligands<sup>3</sup>. Since the bidentate ligands occupy two bonding sites each, it takes only four ligands to fill the available sites of the europium ion (one site is left unbonded). The remaining site is probably not filled by one ligand branch due to steric hindrance from the surrounding, bonded ligands<sup>19</sup>. Ideally, the europium:Ligand ratio would be 1:4, but excess ligand was included to assure full coordination. Previous experiments have applied a Eu:TTA:OP ratio of 1:3:3 to assure the fullest possible europium coordination and the presence of at least one OP ligand per complex<sup>2</sup>. The presence of the OP ligand aids in obtaining good water quenching of complex that doesn't react with explosive traces<sup>3</sup>. This study has applied the same ratio, based on the same logic. This ratio also represents the smallest increase in ligand quantity over the ideal ratio that maintains an equal amount of the two ligands. When the OP ligand was excluded, a 1:5 Eu/TTA ratio was used. It is assumed that the excess ligands do not significantly affect the results because they do not exhibit strong fluorescence in the emission wavelength of interest.

Finally, to form the explosive and europium complex solution, the nitroglycerin / water solution was combined with the europium complex / methanol solution.

#### 4.4.2 Practical Solubility Limit Determinations

The less methanol in the final analysis solution, the better from many standpoints. If the europium / methanol solution is highly concentrated, an UUV would be required to carry less overall volume of the solution to deliver the correct amount of europium complex into a seawater sample for analysis. Additionally, large percentages of methanol in the overall solution were found to adversely affect the solubility of nitroglycerin and seawater components. It is believed that this is due to the fact that methanol is much less polar than water and may allow dissolved ions to combine into insoluble salts. Also, less methanol translates into less waste generation during operation.

In order to determine the minimum amount of methanol required, it is necessary to determine the solubility limits of the different europium complexes in methanol. Accurate solubility limit curves require attention to temperature and chemical kinetics<sup>39</sup>, which is very time consuming and beyond the goals of this thesis. The aim of this experiment is not to produce a highly accurate solubility curve for the involved chemicals, but to establish a rough baseline of the quantity of each compound that could be dissolved in methanol for mixing purposes. Thus, temperature was not altered from room temperature and the waiting period for dissolving was relatively short in comparison to rigorous solubility determinations. Following reference 40, solubility limits were determined by starting with a saturated solution and adding solvent in .25 ml increments until all of the europium complex remained in solution. Solubility was determined by

visual examination, and a waiting period of 20 minutes was allowed before concluding that a solution was completely dissolved.

#### 4.4.3 Handheld UV Testing

Before beginning time-consuming luminescence spectrometer analysis, several samples of different europium compounds in different mixtures were analyzed with the handheld UV light. The purpose of this effort was to generally identify the fluorescent behavior of the different compounds and mixtures. This helped to efficiently determine which compounds are fluorescent, what concentrations are required, which compounds and concentrations are responsive to NG, which compounds and concentrations are quenched by water, and how other additives such as calcium and acid affect the compounds. The handheld UV light provided a quick, hands-on feel for rapidly evaluating different samples. The handheld UV light outputs energy at 370 nm wavelength, which is within the excitation range of TTA.

#### 4.4.4 Excitation and Emission Wavelengths for Analysis

Before testing could begin, excitation and emission wavelengths had to be determined. To make this determination, two important questions needed to be answered. First, can a standard LED be used for excitation? If the optimum excitation wavelength was near a standard LED wavelength, the LED wavelength was chosen for field practicality. Second, does the addition of the various compounds to the europium ion shift its emission wavelength?

The expected emission wavelength of europium (613 nm) was already known<sup>3,4</sup>. With that information, it was possible to use the luminescence spectrometer to find the optimal excitation wavelength to achieve the highest intensity of the europium 613 nm emission for each particular compound. This was done by setting the luminescence spectrometer to receive emission light at only 613 nm, while programming it to scan through a range of excitation wavelengths. If the optimum excitation wavelength was determined to be close to 370 nm, 370 nm was chosen as the excitation wavelength to excite the compound thereafter. 370 nm was preferred because it is an achievable UV wavelength via LED light sources and can be implemented in an UUV package.

After establishing 370 nm as an acceptable excitation wavelength, each compound was tested for emission to determine if the characteristic europium emission wavelength (613 nm) had been shifted by the addition of the other chemicals and solvents. If the peak emission of the compound remained at 613

nm, it was concluded that the addition of the other components did not shift the characteristic emission wavelength of the europium.

#### 4.4.5 Luminescence Spectrometer Background Fluorescence Analyses

To fully evaluate the fluorescent signature obtained from a given sample including the europium complex, the background signature of the solvent must be ascertained. Comparing to the background permits the evaluation of the change in fluorescence that occurred.

Background fluorescence analysis was conducted in the luminescence spectrometer for the cuvette only, distilled water, seawater, methanol, a nitroglycerin / seawater mixture, and five percent methanol / seawater mixtures with and without nitroglycerin. The same excitation light wavelength was used as in the europium complex testing (370 nm).

When examining fluorescence data of various europium mixtures, the background profiles were subtracted to emphasize the fluorescence behavior of interest.

#### 4.4.6 Luminescence Spectrometer Europium Complex Comparisons

Europium was chosen for its known fluorescent behavior and its tendency to lose its fluorescence when exposed to water. TTA and OP were chosen as sensitizing ligands, based on their prior, successful use as sensitizers to europium<sup>2</sup>. The question remains: Which of these ligands (or both) work best with europium for the purpose of this thesis, and in which orders should they be combined? This question concerns both retained fluorescence in the presence of explosives and lost fluorescence without explosives and in the presence of water. Additionally, the question of optimal concentration needed to be answered.

The compounds; Eu/TTA, Eu/TTA/OP and Eu/OP/TTA were evaluated through a range of concentrations to determine which one, at what concentration, provides the largest difference in emitted light intensity between explosive-laden and non-explosive-laden solutions. Eu/OP was not evaluated, because preliminary investigations with the handheld UV light indicated that it did not produce fluorescence when excited with 370 nm UV light. This is corroborated by the reported excitation wavelength range required for the excitation of the OP ligand (less than 300 nm)<sup>18</sup>.

After establishing the appropriate excitation and emission wavelengths, each compound was mixed in seawater solutions with and without nitroglycerin. The overall europium complex concentrations in the seawater samples ranged from  $10^{-4}$  M to  $10^{-6}$  M. These concentrations were based on preliminary investigations into the sensitivity of the luminescence spectrometer. If the

concentration was too high, the emitted light intensity saturated the spectrometer, and if the concentration was too low, the spectrometer didn't detect it.

Additionally, the nitroglycerin concentration was maintained at  $10^{-3}$  M, which was chosen based on successful testing with the handheld UV light.

#### 4.4.7 Luminescence Spectrometer Solvent Investigation: Methanol / Water Ratio

During preliminary investigations with the handheld UV lamp, it was observed that the amount of methanol in the total solution affected both the clarity of the solution and the observed fluorescence. As mentioned above, methanol (or another inert solvent) is required to deliver the europium complex into the seawater solution, because it won't cause fluorescence quenching of the europium compound like water will. Maximizing the fluorescence output of the europium compounds is important for obvious reasons and achieving a clear solution is important to reduce light scattering so that a precise fluorescence level can be ascertained. Methanol is relatively nonpolar and appears to be easily displaced from the europium ion by water and nitroglycerin as long as there is not too much of it. Further studies may indicate that the europium compound can be delivered in water, but that would mean that an explosive trace would have to first displace a water molecule before bonding to the europium compound. At this time, it is unknown whether explosive traces can actually displace bonded water molecules or if they just get to the europium compound first. For this reason, the europium



complex was not delivered in methanol, versus water in the experiments described herein.

For the methanol / water ratio experiment, a particular europium compound was chosen based on good performance in the “Europium Complex Comparisons” section (4.4.6). Then the percentage of methanol in the total analysis solution was varied, while the europium complex and nitroglycerin concentrations were kept constant. Nitroglycerin-containing solutions were compared to nitroglycerin-absent solutions for each methanol percentage to illustrate the explosive-detecting ability of each methanol / seawater ratio.

In addition to fluorescence analysis, photography was utilized as a method of illustrating the effect of methanol in the solutions. For each different methanol percentage, a photograph was taken of both the nitroglycerin and non-nitroglycerin solutions. These photographs help illustrate the effect of methanol on the clarity of the analysis solutions.

#### 4.4.8 Luminescence Spectrometer Nitroglycerin Concentration Investigations

One of the goals of this thesis is to determine the detection limit of explosive compounds with a field-deployable device, not the detection limit of explosive compounds in a sensitive laboratory device. However, laboratory nitroglycerin detection limit investigations were conducted for information and to provide insight into the behavior of the detection method when nitroglycerin concentrations are altered.

For this experiment, a specific europium compound, concentration and methanol percent were chosen based on good results from the “Europium Complex Comparisons” and “Methanol / Water Ratio” experiments described above (sections 4.4.6 and 4.4.7, respectively). Then fluorescence data was recorded through a range of nitroglycerin concentrations, while the europium complex concentration and overall methanol percent remained constant. The fluorescence data was compared to an identical solution without nitroglycerin as a baseline.

#### 4.4.9 Luminescence Spectrometer Non-Ideal Excitation Wavelength Verification

As noted previously, there is a discrepancy between the perfect excitation wavelength for europium and the light wavelength provided by common off-the-shelf LED's. Off-the-shelf LED's come in pre-defined increments. While possible to combine LED's and filters to obtain the exact, optimum excitation wavelength for europium, it is not necessary nor practical to do so if the nearest off-the-shelf LED wavelength will suffice.

To evaluate how much performance is lost through the use of a standard LED, two tests were conducted. First, the luminescence spectrometer was used to identify the optimum excitation wavelength to produce the highest intensity 613nm fluorescence. Keep in mind that it had already been determined that none of the compounds used shifted the europium fluorescence wavelength away from 613 nm. After identifying the optimum excitation wavelength, an analysis was

conducted using this wavelength that was similar to those in the “Europium Complex Comparisons” section. Then the results obtained with 370nm excitation were compared with those obtained with the optimum excitation wavelength to determine how much, if any, performance was lost by not using the exact excitation wavelength.

#### 4.4.10 Luminescence Spectrometer Water vs. Seawater Investigation

There are many constituents of seawater that may or may not play a role in the reaction that takes place among the europium compound, explosive, and water. They may hinder, boost, or play a neutral role in the detection of explosive traces. To determine the overall effect of the many seawater constituents, tests were conducted in freshwater for comparison. Distilled water was used and the testing parameters used were chosen to match the optimum seawater results already obtained. Through the previous seawater testing, a specific europium complex, excitation wavelength, and methanol/water ratio was chosen as favorable and extended to the freshwater testing.

Since a difference was found between the detection method performance in fresh water and seawater, experiments were conducted in an acidic solution and in a calcium-rich solution. These tests were performed, not to quantify the effects of acid and calcium, but to help explain the water, seawater difference and confirm that the acid and metal ion effects described by others<sup>12,15,20,21</sup> can be extended to this underwater detection method.

For these tests, distilled water solutions of sodium chloride (NaCl), calcium chloride (CaCl<sub>2</sub>), and hydrochloric acid (HCl) were prepared. Because all of these salts included chloride, the concentrations were adjusted to keep chloride constant through all of the solutions. This method was to eliminate the chloride ion as a variable. The overall amounts used were based on the typical chloride concentration in the ocean. Reference 35 notes that there is 19.35 grams of chloride ion per each kg of seawater. Accounting for the mass of chloride (35.45 g/mol), this translates into a concentration of 0.55 M of sodium chloride. Because HCl also contains only one chloride ion, the concentration of HCl used was identical at 0.55 M. CaCl<sub>2</sub>, however, contains two chloride ions per compound, so its concentration was halved to maintain chloride ion consistency. This ratio resulted in a 0.27 M CaCl<sub>2</sub> concentration.

#### 4.4.11 Deployable Detector Performance Characterization

The custom-designed fluorometer differs in sensitivity from the laboratory luminescence spectrometer. Thus, it was necessary to determine the fluorometer's particular nitroglycerin detection ability. This testing was performed by plugging one end of the fluorometer and filling it with the appropriate amounts of solutions. A flow-through configuration was not used in these tests because the supply of nitroglycerin and reagents was limited, and it is more difficult to assess problems when a flow-through system is used. The fluorometer was powered by a "battery eliminator" source, set to 9 volts, and the output was measured with a digital multimeter. The setup is shown in Figures 17 and 18.

The test procedure was as follows:

- 1) Add 1 ml of the seawater/ nitroglycerin solution to the open end of the fluorometer.
- 2) Add .64 ml of the europium complex / methanol solution to the fluorometer.
- 3) Vigorously fill the fluorometer with seawater / nitroglycerin solution by quickly injecting it with a syringe to conduce mixing of the solutions.
- 4) Cover the open end of the fluorometer to limit the intrusion of outside light.
- 5) Monitor the multimeter for 5 minutes to determine the voltage output from the fluorometer once the reagents have reacted.

- 6) Empty the fluorometer, rinse thoroughly with fresh water, and proceed to the next test.

#### 4.4.12 Deployable Detector Filtration Study

Turbidity measurements with a CTD were conducted to evaluate the turbidity conditions of port water (Port Everglades). This is pertinent because the CCST UUV's will be expected to operate in port environments. These measurements were brief and are not likely to encompass the full range of turbidity that may be encountered in port environments, but they do provide insight into what to expect. To fully evaluate port turbidity conditions, many factors must be considered, such as time of day, season, and weather. From these few measurements, it was found that port water is significantly more turbid than the open sea. Figure 28 shows the locations at which turbidity measurements were taken and Figure 29 shows the resulting turbidity profiles at each location, plotted from MATLAB. Each location's turbidity measurement includes a reading during the lowering and raising of the CTD.

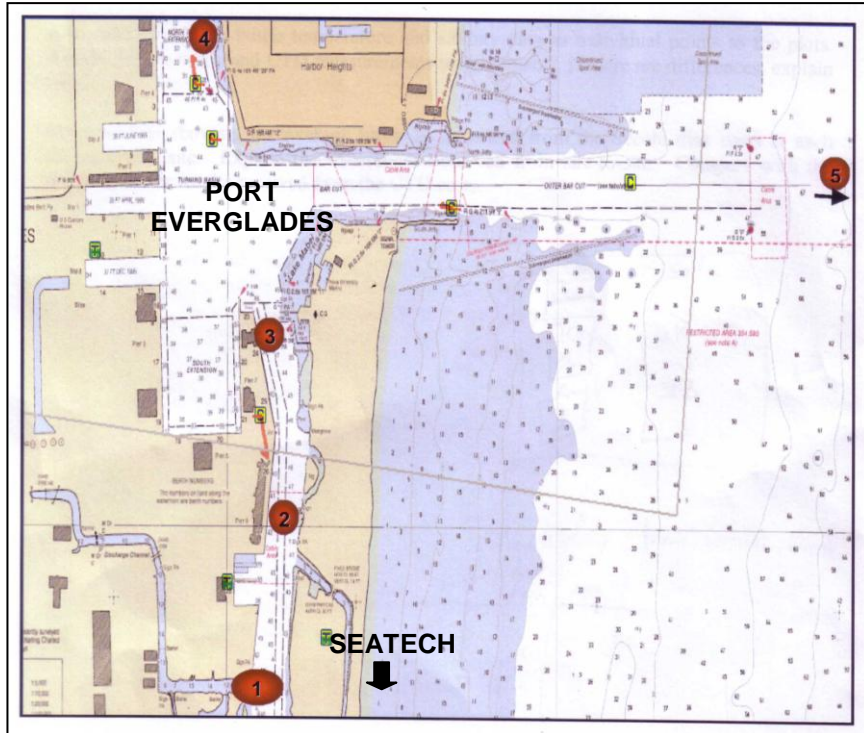


Figure 28 – Turbidity measurement locations

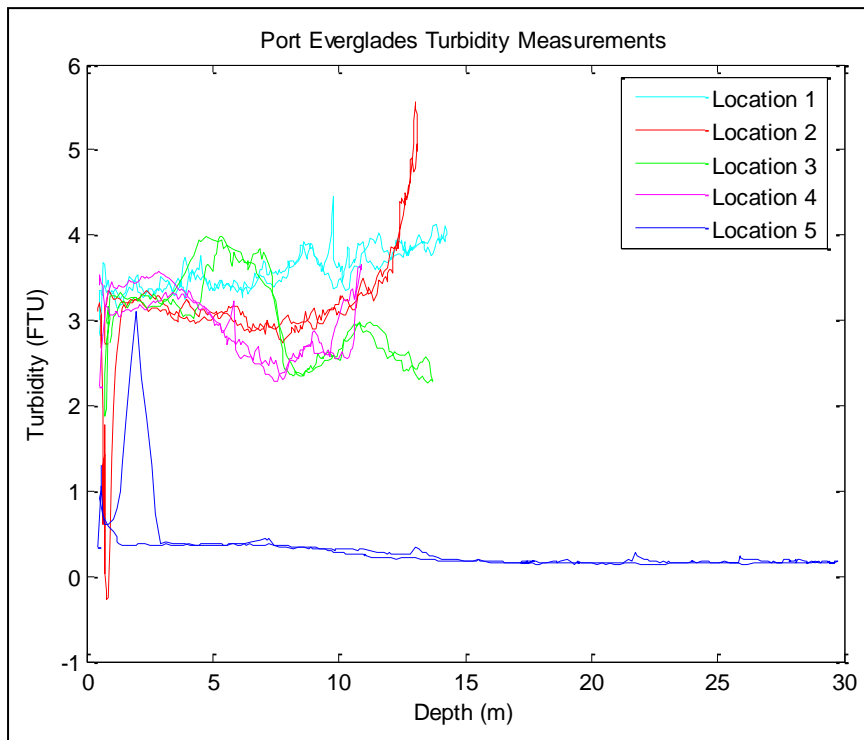


Figure 29 – Turbidity measurement results

Some degree of filtering will be required for the detection system. Water sample cleanliness could affect the fluorescence measurements as well as the pumps that may be used to ultimately supply the fluids to the detector in the field. To investigate the amount of filtering required, water was obtained from Port Everglades and individual samples were filtered with different filter retention sizes. Preliminary investigations indicated that pumps will likely require filtering in the 5  $\mu\text{m}$  range, so this was chosen as the upper end of the filtration range tested. Three filtration levels were tested; no filtering, 5  $\mu\text{m}$  and 0.45  $\mu\text{m}$  filtering. Unfortunately, the CTD that was used for the port turbidity studies was not available to check the turbidity of the water samples after filtration. Because of this, the effect of filtration size on the detector's performance can be evaluated, but no direct link between turbidity and filtration can be made.

#### 4.4.13 Proof of Design

After designing the chemical detection method and detector, a laboratory setup was used to prove that the design works in simulated field conditions. The laboratory setup has been described in section 4.2.6. The setup was adjusted to deliver the proper ratio of solutions under flow conditions that were reasonable for the equipment used.

To determine what qualified as reasonable flow conditions, the restrictor valve used to control the europium solution flowrate was closed until a minimal,



but constant, flowrate was achieved. Based on the methanol solution flowrate, the seawater flowrate was adjusted to provide an acceptable mixing ratio.

Once the appropriate flowrates had been achieved, measurements were taken with the fluorometer to analyze the following flows:

- Seawater
- Seawater + Eu/TTA in Methanol
- Nitroglycerin / Seawater + Eu/TTA in Methanol

The concentrations used in proof of concept testing were chosen based on the results of the deployable detector performance characterization tests.

## CHAPTER 5

### EXPERIMENTAL RESULTS AND DISCUSSION

#### 5.1 SOLUBILITY LIMIT RESULTS

Solubility limits were determined as described in section 4.4.2 for all three europium compounds and the results are tabulated below. It was found that the presence of OP in the compound significantly reduced the solubility. Since europium is ninefold coordinate (can accept 4 bidentate ligands), the Eu/TTA ratio of 1:5 was chosen to provide one extra TTA compound per europium ion. The excess ligand over the stoichiometric proportion was included to improve the likelihood that all of the europium ions were fully coordinated with TTA. The Eu/TTA/OP and Eu/OP/TTA ratio of 1:3:3 is the minimum ratio that will provide a ligand excess, while keeping the ligand ratios equal.

<b>Compound</b>	<b>Eu/TTA</b>	<b>Eu/TTA/OP</b>	<b>Eu/OP/TTA</b>
Mass of EuCl <sub>3</sub>	.01116 g	.01131 g	.01120 g
Mass of TTA	.03321 g	.02062 g	.02051 g
Mass of OP	-	.01672 g	.01641 g
Volume of Methanol	3 ml	6.75 ml	6.75 ml
Mixing Ratio	1:5	1:3:3	1:3:3
<b>Solubility Limit</b>	<b>1.02 x 10<sup>-2</sup> M</b>	<b>4.57 x 10<sup>-3</sup> M</b>	<b>4.53 x 10<sup>-3</sup> M</b>

Table 1 – Europium compound solubility results in methanol

## 5.2 LUMINESCENCE SPECTROMETER RESULTS

### 5.2.1 Excitation

The optimum excitation wavelength was found to be 382 nm (Figure 30). It was judged that this was close enough to the standard LED wavelength of 370 nm to continue with a 370 nm excitation for the experiments. To confirm that this decision was acceptable, a small group of particular tests was conducted at 382 nm excitation to evaluate the amount of performance lost by using a non-ideal excitation wavelength. This comparison is discussed in the “Luminescence Spectrometer Non-Ideal Excitation Wavelength Verification” section 4.4.9.

For practicality, a 370 nm excitation wavelength is preferred over 382 because it is available as a standard LED. LED’s that produce light nearer to the 382 nm goal are available, but they are likely outliers in the production process

that are just tested and sorted. These outliers are likely to be less intense light sources and it becomes more difficult to reproduce this wavelength if additional units or replacements are required<sup>34</sup>. Additionally, LED's produce light through a band of wavelengths, centered at a specific frequency. With this tolerance, the gap between 370 nm and 382 nm is reduced.

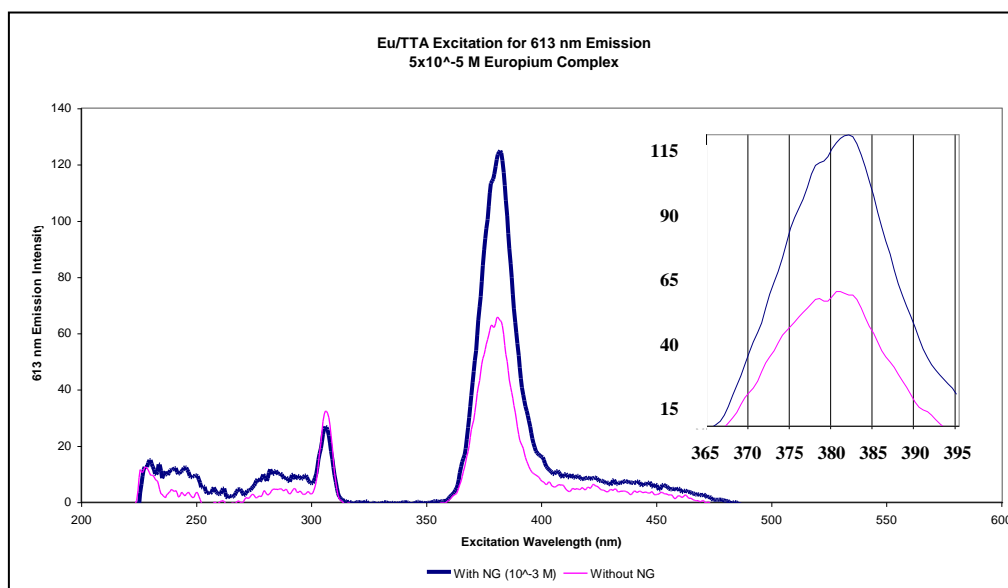


Figure 30 – Eu/TTA peak excitation when scanning for 613 nm emission, with and without nitroglycerin

Referring to Figures 31, 32 and 33, it is apparent that all of the compounds tested (Eu/TTA, Eu/TTA/OP and Eu/OP/TTA) are excited in the 382 nm range. It is assumed that this is due to their common TTA ligand, which absorbs in this range. Also notable, Eu/TTA/OP and Eu/OP/TTA are strongly excited near 310 nm, while Eu/TTA is not. This is apparently due to the ability of the OP ligand to absorb radiation in this far UV range and transfer it to the europium. This

observation differs slightly from that obtained elsewhere, where OP was observed to absorb primarily below 300nm<sup>18</sup>.

Another feature that can be ascertained from Figures 31, 32 and 33 is the quenching of Eu/TTA without nitroglycerin, and the lack thereof for the Eu/TTA/OP and Eu/OP/TTA compounds. Without nitroglycerin present, the Eu/TTA compound provides very little response to any of the excitation wavelengths applied, but Eu/TTA/OP and Eu/OP/TTA respond strongly to a range of excitation wavelengths whether nitroglycerin is present or not.

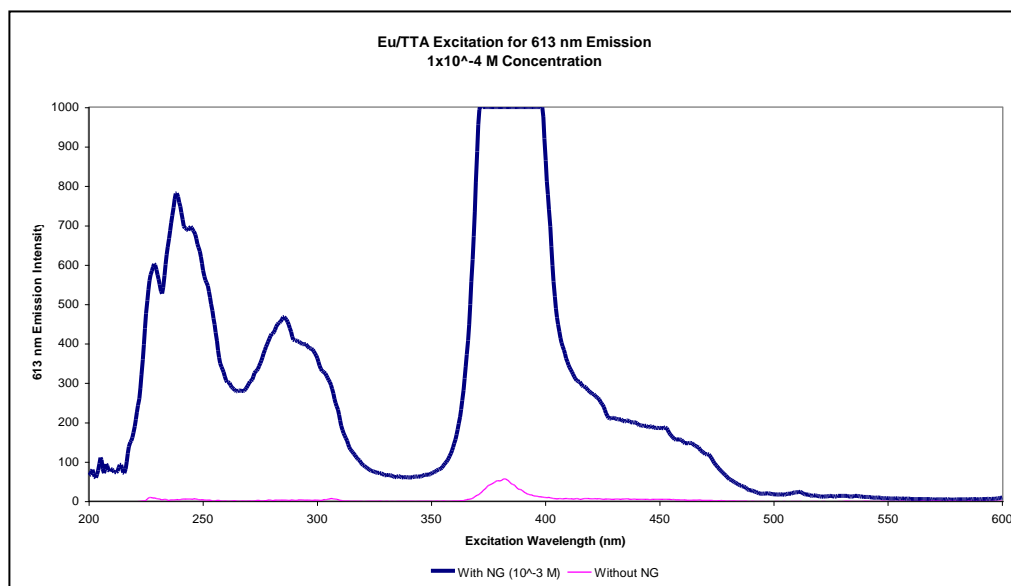


Figure 31 – Eu/TTA excitation when scanning for 613 nm emission, with and without nitroglycerin

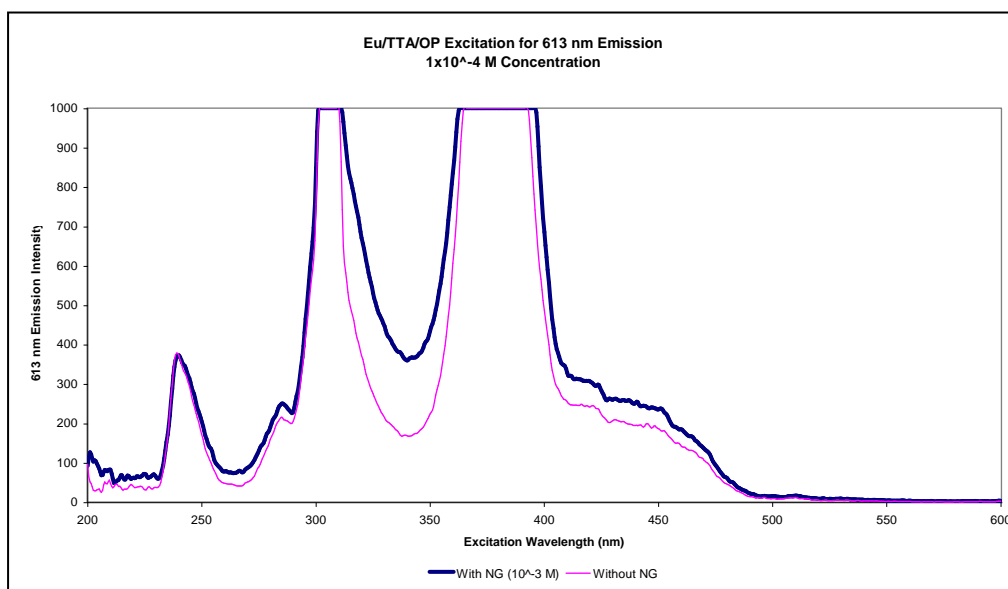


Figure 32 – Eu/TTA/OP excitation when scanning for 613 nm emission, with and without nitroglycerin

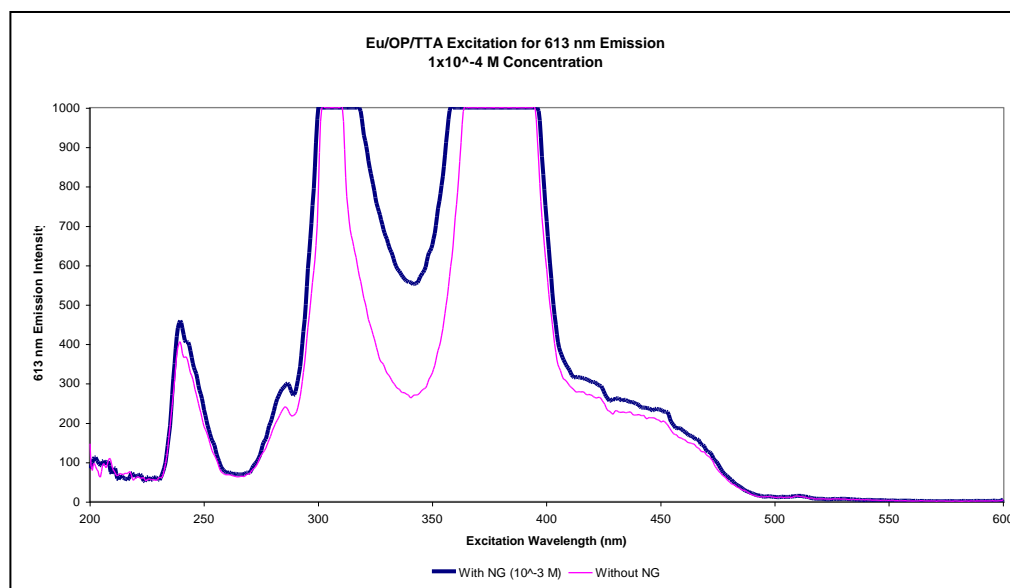


Figure 33 – Eu/OP/TTA excitation when scanning for 613 nm emission, with and without nitroglycerin

### 5.2.2 Emission

It is important to determine the characteristic wavelength of the explosive-laden compound so that it can be detected. Also of importance is knowing if the characteristic wavelength is prone to shifting with the addition of the other compounds involved in the reaction. In other words, will the emission always be the characteristic emission of europium (613 nm)?

Figures 34, 35 and 36 indicate that the emission wavelength for all three europium compounds remained consistent with the characteristic emission wavelength of europium alone (613 nm), regardless if nitroglycerin was present. Minimal, if any, shifting of the characteristic wavelength occurred with the addition of OP, TTA, nitroglycerin, methanol and seawater to the europium ion. In these figures, different europium compound concentrations were used to capture a peak that was visible, but didn't saturate the spectrometer.

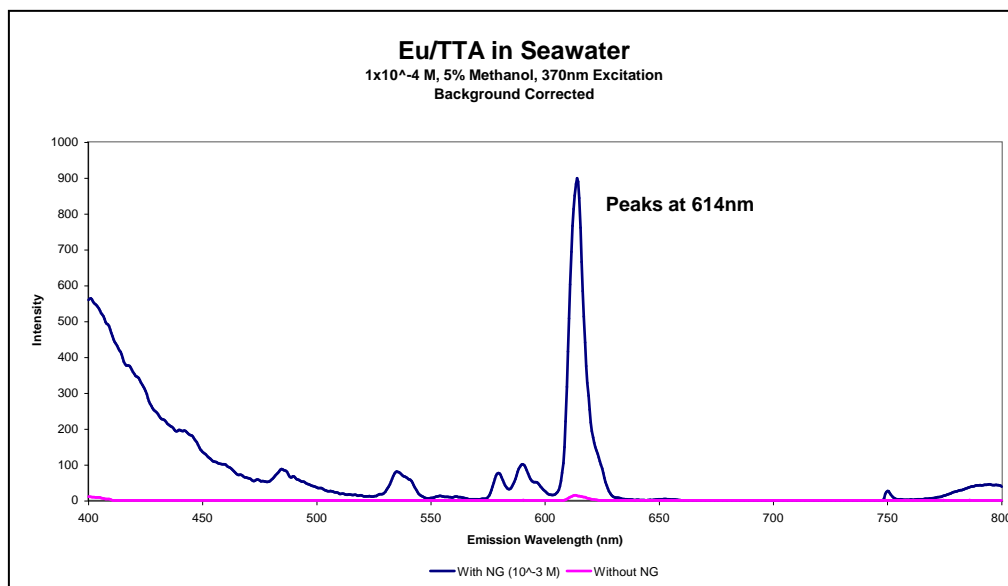


Figure 34 – Eu/TTA emission in seawater, excited at 370 nm

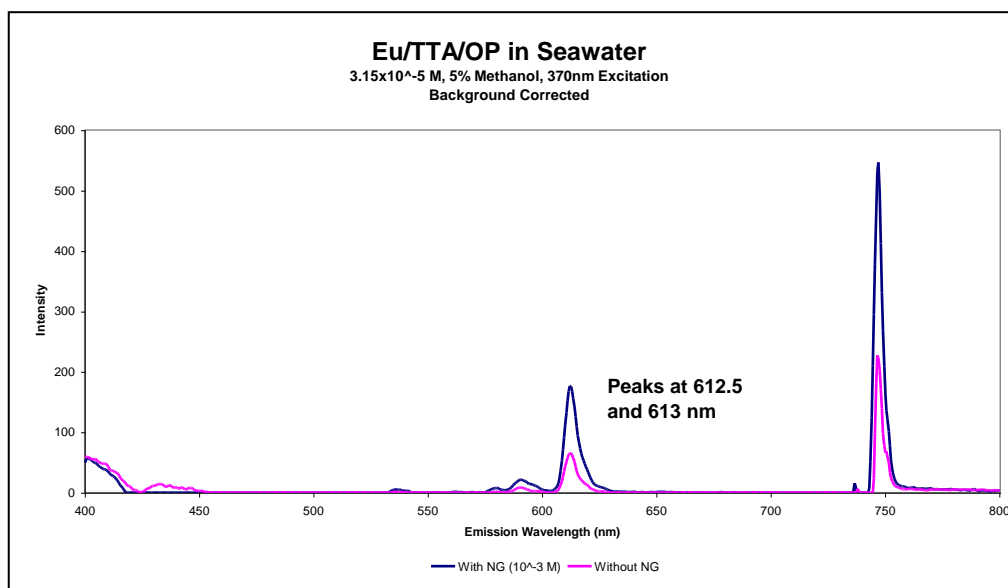


Figure 35 – Eu/TTA/OP emission in seawater, excited at 370 nm



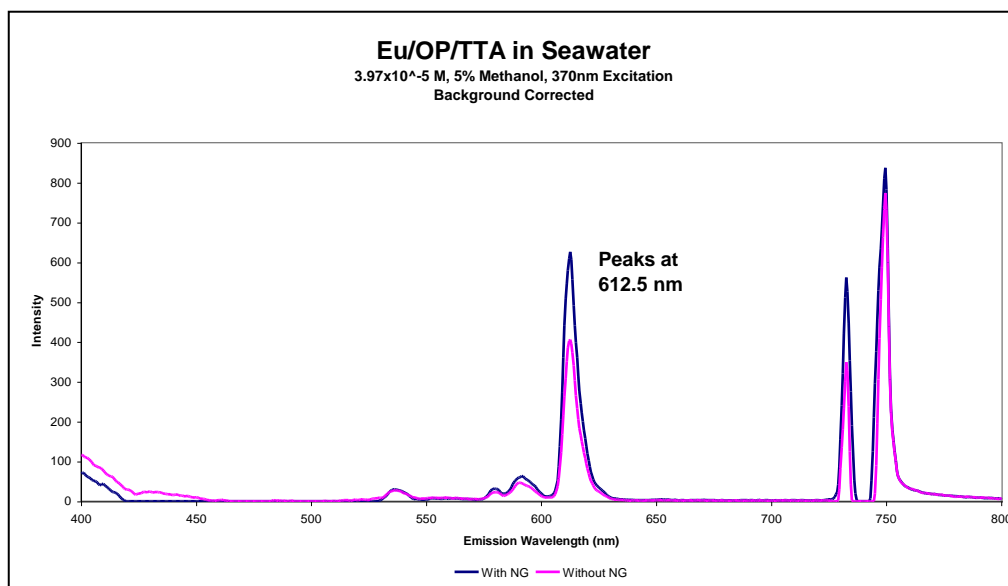


Figure 36 – Eu/OP/TTA emission in seawater, excited at 370 nm

### 5.2.3 Background

To clearly evaluate the changes in fluorescence due to the addition of nitroglycerin to a given solution, the background fluorescence profile for several solutions was acquired. These profiles are shown in Figures 37 through 43. To analyze luminescence spectrometer results, the appropriate background profile was first subtracted.

One of the most notable features, common to all of the background profiles shown, is the large peak centered around 740 nm. Since this peak shows up with the empty analysis cuvette, it was assumed that this peak results from the container and was ignored.

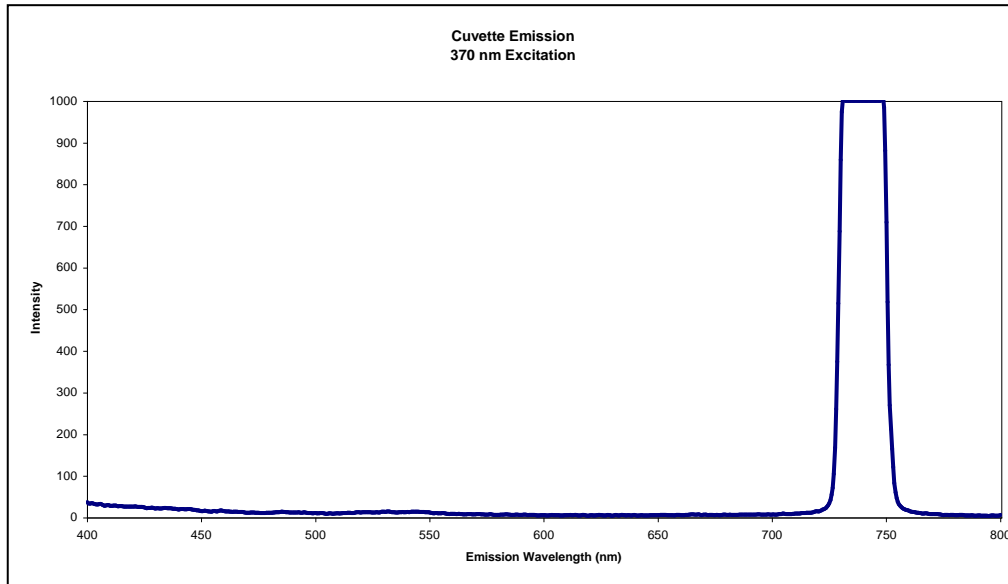


Figure 37 – Luminescence spectrometer cuvette emission, excited at 370 nm

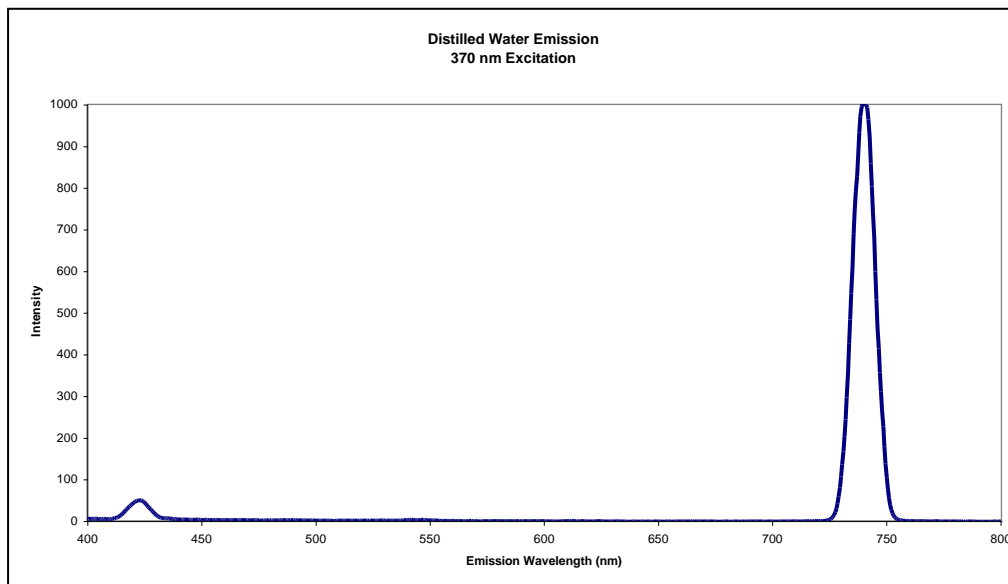


Figure 38 – Distilled water emission, excited at 370 nm

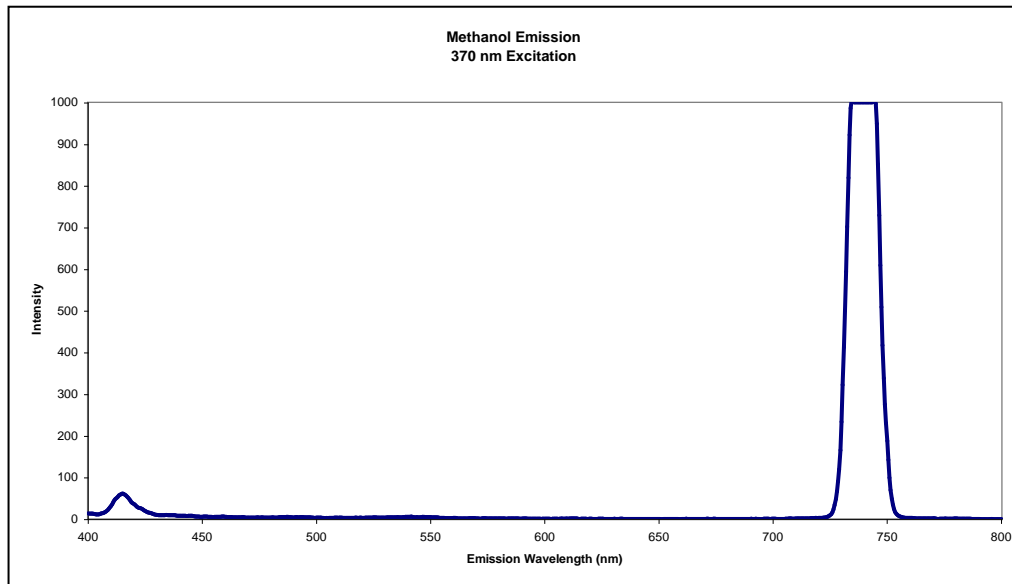


Figure 39 – Methanol emission, excited at 370 nm

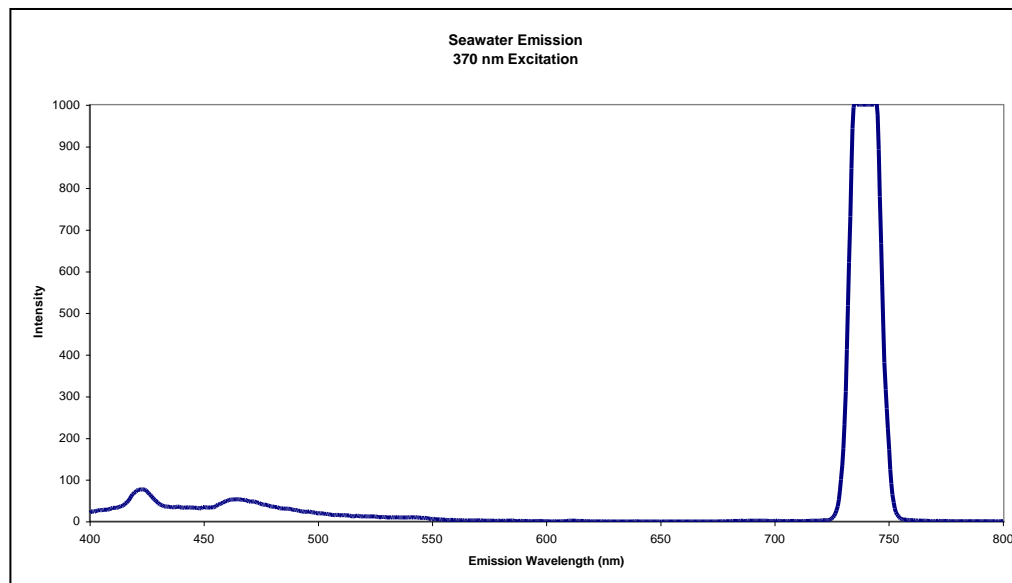


Figure 40 – Seawater emission, excited at 370 nm

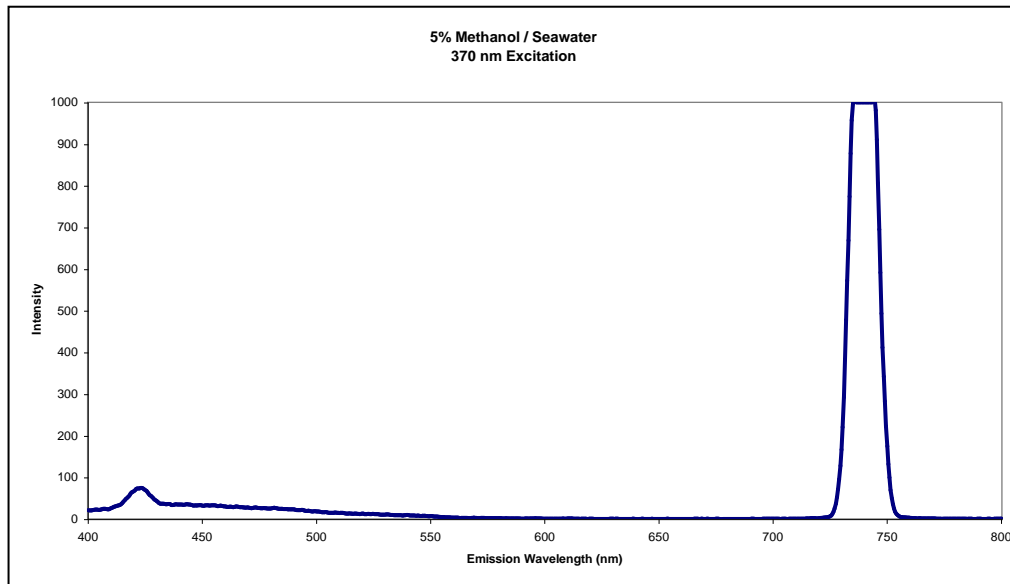


Figure 41 – 5% methanol / seawater solution emission, excited at 370 nm

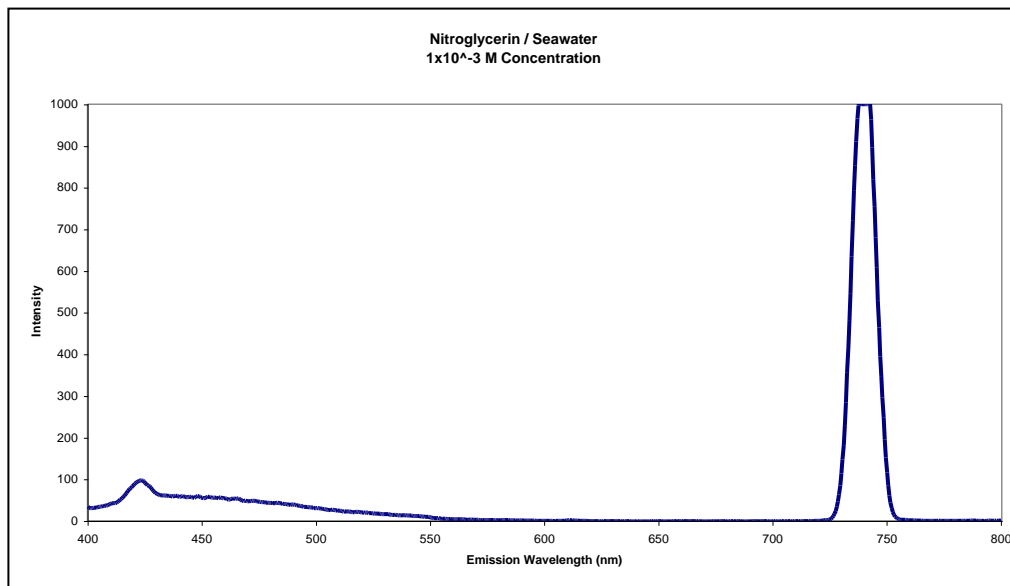


Figure 42 – Nitroglycerin and seawater emission, excited at 370 nm

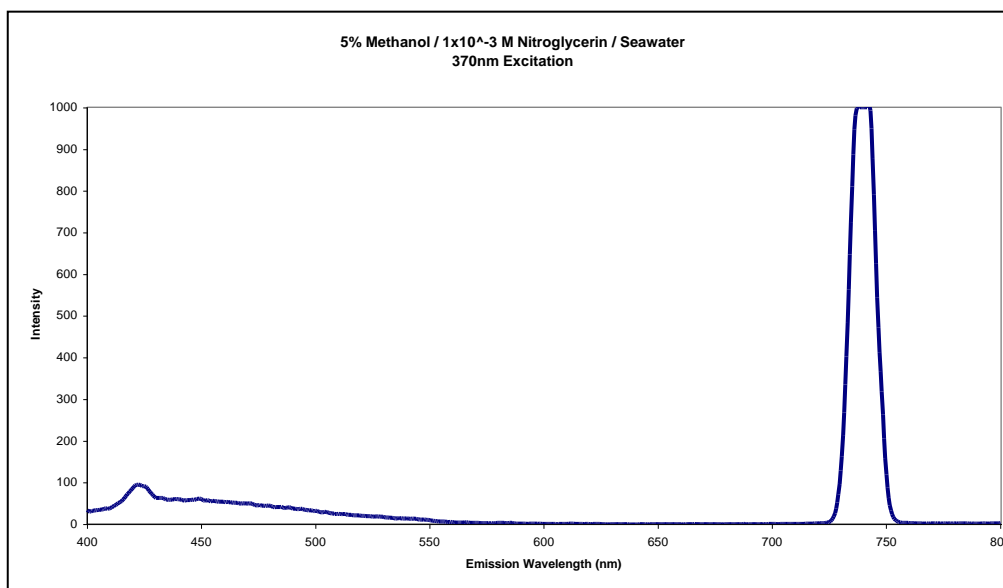


Figure 43 – 5% methanol /  $1 \times 10^{-3}$  M nitroglycerin / seawater solution emission, excited at 370 nm

#### 5.2.4 Luminescence Spectrometer Europium Complex Comparisons

Luminescence spectrometer testing as described in section 4.4.6 yielded the results shown in Figure 44. Upon review of Figure 44, it becomes obvious that there are only narrow ranges in Eu/OP/TTA and Eu/TTA/OP concentrations that fall within the luminescence spectrometer's detection limits. There is a quick jump from virtually undetectable fluorescence to too much fluorescence through a relatively small change in europium complex concentration. This sharp increase in intensity also occurs for the Eu/TTA compound in the presence of

nitroglycerin. However, the Eu/TTA solution without nitroglycerin did not fluoresce intensely at any concentration tested.

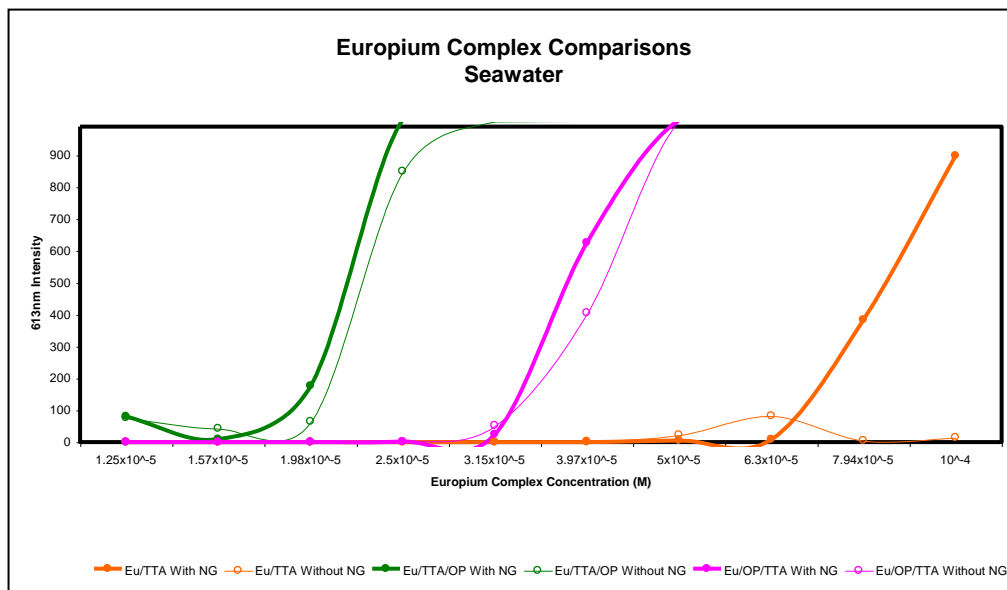


Figure 44 – Response of all three europium compounds in seawater, with and without nitroglycerin, excited at 370 nm

The purpose of this test was to identify the europium compound that provided the greatest fluorescence intensity difference between nitroglycerin-containing and nitroglycerin-absent solutions that are otherwise identical. All three compounds tested showed a difference between solutions with nitroglycerin (NG) and without NG, but Eu/TTA displayed the greatest difference. This is mostly because the Eu/TTA solution without NG never exhibited strong fluorescence. It is assumed that the Eu/TTA compound is more thoroughly quenched by water than the Eu/TTA/OP and Eu/OP/TTA compounds. Figure 45 illustrates the difference in intensity between NG-containing and NG-absent

solutions for all three compounds. The Eu/TTA solution provided a markedly larger difference in intensity than the other compounds.

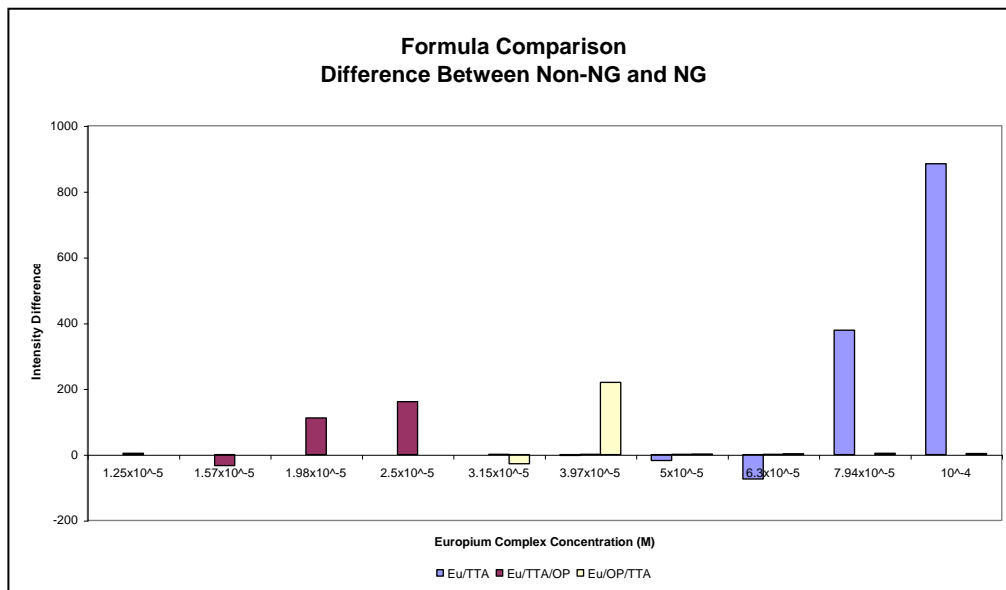


Figure 45 – Difference in intensity between nitroglycerin-laden and nitroglycerin-absent solutions for each europium compound. Excited at 370 nm.

An additional point of interest that this experiment brings to light is that each compound begins to intensify at a different concentration than the others. Eu/TTA/OP's fluorescence intensifies at the lowest concentration and Eu/TTA's fluorescence begins to intensify at the highest concentration. Because Eu/TTA/OP and Eu/OP/TTA show differences relating to concentrations, it can be assumed that the compounds behave differently even though they contain the exact same chemicals in the same ratios. Apparently, mixing order (reaction order) plays a role in the final compound.

While the compounds behaved as expected in that the NG-containing solution fluoresced more intensely than the NG-absent solution, there was a point for each compound at which the NG-absent solution fluoresced more intensely than the NG-containing solution. This anomaly was reversed when the compounds were excited with their exact excitation wavelength, vice the 370 nm used for the majority of the testing. See Figures 51, 52 and 53 for a comparison of the exact excitation wavelength (382 nm) versus the 370 nm excitation. To reiterate, the exact excitation wavelength was not used for luminescence spectrometer testing, because while this can be produced in the laboratory, only certain wavelength increments are likely to be available in the field at low cost. The excitation wavelength used (370 nm) happens to be an available LED wavelength, and it was anticipated that LED's would be the desired light source for the field-deployable detector. It is assumed that an LED with 370 nm peak output is close enough to the exact excitation wavelength of 382 nm to suffice, especially when considering that LED output will include a range of wavelengths surrounding the peak wavelength. A 370 nm LED is expected to have a half-peak range of 10-15 nm, meaning that the width of the excitation peak at one half of the maximum intensity will be 10-15 nm<sup>34</sup>.



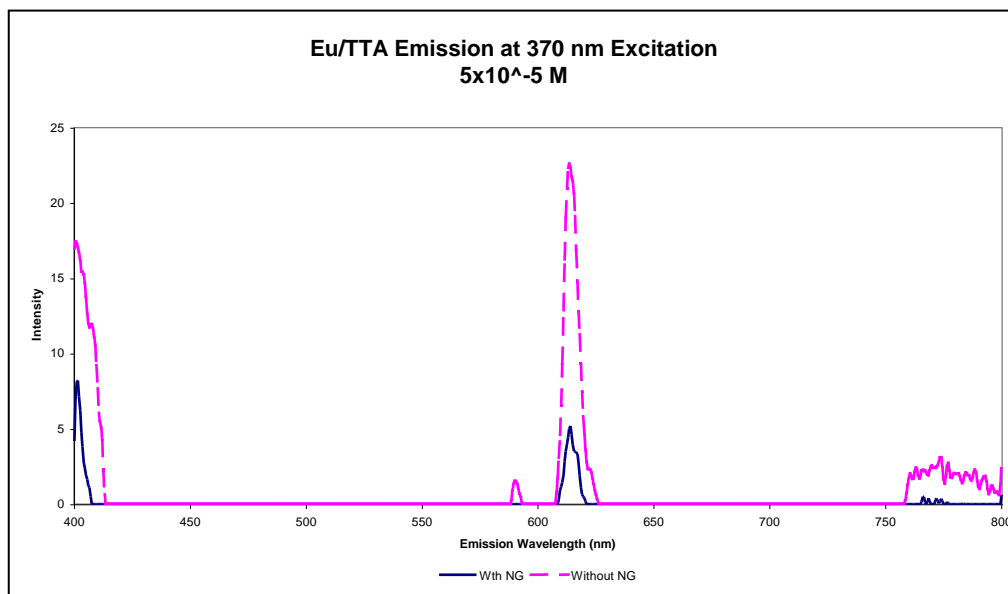


Figure 46 – Eu/TTA emission, excited at 370 nm, with and without nitroglycerin

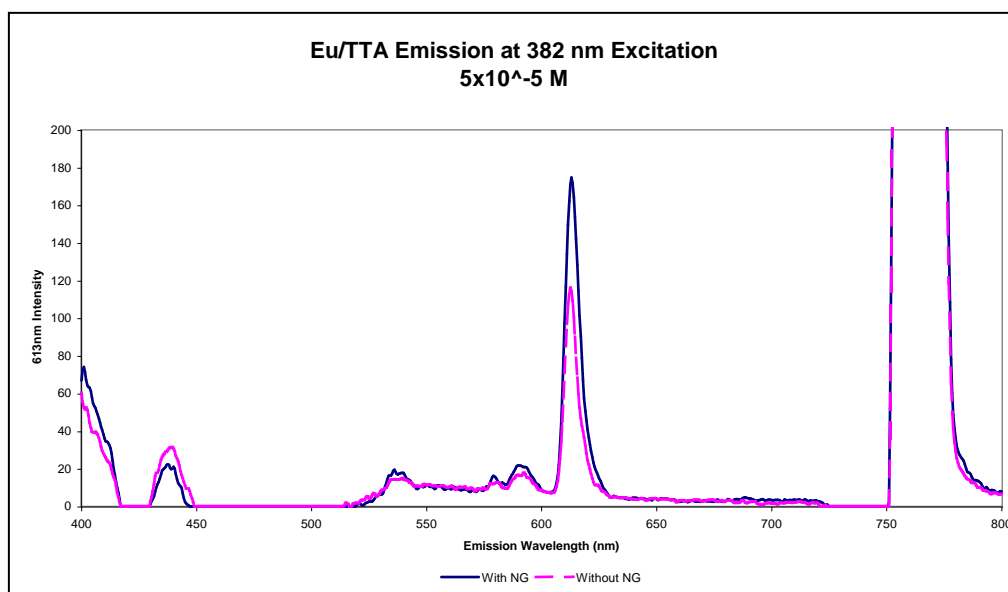


Figure 47 – Eu/TTA Emission, excited at 382 nm, with and without nitroglycerin

Figures 69 through 86 (Appendix A1-1) contain the complete luminescence spectrometer results for Eu/TTA, Eu/TTA/OP and Eu/OP/TTA, with and without nitroglycerin, under 370 nm excitation. Figures 87 through 93 (Appendix A1-2) contain the luminescence spectrometer results for Eu/TTA with and without nitroglycerin, under 382 nm excitation.

#### 5.2.5 Solvent Investigation: Methanol / Seawater Ratio

The amount of methanol used to deliver the europium compound into the seawater solutions was found to affect both the clarity of the solution and the resulting fluorescence output.

Methanol effect studies were conducted for the Eu/TTA compound only, based on the results of the “Luminescence Spectrometer Europium Complex Comparisons” section (5.2.4), which indicated that Eu/TTA is the most promising compound to use for the purposes of this thesis. Figure 48 shows the resulting fluorescence levels for explosive-laden and non-explosive solutions, when the percentage of methanol is varied. Figure 48 shows that too much methanol can adversely affect the ability to detect nitroglycerin. All of the luminescence spectrometer fluorescence profiles for this experiment are attached in Appendix A1-3, Figures 94 through 102.

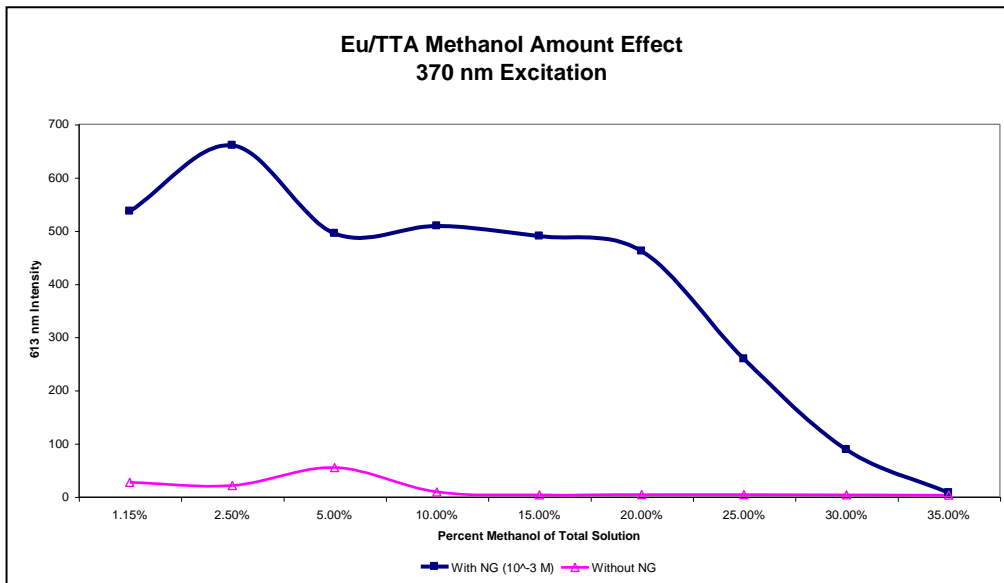


Figure 48 – 613 nm fluorescence intensity as a function of solution methanol percentage.

Additionally, it was found that there was a general reduction of clarity with an increase in methanol percentage when nitroglycerin was present. When there was no nitroglycerin, methanol only slightly affected the clarity. It is possible that high methanol content drives the nitroglycerin to collect together, instead of dispersing. Grouping of the nitroglycerin would also explain the loss of nitroglycerin detecting ability with increased methanol percentage. Solution clarity is important to measuring fluorescence, because cloudy solutions can result in light scattering, which affects the precision of the fluorescence measurement. Figure 49 shows the variation of clarity with methanol percentage in both nitroglycerin-containing and non-nitroglycerin solutions.

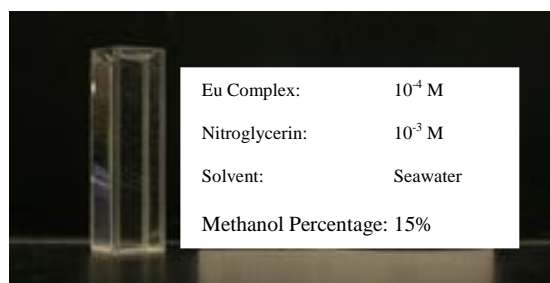
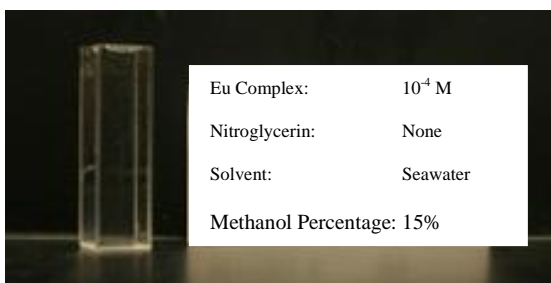
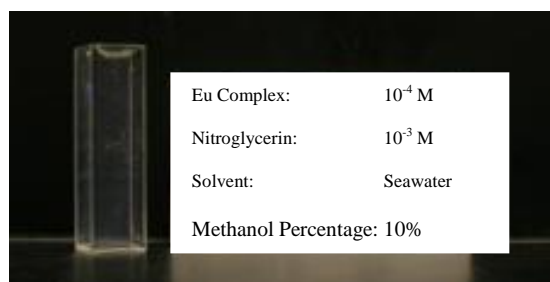
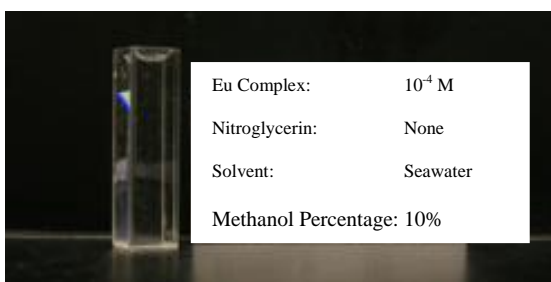
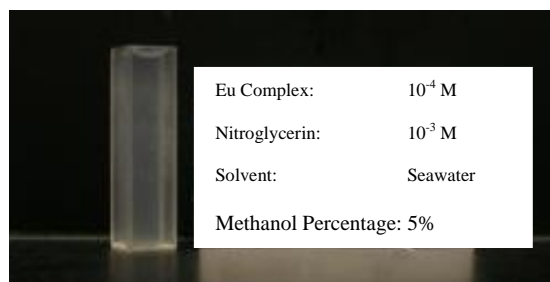
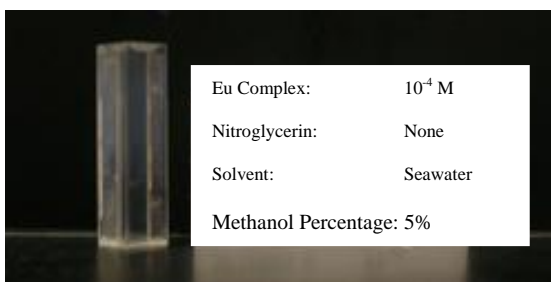
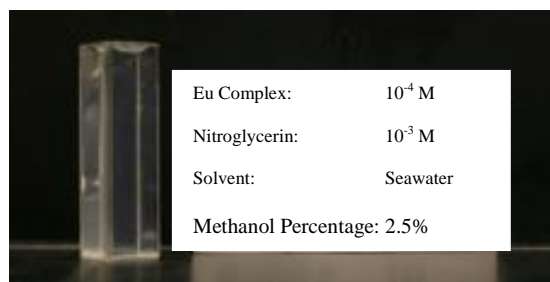
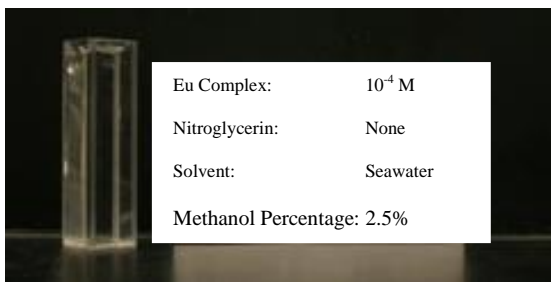
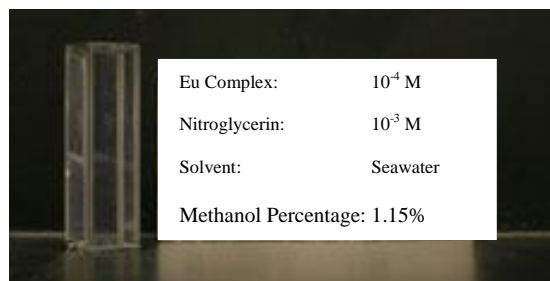
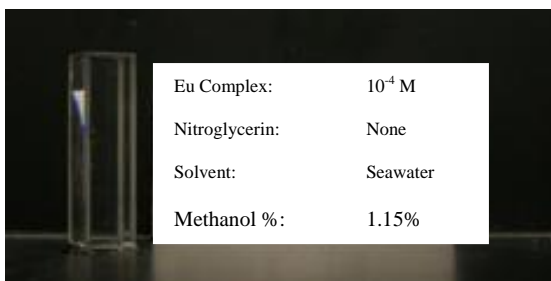


Figure 49, Part 1 – Solution clarities with varying amounts of methanol

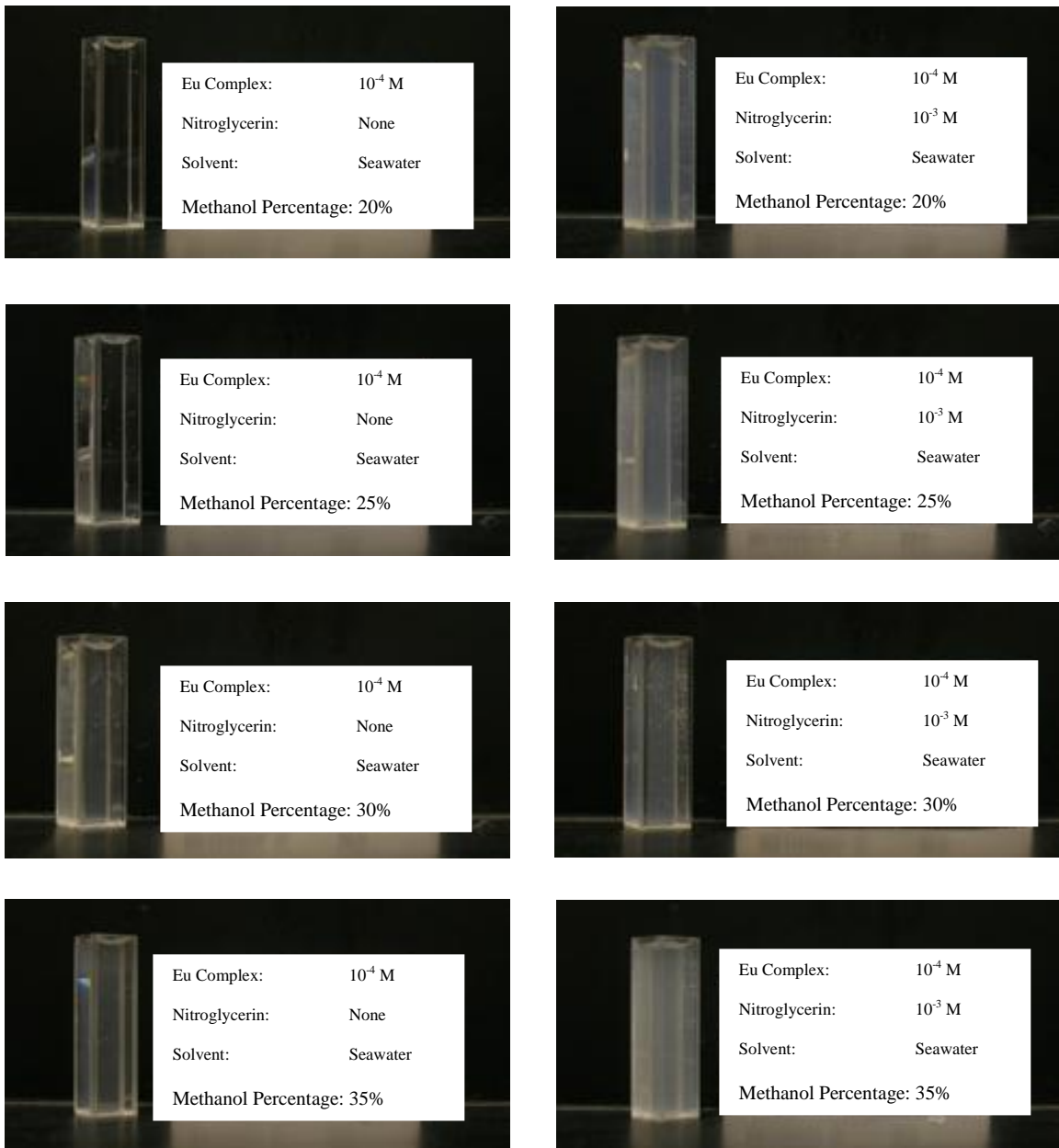


Figure 49, Part 2 – Solution clarities with varying amounts of methanol

## 5.2.6 Luminescence Spectrometer Nitroglycerin Concentration Investigations

The luminescence spectrometer provided a sensitive method of determining the limits of the detection method when the nitroglycerin concentration was gradually reduced. This is not directly related to the detection limits of the field-deployable detector because their sensitivities differ, but the luminescence spectrometer testing provided both insight into the behavior of the detection scheme and a starting point in the later determination of the field device detection limits. Figure 50 shows the fluorescence intensity derived from solutions with varying nitroglycerin content. Review of Figure 50 suggests that this method can identify nitroglycerin in solutions as diluted as approximately  $4.88 \times 10^{-7}$  M (approximately 56 ppb). At higher nitroglycerin concentrations, the emission intensity was found to be somewhat erratic. It is believed that this is because there is a reaction speed factor that must be considered at higher concentrations. It was found during the deployable detector tests, that the fluorescence output at high concentrations oscillates in intensity for a significant time period before stabilizing. Appendix A1-4, Figures 103 through 121, contains all of the luminescence spectrometer runs contributing to Figure 50.

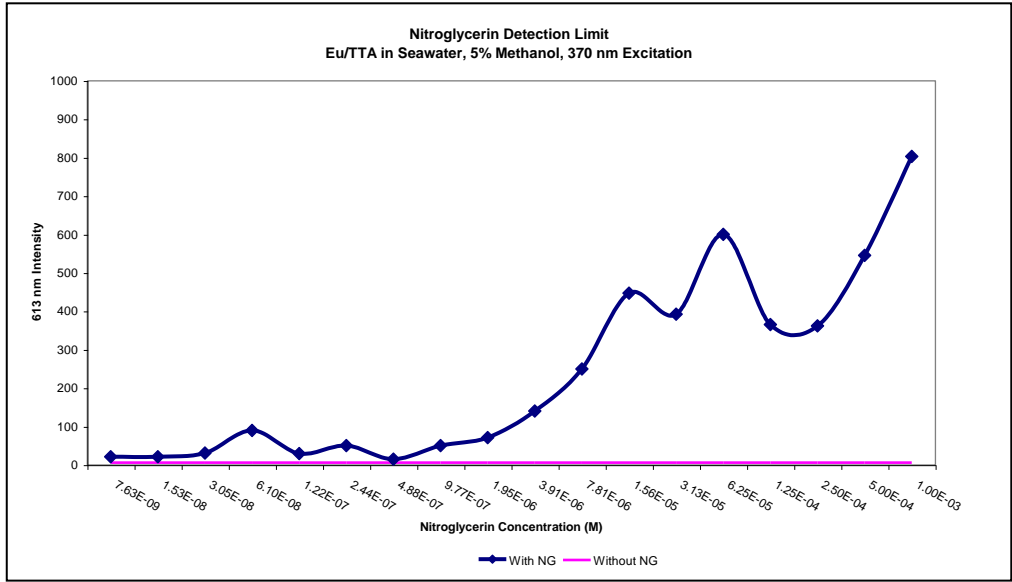


Figure 50 – 613 nm intensity as a function of nitroglycerin concentration

5.2.7 Non-Ideal Excitation Wavelength Verification

As mentioned earlier, testing was not conducted with what was found to be the optimum excitation wavelength for the various europium compounds. Instead, a standard LED wavelength that was close to the optimum excitation wavelength was used. Because of this compromise, it is pertinent to investigate how much performance is sacrificed. Figure 51 displays the results obtained at the standard LED wavelength (370 nm) and Figure 52 shows those obtained at the exact excitation wavelength (382 nm). Figure 53 compares results from both wavelengths. There is some, but minimal, performance loss with the standard LED wavelength. Furthermore, the luminescence spectrometer is capable of very

narrowband excitation, but the LED's that will be used in the field unit have a much larger tolerance. Thus, due to wavelength peak width, the gap between 370 nm and 382 nm is reduced, as well as the difference in explosive detection performance between the two.

Additionally, as discussed earlier, use of the non-ideal excitation wavelength caused an anomaly at  $5 \times 10^{-5}$  and  $6.3 \times 10^{-5}$  molar concentrations, in which the explosive-laden solution output less fluorescence than the non-explosive solution. This can be observed in Figure 51. As can be seen in Figure 52, this doesn't occur with the exact excitation wavelength.

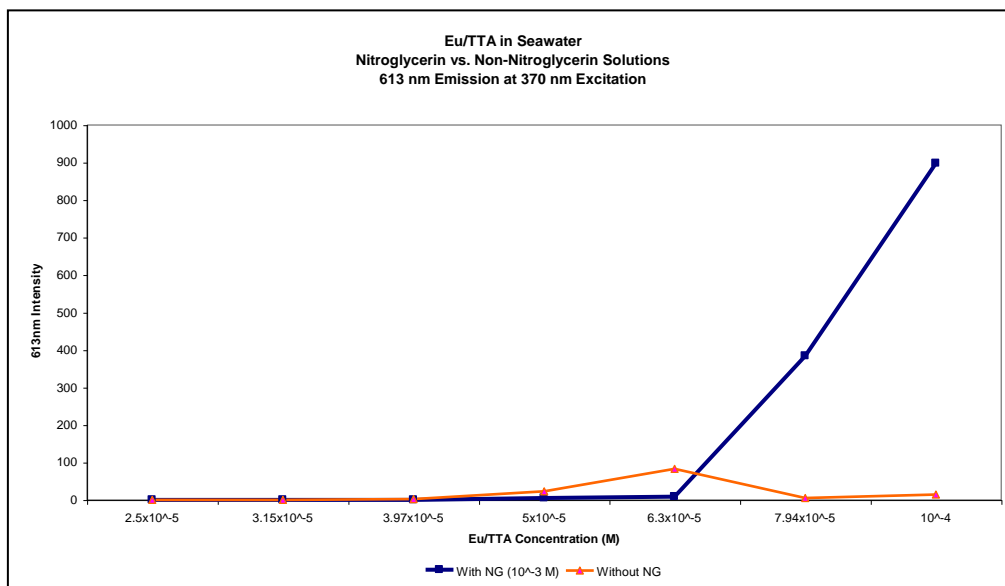


Figure 51 – Eu/TTA 613 nm emission, 370 nm excitation, with and without nitroglycerin



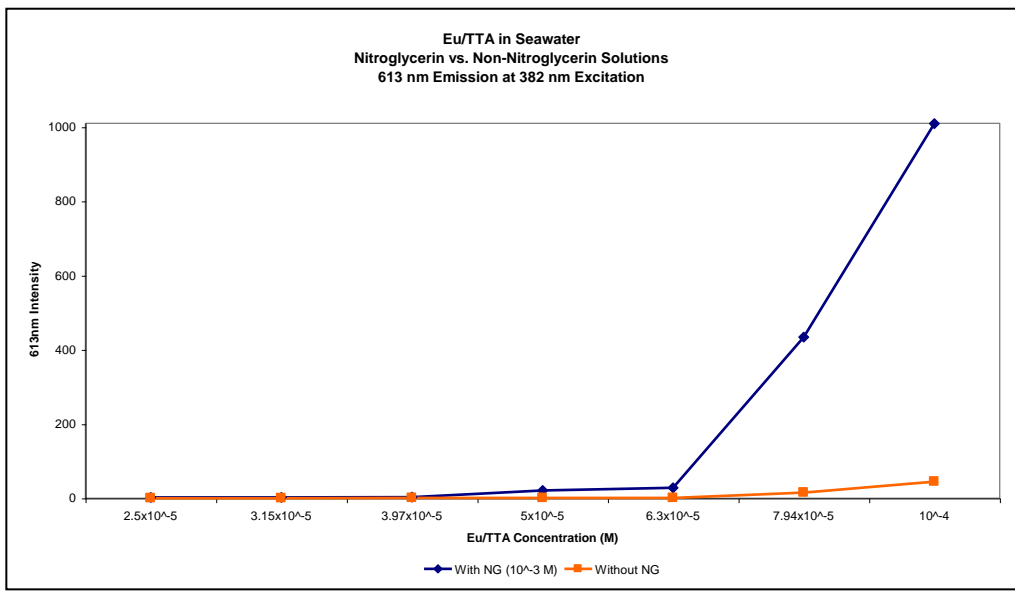


Figure 52 – Eu/TTA 613 nm emission, 382 nm excitation, with and without nitroglycerin

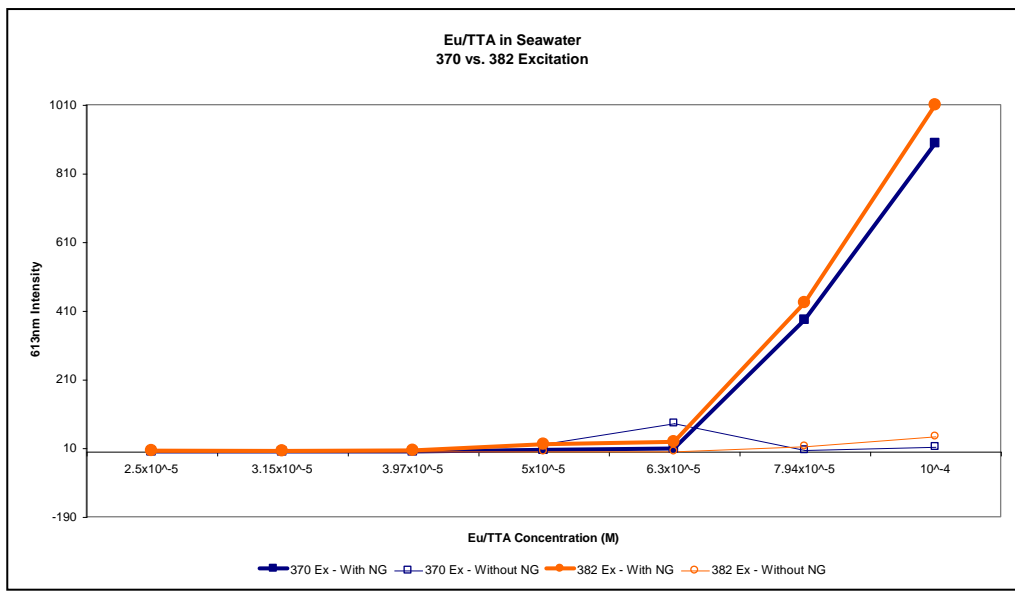


Figure 53 – Eu/TTA 613 nm emission, 370 nm and 382 nm excitation, with and without nitroglycerin

## 5.2.8 Water vs. Seawater

It was found that the detection method performed better in water than it did in seawater. Nitroglycerin could be identified by fluorescence at a lower europium complex concentration in water, down to approximately  $5 \times 10^{-6}$  M. Additionally, in seawater, the change from minimal fluorescence to great fluorescence of an explosive-laden solution occurred over a short range in europium complex concentration. In freshwater, this change occurred over a wider concentration range that began at a much more dilute level. These comparisons can be viewed in Figures 54 and 55.

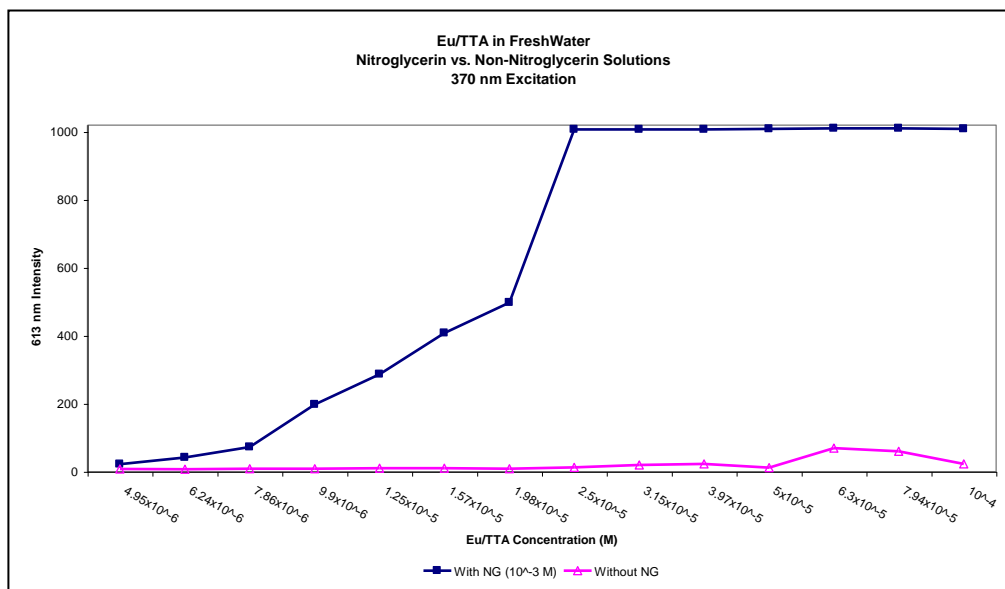


Figure 54 – Fresh water Eu/TTA 613 nm emission, 370 nm excitation, with and without nitroglycerin

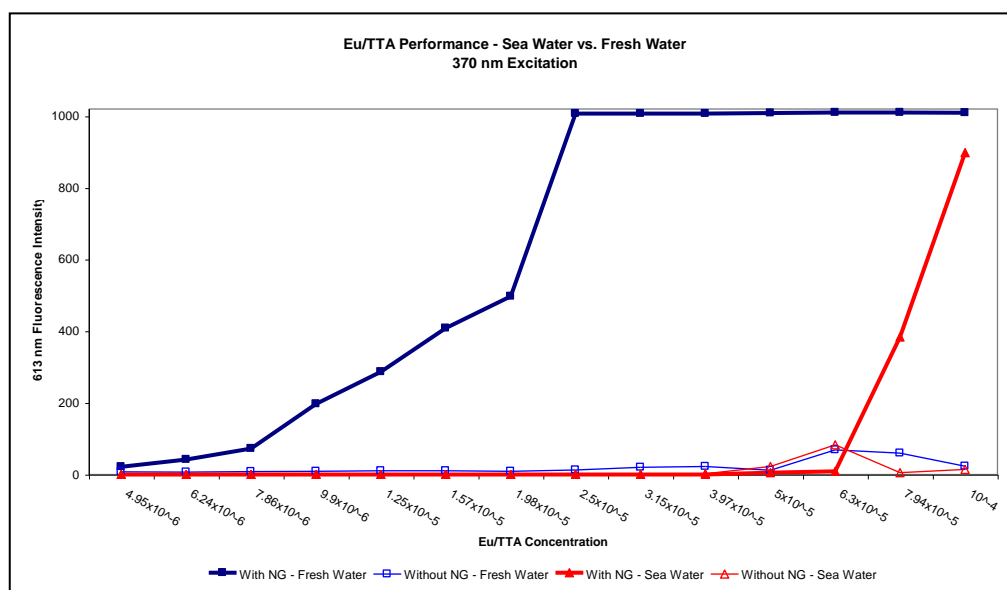


Figure 55 – Fresh water and seawater Eu/TTA 613 nm emission, 370 nm excitation, with and without nitroglycerin

These results indicate that there are components in seawater that adversely affect the detection method, at least at lower europium complex concentrations. As mentioned before, low pH and the presence of additional metal ions has been reported to negatively affect the fluorescence of lanthanide complexes<sup>12,15,20,21</sup>. The pH effect has been noted to occur at pH lower than 4 or 5<sup>12,20,21</sup>, which is out of the range of seawater pH at 7.5-8.4<sup>22</sup>. Despite this, a test was performed to confirm the potential effect of low pH on the Eu/TTA compound with nitroglycerin.

Alkaline earth metal ions have been reported to support metal-exchange reactions with the lanthanide ions, leaving lanthanide ions lacking ligands and prone to water quenching. This effect has been specifically noted to occur with

Calcium, but Magnesium is another member of this group that can be found in seawater<sup>35</sup>. To investigate this effect, a test to verify the calcium effect on the Eu/TTA compound was also performed.

These tests were not performed to quantify the effects of calcium and acid on the Eu/TTA method, but to prove that these effects, which have been found in other studies, do extend to this detection method. These effects were not completely quantified for this case because the calcium content, magnesium content and pH of seawater are not expected to vary considerably from that used for experimentation.

As discussed in section 4.4.10, these tests were conducted in distilled water solutions of NaCl, CaCl<sub>2</sub>, and HCl. The concentrations were calculated to match the chloride ion concentration with that from the ocean and to maintain it as constant across all three solutions. This eliminated chloride as a variable across the solutions. The only drawback of maintaining the chloride ion constant was that the concentration of the calcium ion was half of that of the sodium and hydrogen ions. Despite this irregularity, the results proved meaningful. Figure 56 indicates that both calcium and hydrogen ions strongly quench the Eu/TTA – nitroglycerin fluorescence in comparison with sodium ions.

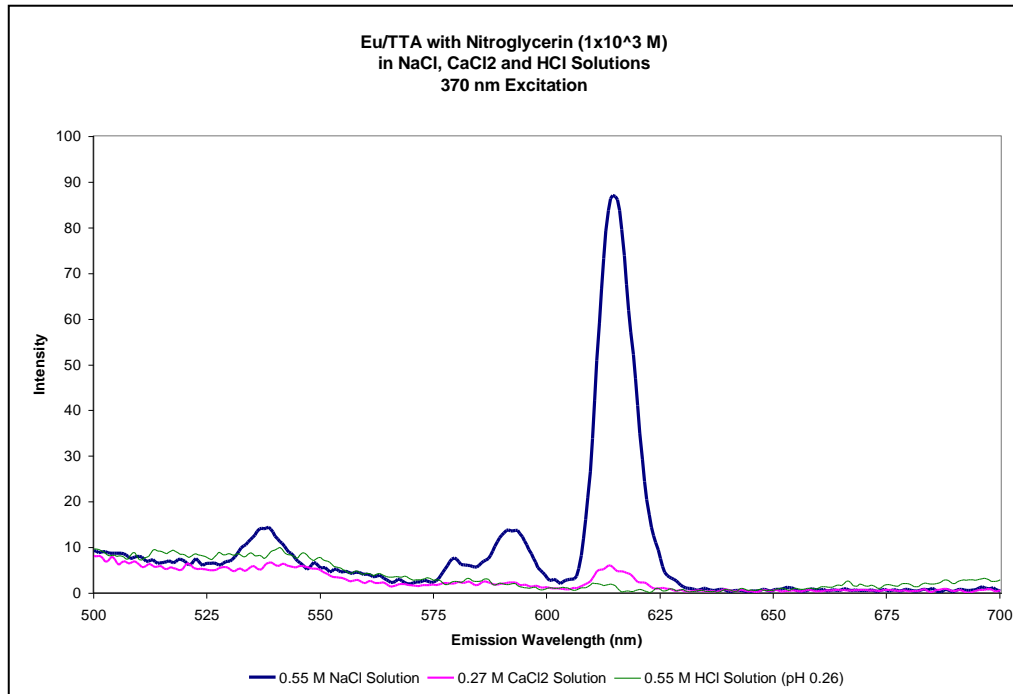


Figure 56 – Eu/TTA emission in the presence of sodium, calcium and hydrogen ions, 370 nm excitation, with nitroglycerin

### 5.3 FIELD-DEPLOYABLE DETECTOR RESULTS

#### 5.3.1 Deployable Detector Performance Characterization

The deployable detector was evaluated with a range of Eu/TTA concentrations and was found to be sensitive to nitroglycerin in seawater. However, there was a set of results that identifies a likely flaw in the detector that must be avoided. The detectability of nitroglycerin improved with increasing Eu/TTA concentration, until a point was reached where the fluorometer was saturated and reported that solutions with nitroglycerin produced less intense

fluorescence than solutions without nitroglycerin. This behavior is in contradiction to the results obtained with the luminescence spectrometer and with direct visual observation. While the WETStar indicated that fluorescence decreased with increasing nitroglycerin content, it was readily apparent that the opposite was true. Figures 57 and 58 are photographs from the open end of the WETStar during analysis that clearly show more fluorescence with nitroglycerin than without at these higher Eu/TTA concentrations. Not only could a stronger fluorescence be observed when nitroglycerin was present, it could also be seen that the fluorescence grew stronger as more nitroglycerin was added. Due to the discrepancy between the WETStar output and visual observation and luminescence spectrometer results, it must be assumed that the results from the WETStar are inaccurate when the Eu/TTA concentration is too high. It would be expected that the WETStar would be saturated at 5 V during these measurements, but it instead produces an immediate voltage that is lower than the nitroglycerin-lacking baseline. When this anomaly was observed, readings were taken via the analog channel, thus ruling out analog to digital conversion errors. This problem will be addressed with the vendor of the WETStar sensor.



Figure 57 – Strong visible fluorescence with nitroglycerin ( $10^{-3}$  M) at Eu/TTA ( $8 \times 10^{-4}$  M in Methanol)



Figure 58 – Weak visible fluorescence without nitroglycerin at Eu/TTA ( $8 \times 10^{-4}$  M in Methanol)

It was also found that at Eu/TTA concentrations that were fairly high (but less than 5 V saturation), the fluorescence output oscillated before reaching equilibrium, imposing a required waiting time for reaction completion. Looking through the end of the WETStar during these oscillations, a turbid state of reaction was observed in which the fluids swirled and the light intensity varied. The resulting voltage oscillations were too erratic to measure with the multimeter, so a waiting period of five minutes was employed so the different solutions could be compared. At lower concentrations, almost no waiting was necessary, but the reactions could take minutes at higher concentrations. Five minutes was more

than enough for all concentrations evaluated, with most reactions completing in less than three. Each Eu/TTA concentration was analyzed for a range of nitroglycerin concentrations. The results are shown below in Figures 59 through 64.

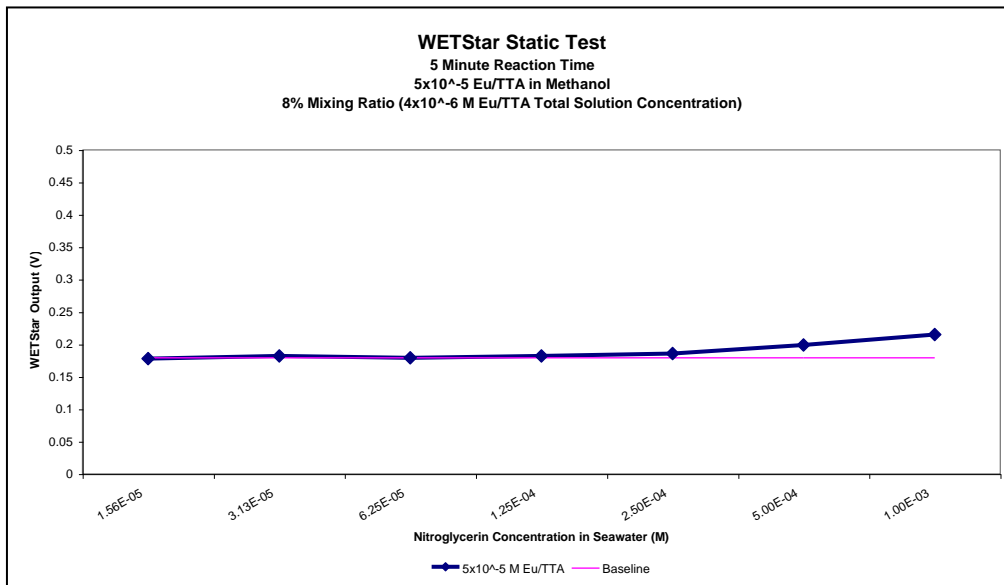


Figure 59 – Deployable detector static test with  $5 \times 10^{-5}$  M (Me) europium concentration



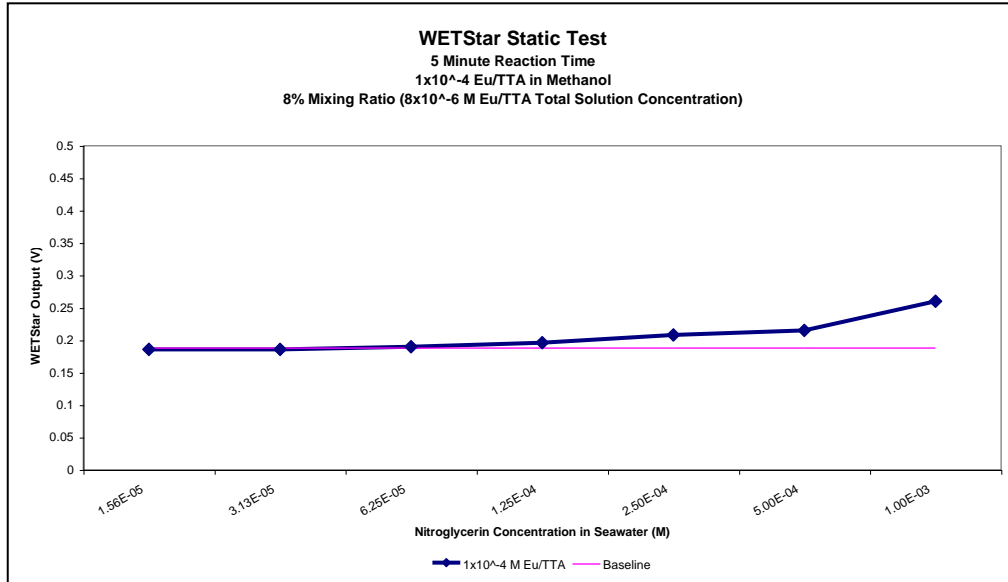


Figure 60 – Deployable detector static test with 1x10<sup>-4</sup> M (Me) europium concentration

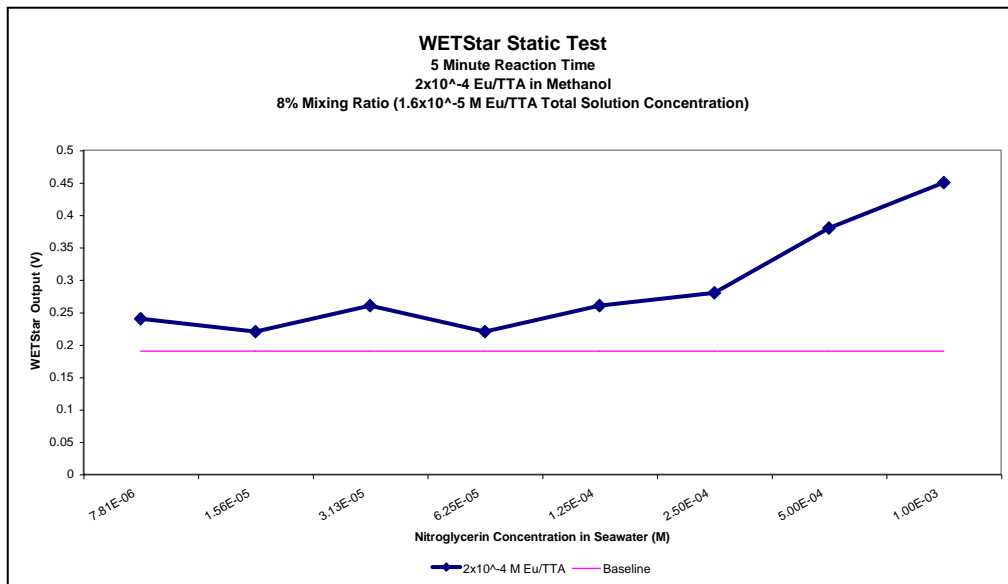


Figure 61 – Deployable detector static test with 2x10<sup>-4</sup> M (Me) europium concentration

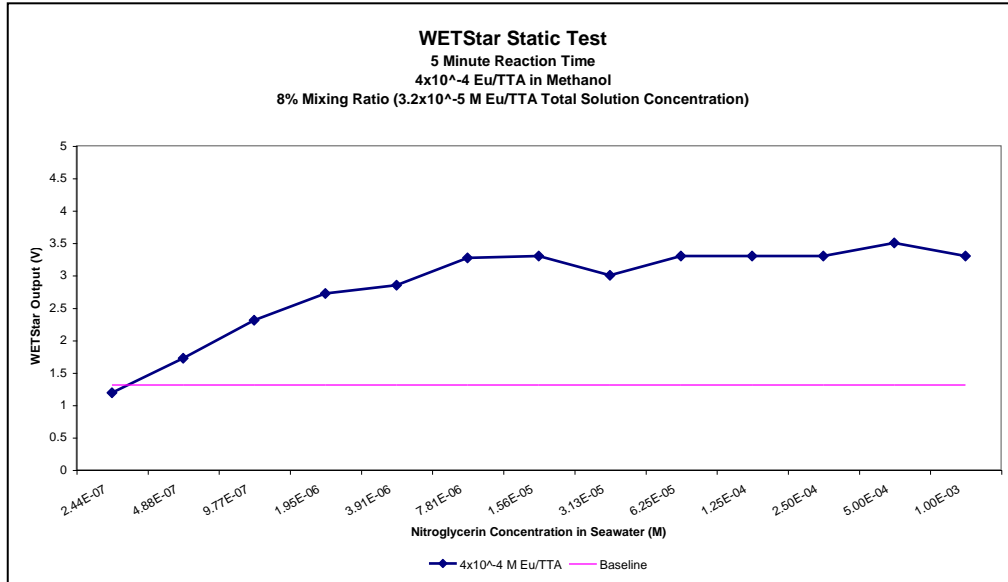


Figure 62 – Deployable detector static test with 4x10<sup>-4</sup> M (Me) europium concentration

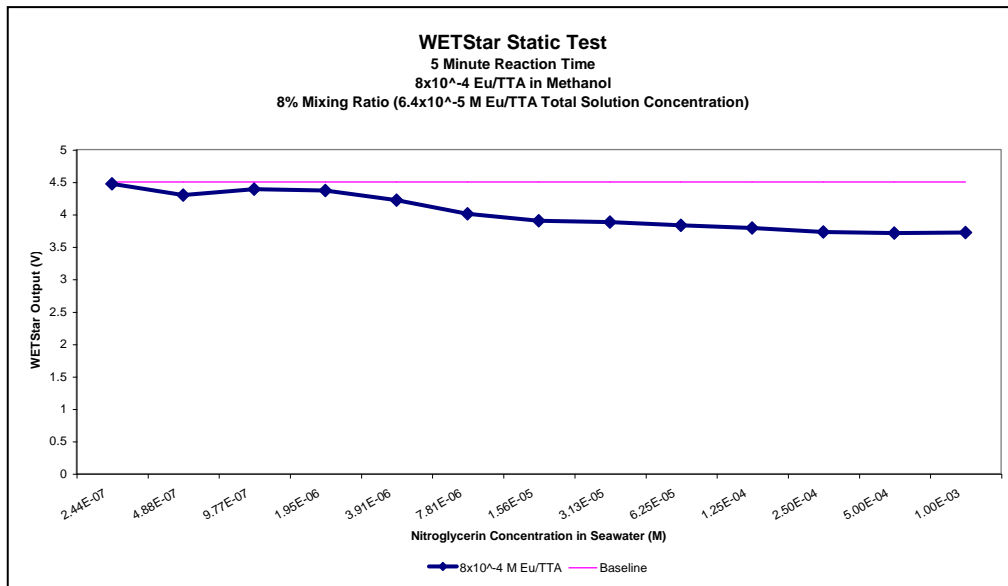


Figure 63 – Deployable detector static test with 8x10<sup>-4</sup> M (Me) europium concentration

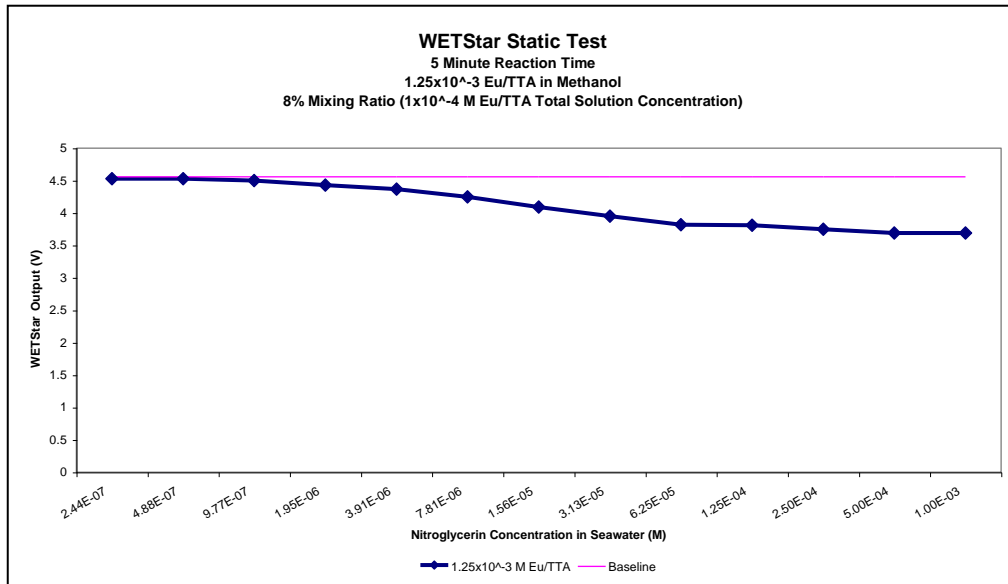


Figure 64 – Deployable detector static test with 1.25x10<sup>-3</sup> M (Me) europium concentration

### 5.3.2 Deployable Detector Filtration Study

In a static test, the fluorescence measurement improved slightly with finer filtering for both the nitroglycerin-laden and nitroglycerin-absent solutions. The improvement was very slight and the relative difference between solutions with and without nitroglycerin did not seem to change with filtration. The results are shown below in Figure 65. Based on these results, it is envisioned that no additional filtering beyond the pump requirements will be necessary or practical.

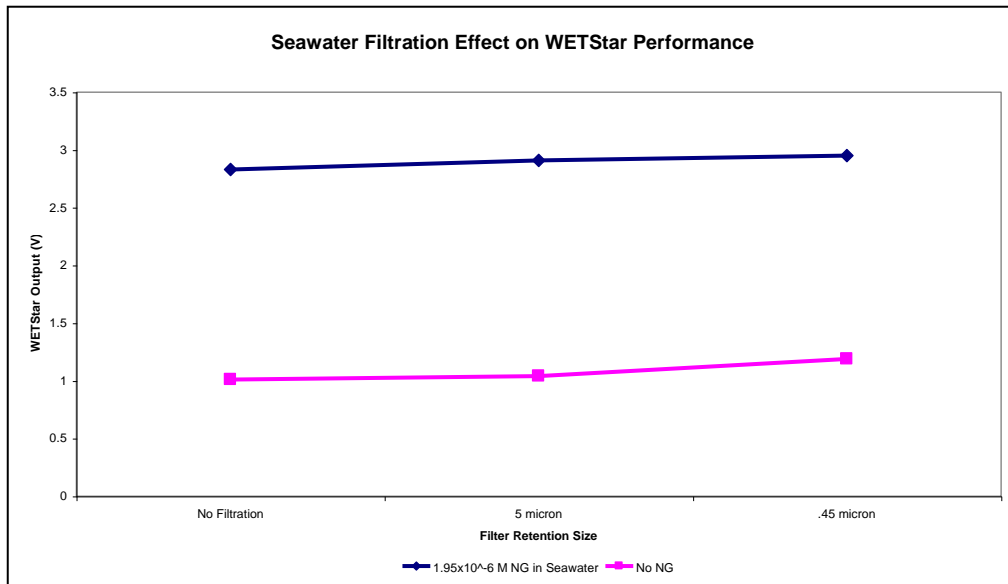


Figure 65 – Filtration effects on the deployable detector performance

#### 5.4 PROOF OF DESIGN

The detector was used in a flow-through configuration that included the static mixer and a method to provide the different solutions in the proper ratios. The point of this test was to prove the feasibility of the design. An additional length of tubing was included between the mixer and the detector to allow extra reaction time, but it is unknown if this length provided enough time for the reactions to complete. It is suspected that an even longer reaction time would have given better results.

The concentrations used for this test were selected based on previous detector characterization results, keeping in mind that the chemical supplies were limited and the flow-through setup rapidly uses supplies. The fact that higher concentrations require longer reaction times was also considered. The nitroglycerin concentration in seawater used was  $5 \times 10^{-4}$  M. The added europium complex concentration in methanol was  $2 \times 10^{-4}$  M, and the mixing ratio was adjusted so that the europium solution comprised 8.73% of the total solution. This resulted in a europium complex concentration of  $1.75 \times 10^{-5}$  M with respect to the total solution. Keep in mind, for comparison purposes, that most of the references to europium concentrations in other sections of this paper refer to the europium concentration in the *total* solution.

The design was validated through this test. Nitroglycerin was detected in the flow through configuration. Measurements were taken for seawater, seawater mixed with the europium complex, and seawater / nitroglycerin mixed with the europium complex. The results are shown below in Figure 66.

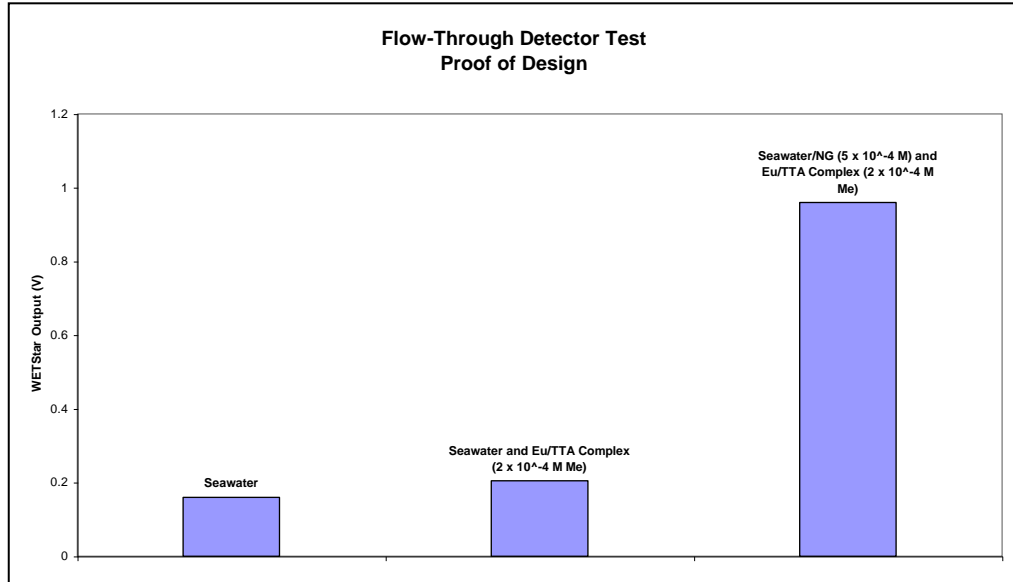


Figure 66 – Flow-through detector results from the proof of design tests

## CHAPTER 6

### CONCLUSIONS AND PROPOSED DESIGN CONFIGURATIONS

From these experiments, it was determined that the use of a lanthanide element to fluorescently tag explosive traces is a viable underwater trace explosive detection method. While water quenches europium compound fluorescence, water-borne nitroglycerin is able to protect europium's fluorescent properties. This likely occurs because the explosive trace's negatively charged nitrite moiety is more strongly attracted to the positively charged lanthanide ion's free bonding site than dipolar water molecules are.

To capture the fluorescent properties of a lanthanide ion, radiation-absorbent ligands must be attached to absorb and transfer energy to it. The type of ligand is important, as well as mixing order if multiple ligands are used. It was found that the europium / thenoyltrifluoroacetone (Eu/TTA) chelate produced significantly better results in underwater explosive detection than europium / thenoyltrifluoroacetone / 1,10-phenanthroline (Eu/TTA/OP) and europium / 1,10-phenanthroline / thenoyltrifluoroacetone (Eu/OP/TTA). Eu/TTA fluoresced strongly in the presence of NG, but almost completely lost fluorescence when NG was absent. On the other hand,

Eu/OP/TTA and Eu/TTA/OP fluoresced strongly with and without water-borne nitroglycerin. This suggests that the OP ligand creates a hydrophobic environment around the europium ion, even when NG is not present. The presence of the OP ligand also significantly reduced the solubility of the compound in methanol. Additionally, while Eu/TTA/OP and Eu/OP/TTA solutions contained the same ratios of components, they performed differently, indicating the importance of ligand mixing order.

It was found that the excitation wavelength required to create fluorescence of a lanthanide compound depended strictly on the excitation wavelengths of the attached ligands. When the TTA ligand was used, optimal excitation was found to be 382 nm and when the OP ligand was added, strong excitation also occurred around 310 nm. Excitation near the TTA requirement is easily accomplished via LED sources, whereas the deep ultraviolet wavelengths required by OP are not. Because of this and the better explosive-detection performance without OP, OP was omitted to provide an optimum compound for use. Since this thesis is ultimately aimed at a working design, practicality was factored in and excitation was chosen to be 370 nm for experimentation, versus the optimum wavelength of 382 nm. This choice was made because 370 nm is a standard wavelength available in LED's. To verify the correctness of this choice, testing was conducted on the Eu/TTA compound with both 370 nm and 382 nm excitation wavelengths for comparison, which indicated that very little performance is lost by this shift in excitation. Even less loss is expected in the field due to the fact that the 370 nm and 382 nm gap is closed somewhat due to the actual width of each one's excitation peak.

It is sometimes possible for the characteristic emission wavelength of an element to shift when it is combined with other components to form a compound. It was found



that the characteristic europium emission wavelength of 613 nm persisted, regardless of the compound configuration. This wavelength did not change in the presence of OP, TTA, nitroglycerin or sodium, or in fresh water and seawater solutions.

Because europium fluorescence is quenched by water, it was chosen to combine the europium and sensitizing ligands in methanol before introduction into the seawater and water solutions. It was found that the methanol affects both the final solution clarity and fluorescence. Overall, the less methanol included, the better. For the tests conducted with Eu/TTA, fluorescence fell to negligible levels when the methanol level reached 35 percent of the total solution. Only Eu/TTA was tested for methanol effect because it was chosen as the more favorable compound in an earlier test. Rough solubility limits of the compounds were ascertained to provide some insight into the minimum amount of methanol required. OP had a negative effect on solubility. The maximum solubilities found for Eu/TTA, Eu/TTA/OP and Eu/OP/TTA were  $1.02 \times 10^{-2}$  M, were  $4.57 \times 10^{-3}$  M and were  $4.53 \times 10^{-3}$  M, respectively.

The europium detection method was found to perform considerably better in fresh water than in seawater. A specified amount of nitroglycerin could be detected in fresh water with less than 1/12 the amount of reagent required to detect the same amount of nitroglycerin in seawater. Based on references 12, 15, 20 and 21, it is believed that this is due to metal-exchange reactions with calcium and magnesium in the seawater. References 12, 15, 20 and 21 also note that acidic conditions negatively affect europium compound fluorescence. The impact of metal-exchange reactions and low pH were not quantified because the calcium and magnesium content of seawater is not expected to vary significantly from the seawater samples used for experimentation and the range of

seawater pH is much higher than the problem ranges reported in references 12, 15, 20 and 21<sup>22</sup>. However, tests were conducted to prove that this explosive detection method is susceptible to these conditions and help explain the difference in performance between seawater and freshwater. These tests confirmed that this detection method is compromised by large amounts of calcium ions and low pH.

With Eu/TTA at  $1 \times 10^{-4}$  M concentration (total solution), nitroglycerin could be detected in the laboratory luminescence spectrometer down to concentrations as dilute as approximately  $1 \times 10^{-6}$  M.

After characterizing the chemical detection method in the laboratory with a luminescence spectrometer, tests were performed with a modified commercial fluorometer to move towards a field-deployable design. Static (non-flowing) tests indicated that, with this chemical detection method, a deployable fluorometer is sensitive to nitroglycerin dissolved in seawater. The sensitivity depends on the amount of the europium complex used, with more Eu/TTA translating to better sensitivity. In the WETStar characterization tests, sensitivity was found to be  $2.44 \times 10^{-7}$  M nitroglycerin with the equipment used, a Eu/TTA concentration in methanol of  $4 \times 10^{-4}$  M, and a mixing ratio of 8 percent. This translates to about 28 ppb. However, there is a limit to which the Eu/TTA concentration can be increased before problems are encountered with the particular fluorometer used in this experiment (WETStar). If the Eu/TTA concentration is high enough that the upper output voltage limit (5 V) of the WETStar was surpassed, the WETStar output information that defied visual observation and luminescence spectrometer readings. At these high Eu/TTA concentrations, the WETStar indicated that there was less intense fluorescence with nitroglycerin than without, even

though it was visually obvious that the opposite was true. Based on these comparisons, it was concluded that the WETStar output was erroneous when the Eu/TTA concentration was too high. Therefore, the best performance with this method and equipment is attained when the Eu/TTA complex is as high as possible, without reaching the point where the fluorometer outputs false results. While higher europium complex concentrations bring better sensitivity (before saturation), they also require more reaction time. Until the reaction is completed, the fluorescence output oscillates erratically and produces little usable information. All of the concentrations studied needed less than five minutes to stabilize. Reaction time must also be considered in system design.

The impact of sample filtration was also addressed, and it was found that filtration slightly increases the fluorescence intensity reading from the fluorometer. This slight increase was noted in both the nitroglycerin-laden and nitroglycerin-absent solutions, with very little change in their relative readings. With minimal change in fluorometer output and no noticeable change in relative readings, filtration adds little value to the design. However, if a pump is used to pass the sample through the fluorometer, a minimum amount of filtration will be required to assure pump operation and endurance.

The flow-through trace-explosive detector design was validated with a laboratory hydraulic system. This system combined the seawater/nitroglycerin solution with the europium complex solution in an appropriate ratio and then mixed them, before the final solution was passed through the modified WETStar fluorometer. Using this system, the fluorometer was able to discriminate between plain seawater and seawater that contained traces of nitroglycerin, and the design concept was proven.

It is believed that the negatively charged nitrite moiety of the nitroglycerin compound is what makes it detectable with the chemical method presented herein. Because this characteristic is common to many explosive types, it is believed to be highly likely that this method can be extended to detect many explosive types, in addition to nitroglycerin.

Based on this research, two proposed design options are shown below in Figures 67 and 68. The first design utilizes two small pumps, while the second makes use of one pump and a restrictor combination to control the seawater / reagent ratio. The UUV speed cannot be assumed to be constant, and because the mixing ratio of the seawater and reagent must be controlled, at least one pump is necessary. The two-pump design would be easier to setup, while some tuning would be required to achieve the proper mixing ratio with the restrictor setup. The restrictor setup would be less expensive and likely require less maintenance. cursory research indicates that pumps and restrictors are available that meet the requirements of this design. For example, Micropump Inc. can provide suitable pumps, and The Lee Company produces a range of hydraulic restrictor sizes that will fit this application. Many companies make small pumps, but this application is quite demanding for miniature pumps. The pumps must be accurate in their flowrates and more importantly; they must be able to withstand the internal case pressure that results from water depths that the CCST UUV must be designed to. Static mixers are available from a variety of companies. TAH Industries provided the static mixer used in the proof of design test of this thesis.

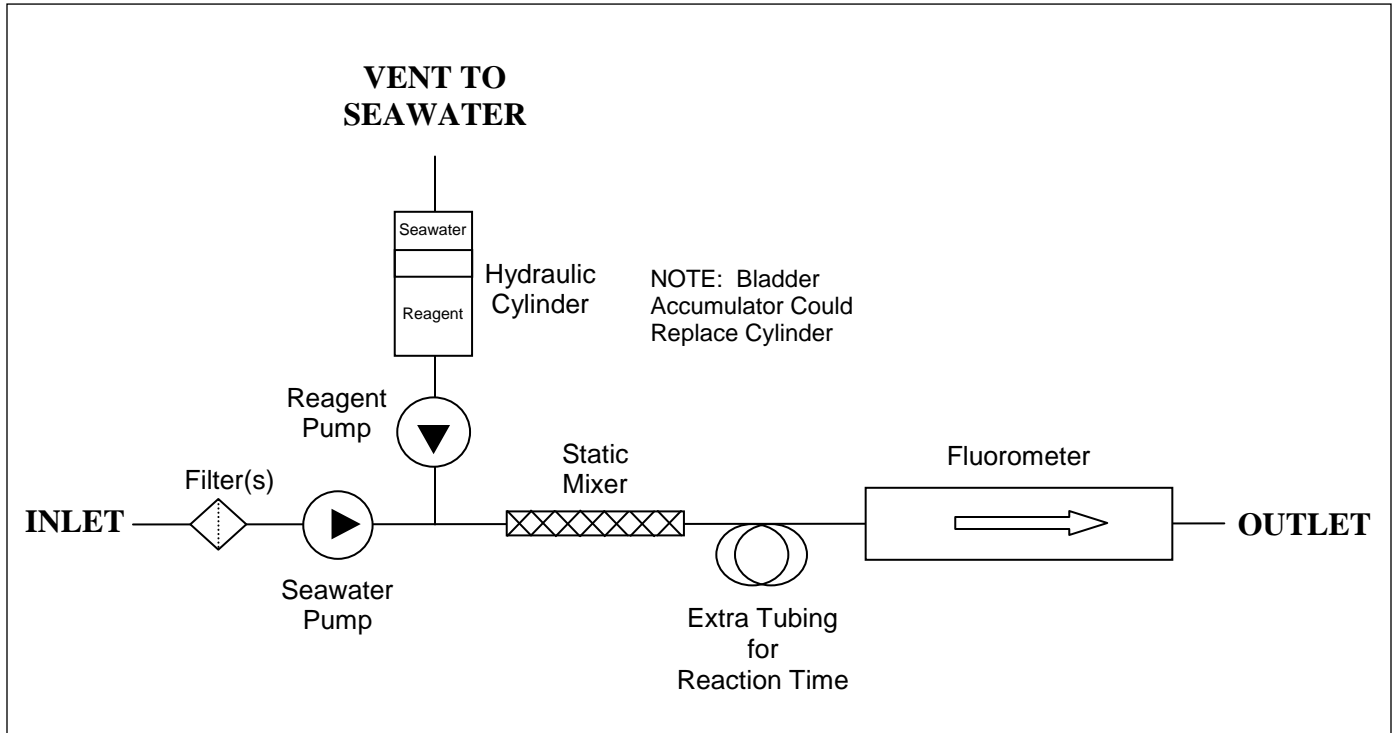


Figure 67 – Proposed design schematic no. 1

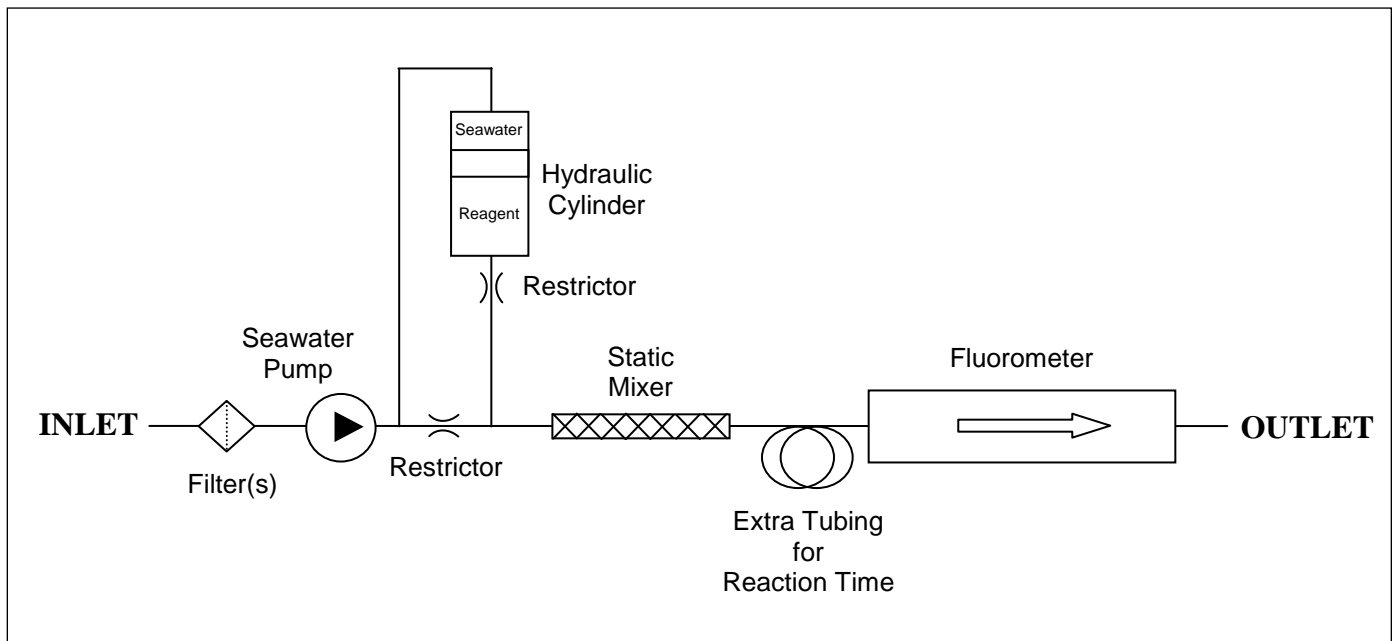


Figure 68 – Proposed design schematic no. 2

## CHAPTER 7

### FURTHER RESEARCH

It is believed that the negatively charged nitrite moiety of the nitroglycerin compound is what makes it detectable with the chemical method presented herein. Because this characteristic is common to many explosive types, it is believed to be highly likely that this method can be extended to detect many explosive types, in addition to nitroglycerin. However, this is just an educated assumption. To verify this extension to other explosive types, this method will have to be tested with them.

In this thesis, the required reaction time between the europium complex and nitroglycerin was noted and considered, but not characterized. Further research to evaluate the reaction kinetics may prove useful in optimizing a deployable detector design.

Because a turbidity measurement device was not available to compare filtration levels with the resulting turbidity, it may prove useful to perform this characterization.

One of the more notable characteristics of europium that hasn't been tapped into in this thesis is its long fluorescence time. Because it fluoresces for a very long time<sup>2</sup>, time-resolved analysis could introduce another level of sensitivity.

Quantum Dots (Q-dots) are manmade semiconductor nanocrystals. They behave like an atom in many ways, and can be designed to be fluorescent. Through manipulation of their size and shape, their characteristic fluorescence wavelength (and color) can be controlled<sup>6</sup>. The ability to control and design fluorescence color could add another dimension to the detectability of explosives by choosing colors that are easily discerned from the ambient background.

## REFERENCES

- 1) J. Yinon, S. Zitrin, *Modern Methods and Applications in Analysis of Explosives*, John Wiley & Sons Ltd., 1993.
- 2) E. Menzel, K. Bouldin, R. Murdock, Trace Explosives Detection by Photoluminescence, *The Scientific World JOURNAL* (2004) 4, 55–66 ISSN 1537-744X; DOI 10.1100/tsw.2004.7.
- 3) E. Menzel, L. Menzel, J. Schwierking, A Photoluminescence Based Field Method of Detection of Traces of Explosives, *The Scientific World JOURNAL* (2004) 4, 725-735 ISSN 1537-744X; DOI 10.1100/tsw.2004.126.
- 4) J. Chen and P. Selvin, Thiol-Reactive Luminescent Chelates of Terbium and Europium, *American Chemical Society, Bioconjugate Chem.* 1999, 10, 311-315.
- 5) Europium, Wikipedia, the Free Encyclopedia, Page Version ID: 60128903, Date of last revision: 23 June 2006,  
<http://en.wikipedia.org/w/index.php?title=Europium&oldid=60128903>.
- 6) Quantum Dot, Wikipedia, the Free Encyclopedia, Page Version ID: 61923994, Date of last revision: 3 July 2006,  
[http://en.wikipedia.org/w/index.php?title=Quantum\\_dot&oldid=61923994](http://en.wikipedia.org/w/index.php?title=Quantum_dot&oldid=61923994).



- 7) Held, P., An Introduction to Fluorescence Resonance Energy Transfer (FRET) Technology and its Application in Bioscience, Bio-Tek Instruments, June 20, 2005.
- 8) Förster, T. (1948) Intermolecular Energy Migration and Fluorescence Ann. Phys 2:55-75.
- 9) Fluorescence, Wikipedia, the Free Encyclopedia, Page Version ID: 62328592, Date of last revision: 6 July 2006, <http://en.wikipedia.org/w/index.php?title=Fluorescence&oldid=62328592>.
- 10) J. Christensen, A. Ladefoged, L. Norgaard, Rapid Determination of Bitterness in Beer Using Fluorescence Spectroscopy and Chemometrics, The Institute of Brewing and Distilling, Publication no. G-2005-0309-278, 2005.
- 11) Bio-Tek, Using the Synergy HT to Measure Time-Resolved Fluorescent Compounds, 2002.
- 12) C. N. Shtykov, T. D. Smirnova, Y. V. Molchanova, Synergistic Effects in the Europium(III)-thenoyltrifluoroacetone-1,10-Phenanthroline System in Micelles of Block Copolymers of Nonionic Surfactants and Their Analytical Applications, Chernyshevsky State University, Saratov, Russia, January 2001.
- 13) Chaplin, M., Water Structure and Behavior: Molecular Vibration and Absorption, (November 2005).
- 14) S. Beltyukova and A. Egorova, Luminescent Properties of Europium (III) in Complexes with Benzoilamidophosphoric Acid Ethers, Chemical Institute of National Academy of Sciences in Ukraine.

- 15) A. Adeyiga, P. Harlow, L. Vallarino, and R. Leif, Advances in the development of lanthanide macrocyclic complexes as luminescent bio-markers, Department of Chemistry, Virginia Commonwealth University, 2006.
- 16) F. Bartha, O. Kapuy, C. Kozmutza and C. Van Alsenoy, Analysis of weakly bound structures: hydrogen bond and the electron density in a water dimer, J. Mol. Struct. (Theochem) 666-667 (2003) 117-122.
- 17) E. D. Isaacs, A. Shukla, P. M. Platzman, D. R. Hamann, B. Barbiellini and C. A. Tulk, Compton scattering evidence for covalency of the hydrogen bond in ice, J. Phys. Chem. Solids 61 (2000) 403-406.
- 18) Menzel, R., RE: Trace Explosives Detection by Photoluminescence, email from R. Menzel to T. Langston, September 28, 2005.
- 19) Steric effects, Wikipedia, the Free Encyclopedia, Page Version ID: 54998731, Date of last revision: 25 May 2006, [http://en.wikipedia.org/w/index.php?title=Steric\\_effects&oldid=54998731](http://en.wikipedia.org/w/index.php?title=Steric_effects&oldid=54998731).
- 20) Perkin Elmer Life Sciences, Stability of the Wallac LANCE™ Eu-chelates, LANCE™ Time-Resolved Fluorescence Detection Application Note.
- 21) Cisbio International, New Europium Cryptates to Probe Molecular Interactions Using HTRF.
- 22) Sea Water, Wikipedia – The Free Encyclopedia, Page Version ID: 52229402, Revised May 8, 2006.
- 23) Expray Kit Technical Background, Mistral Security Inc., Bethesda, MD.
- 24) Photon Micro-Light, High Intensity Black Light, Amberica West, [www.americawest.com](http://www.americawest.com).

- 25) Telephone Conversation with Ian Walsh, WetLabs, Re. Customization of Chlorophyll Fluorometer for Different Absorption and Emission Wavelengths, July 27, 2005.
- 26) Instruction Manuel for the Perkin-Elmer LS50B Luminescence Spectrometer.
- 27) B. Munson, D. Young, T. Okiishi, Fundamentals of Fluid Mechanics, 3<sup>rd</sup> Edition, John Wiley & Sons, Inc., 1998.
- 28) R. Freitas Jr., Nanomedicine: Translational Brownian Diffusion Coefficients for Physiologically Important Molecules Suspended in Water, Robert A. Freitas Jr., 1998.
- 29) T. Ursell, Diffusion of Solid Particles Confined in a Viscous Fluid, 2005.
- 30) J. Bendat, A. Piersol, Random Data: Analysis and Measurement Procedures, 3<sup>rd</sup> Edition, John Wiley & Sons, Inc., 2000.
- 31) B. Van Zeghbroeck, Gaussian, Principles of Semiconductor Devices B. Van Zeghbroeck, 2004.
- 32) Koflo Industries, <http://www.koflo.com/#>.
- 33) A. Kamyshny, S. Magdassi, Y. Avissar, J. Almog, Water-Soaked Evidence: Detectability of Explosive Traces After Immersion in Water, J Forensic Sci, Mar. 2003, Vol. 48, No. 2, Paper ID JFS2002017\_482.
- 34) Telephone Conversation with Doug Hankins, WetLabs, Re. LED Excitation Wavelength, 3/2/06.
- 35) R. Chang, Chemistry, Fifth Edition, McGraw-Hill, Inc., 1994.
- 36) Longmont Official Government Website, What is in Your Tap Water.

- 37) M. Hoffman, F. Bolletta, L. Moggi, G. Hug, Rate Constants for the Quenching of Excited States of Metal Complexes in Fluid Solution, *J. Phys. Chem. Reference Data* 18 219-543, 1989.
- 38) J. Lakowicz, *Principles of Fluorescence Spectroscopy*, 2<sup>nd</sup> Edition, Kluwer Academic/Plenum Publishers, New York, New York, 1999.
- 39) Test Method protocol for Solubility Determination: In Vitro Cytotoxicity Validation Study: Phase III, The National Toxicology Program (NTP) Interagency Center for the Evaluation of Alternative Toxicological Methods (NICEATM), September 24, 2003.
- 40) N. Glagovich, *Procedure for Determining Solubility of Organic Compounds*, Neil Glagovich, 2006.
- 41) B. Evans, The formulation, analysis and stability of glycerol trinitrate in non-aqueous pharmaceutical formulations, *The Pharmaceutical Journal*, (2003), 270, 482-4
- 42) Florida State University, *Molecular Expressions, Exploring the World of Optics and Microscopy*, <http://micro.magnet.fsu.edu/index.html>, 2006.
- 43) Ghasteen, T., Department of Chemistry, Sam Houston State University, Huntsville, Texas, <http://www.shsu.edu/~chemistry/chemiluminescence/JABLONSKI.html>.

## APPENDICES

### A1 Luminescence Spectrometer Data not Shown in Report

#### A1-1 Europium Complex Comparisons

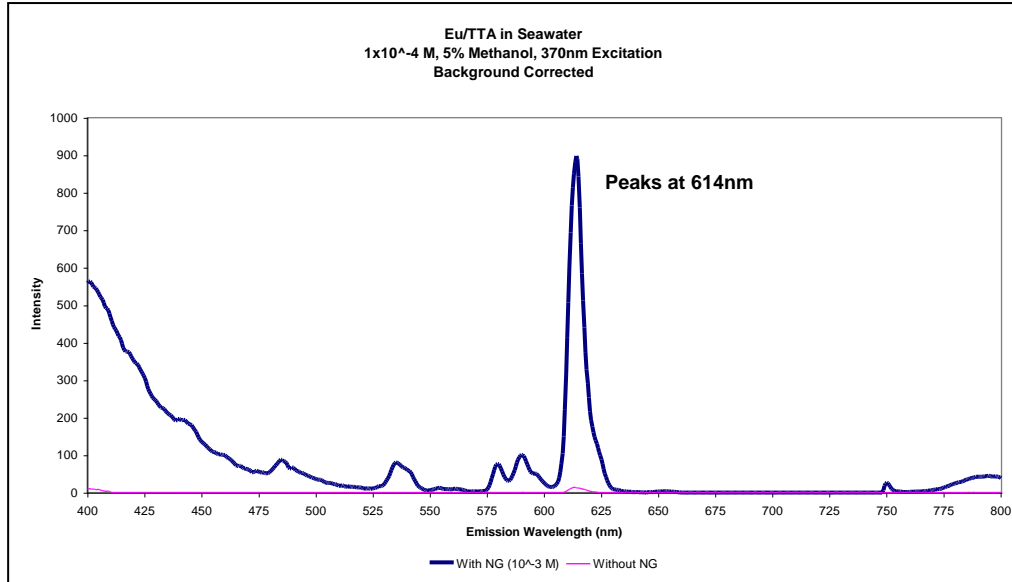


Figure 69 – Eu/TTA 1x10<sup>-4</sup> M Emission in Seawater Under 370 nm Excitation, With and Without Nitroglycerin, 5% Methanol

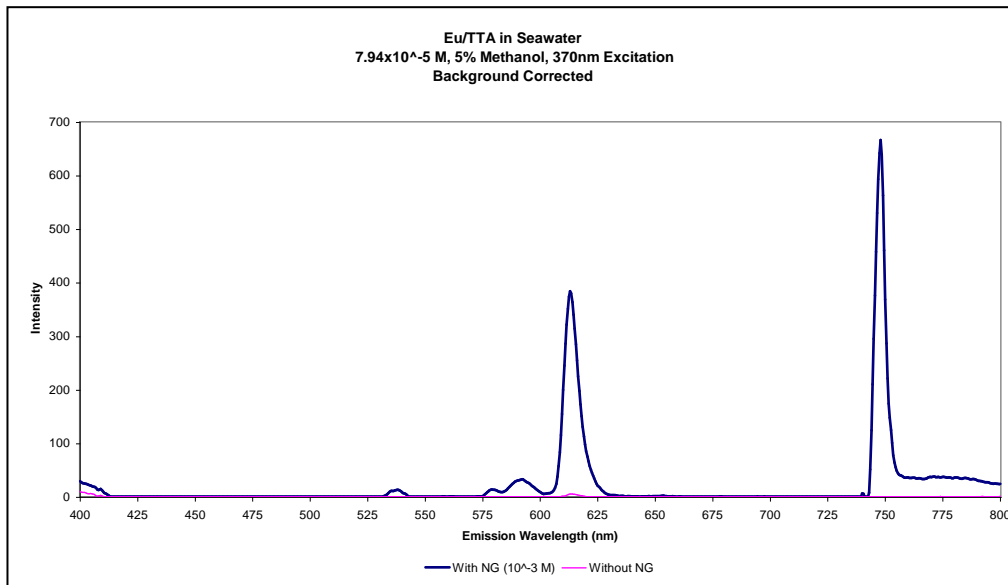


Figure 70 – Eu/TTA 7.94x10<sup>-5</sup> M Emission in Seawater Under 370 nm Excitation, With and Without Nitroglycerin, 5% Methanol

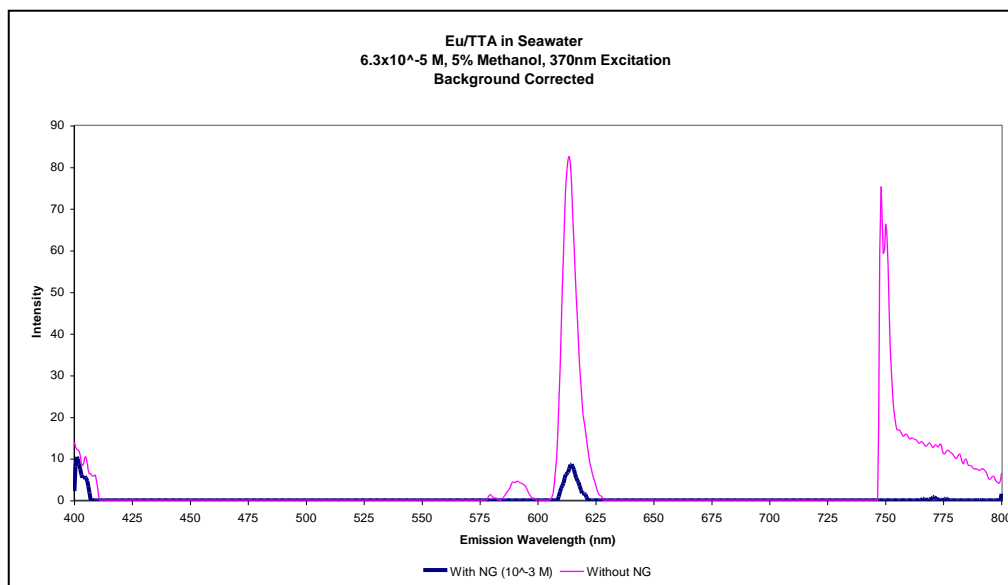


Figure 71 – Eu/TTA  $6.3 \times 10^{-5}$  M Emission in Seawater Under 370 nm Excitation, With and Without Nitroglycerin, 5% Methanol

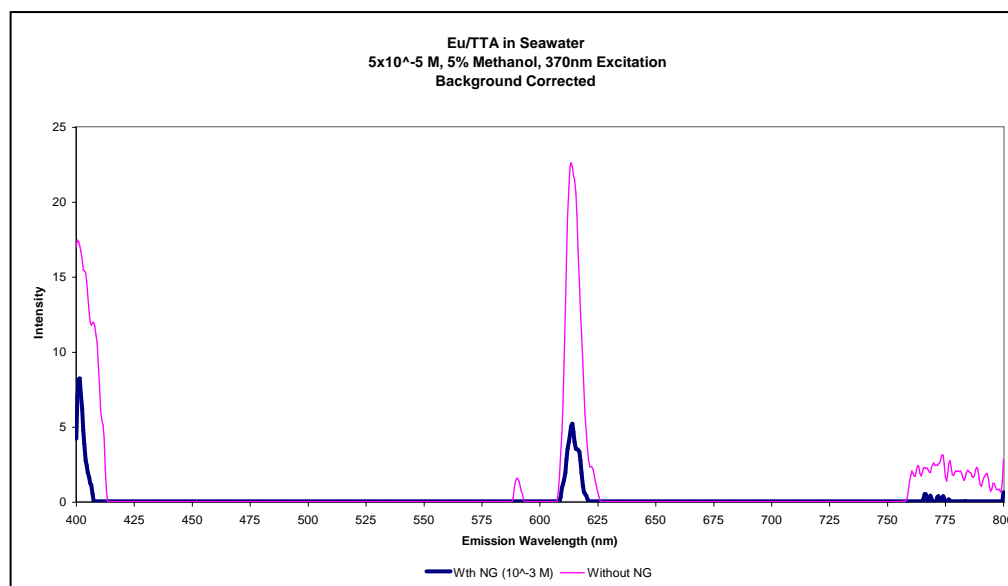


Figure 72 – Eu/TTA  $5 \times 10^{-5}$  M Emission in Seawater Under 370 nm Excitation, With and Without Nitroglycerin, 5% Methanol

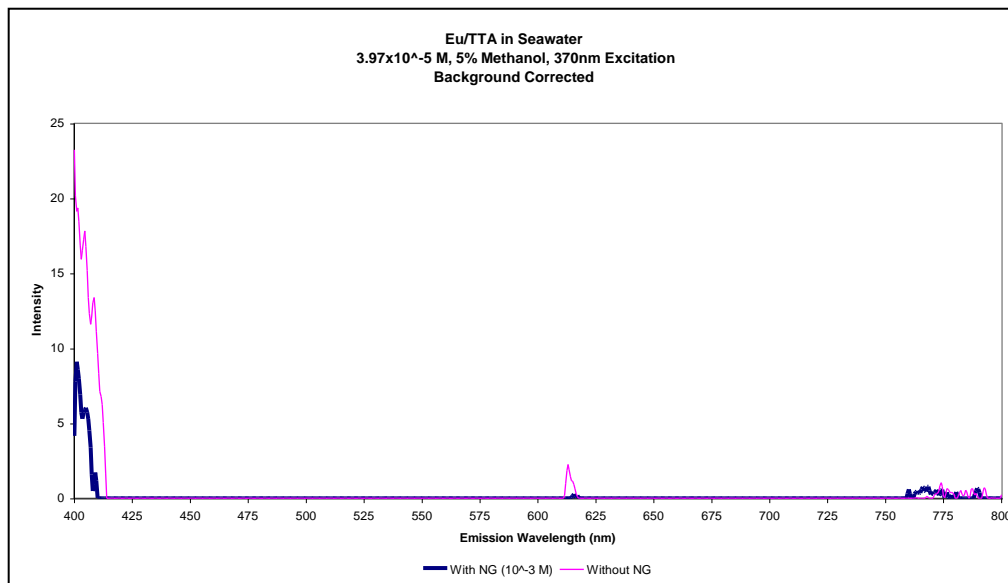


Figure 73 – Eu/TTA  $3.97 \times 10^{-5}$  M Emission in Seawater Under 370 nm Excitation, With and Without Nitroglycerin, 5% Methanol

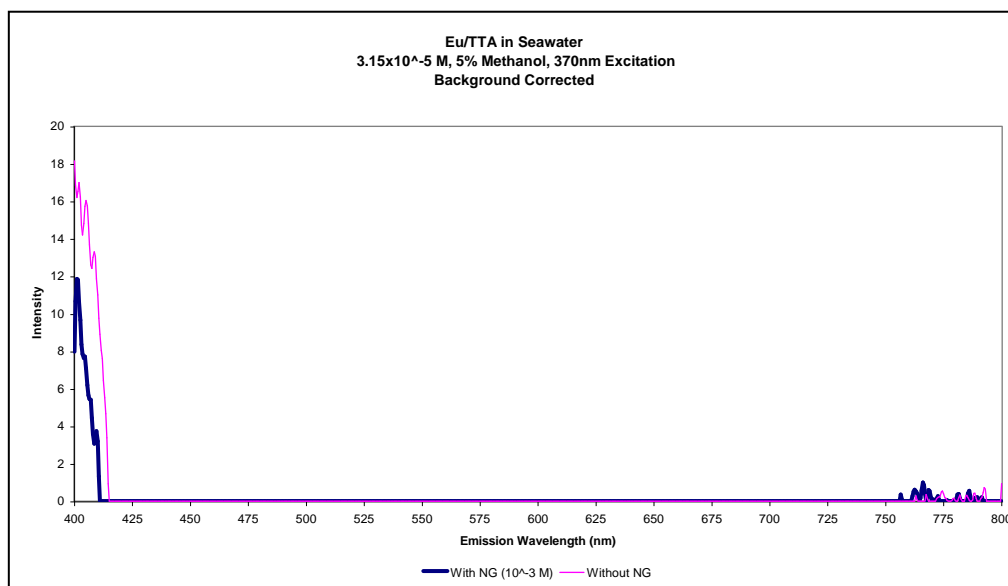


Figure 74 – Eu/TTA  $3.15 \times 10^{-5}$  M Emission in Seawater Under 370 nm Excitation, With and Without Nitroglycerin, 5% Methanol

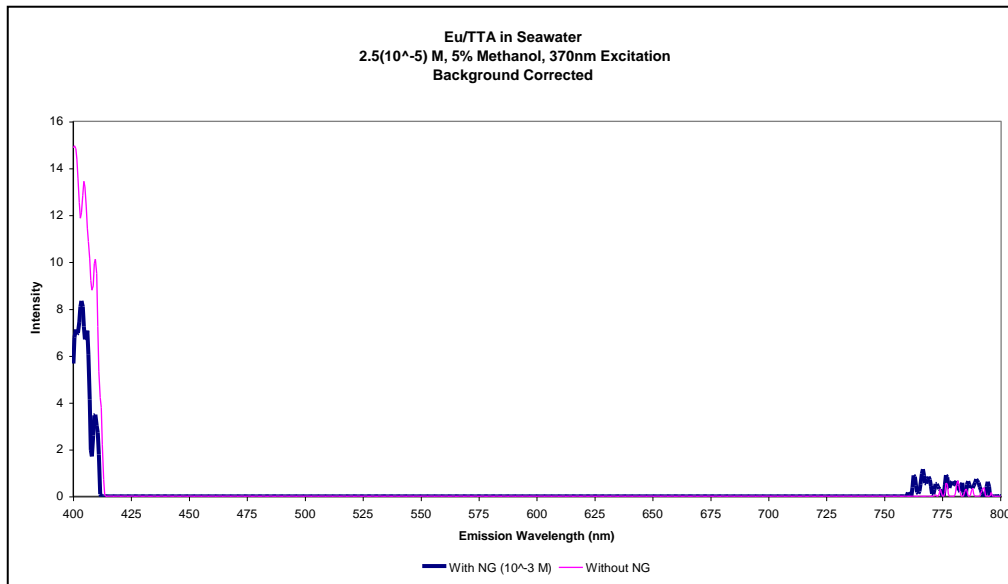


Figure 75 – Eu/TTA  $2.5 \times 10^{-5}$  M Emission in Seawater Under 370 nm Excitation, With and Without Nitroglycerin, 5% Methanol

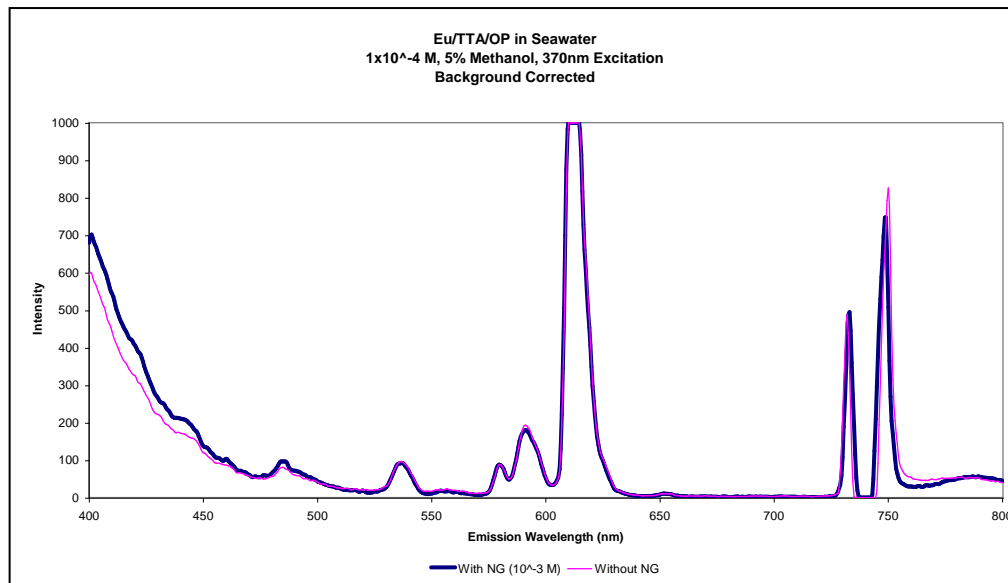


Figure 76 – Eu/TTA/OP  $1 \times 10^{-4}$  M Emission in Seawater Under 370 nm Excitation, With and Without Nitroglycerin, 5% Methanol



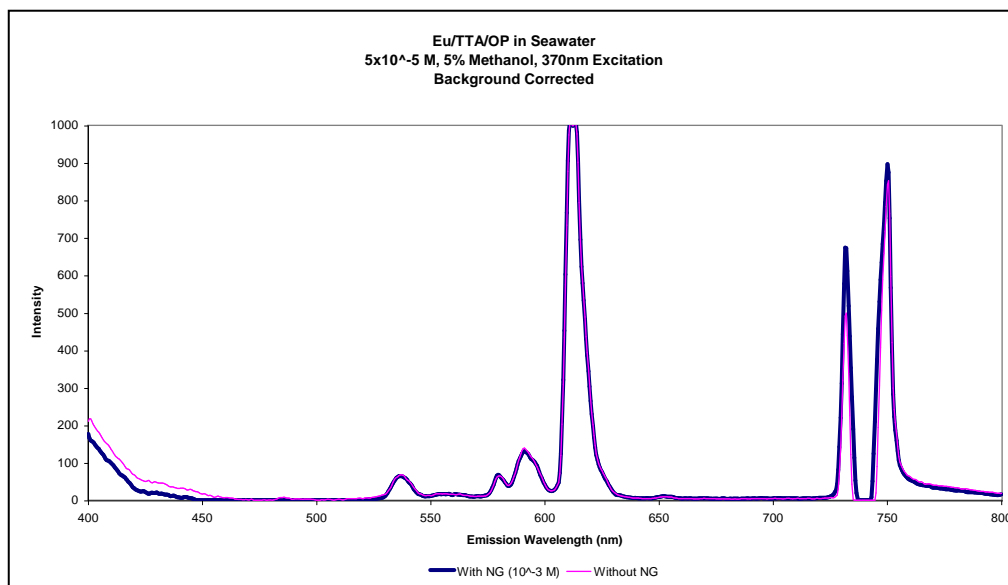


Figure 77 – Eu/TTA/OP 5x10<sup>-5</sup> M Emission in Seawater Under 370 nm Excitation, With and Without Nitroglycerin, 5% Methanol

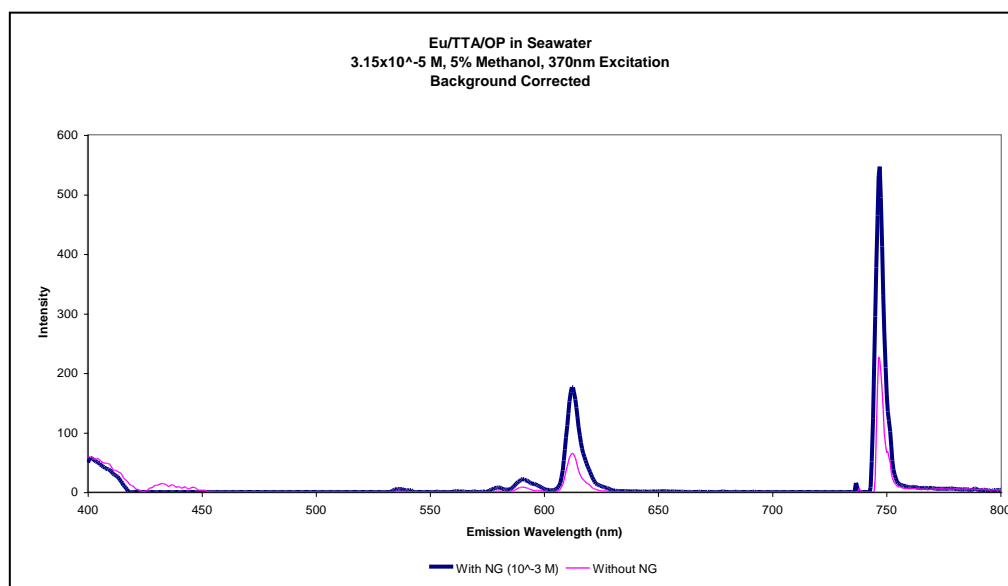


Figure 78 – Eu/TTA/OP 3.15x10<sup>-5</sup> M Emission in Seawater Under 370 nm Excitation, With and Without Nitroglycerin, 5% Methanol

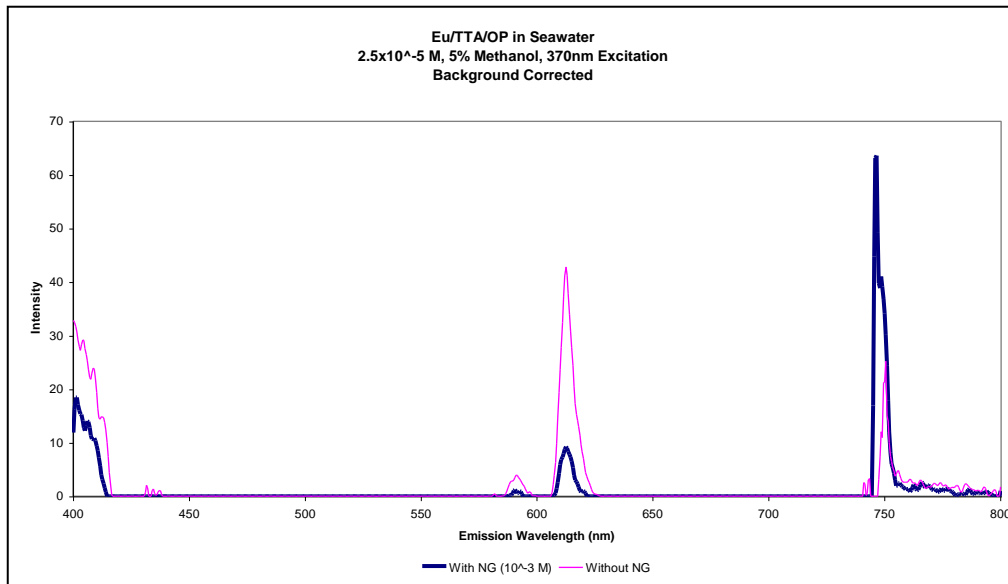


Figure 79 – Eu/TTA/OP  $2.5 \times 10^{-5}$  M Emission in Seawater Under 370 nm Excitation, With and Without Nitroglycerin, 5% Methanol

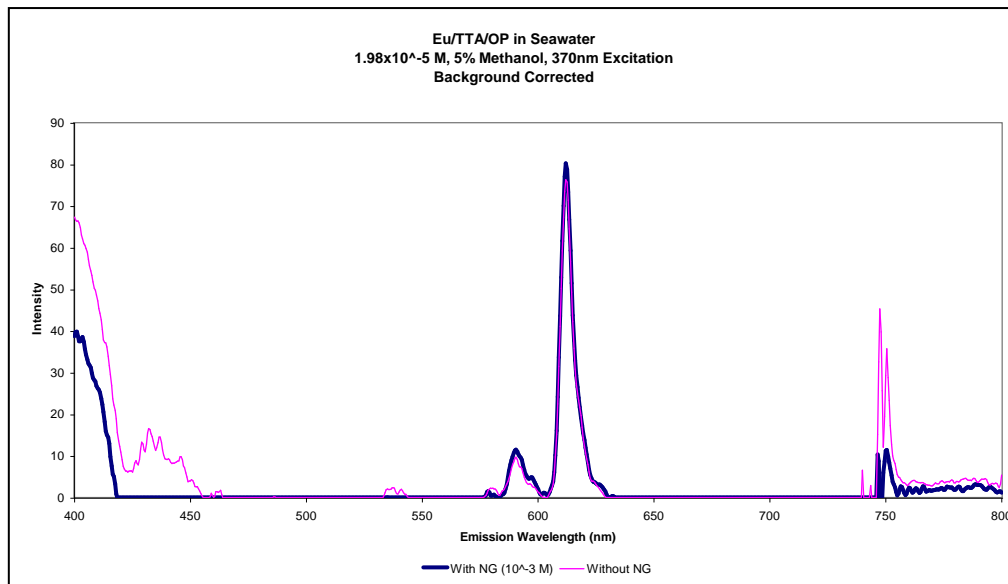


Figure 80 – Eu/TTA/OP  $1.98 \times 10^{-5}$  M Emission in Seawater Under 370 nm Excitation, With and Without Nitroglycerin, 5% Methanol

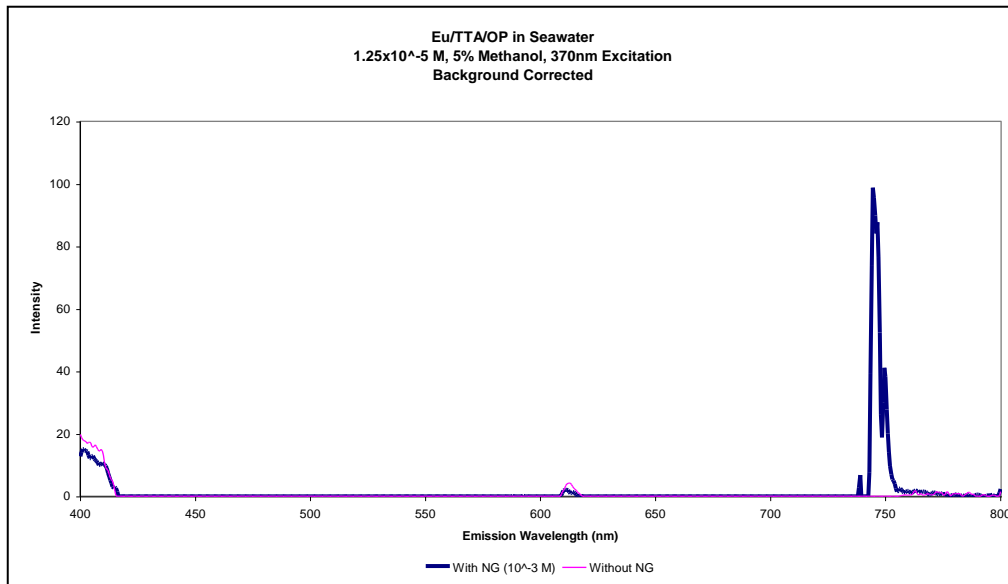


Figure 81 – Eu/TTA/OP  $1.25 \times 10^{-5}$  M Emission in Seawater Under 370 nm Excitation, With and Without Nitroglycerin, 5% Methanol

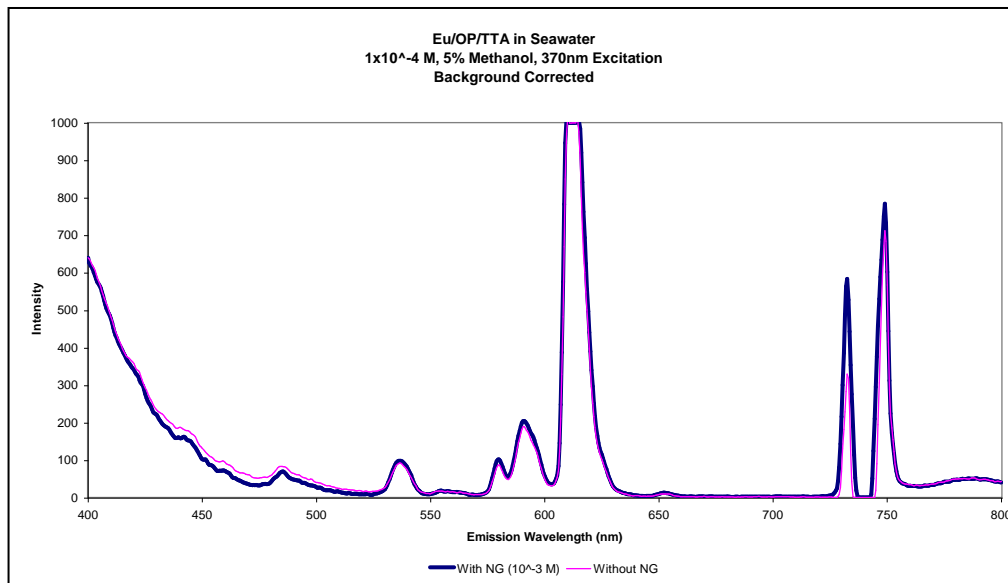


Figure 82 – Eu/OP/TTA  $1 \times 10^{-4}$  M Emission in Seawater Under 370 nm Excitation, With and Without Nitroglycerin, 5% Methanol

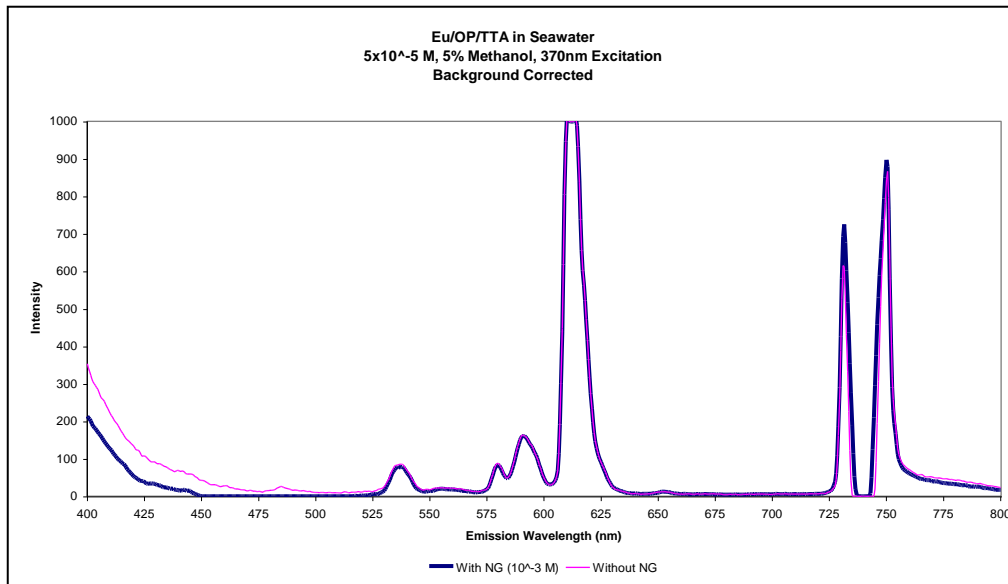


Figure 83 – Eu/OP/TTA  $5 \times 10^{-5}$  M Emission in Seawater Under 370 nm Excitation, With and Without Nitroglycerin, 5% Methanol

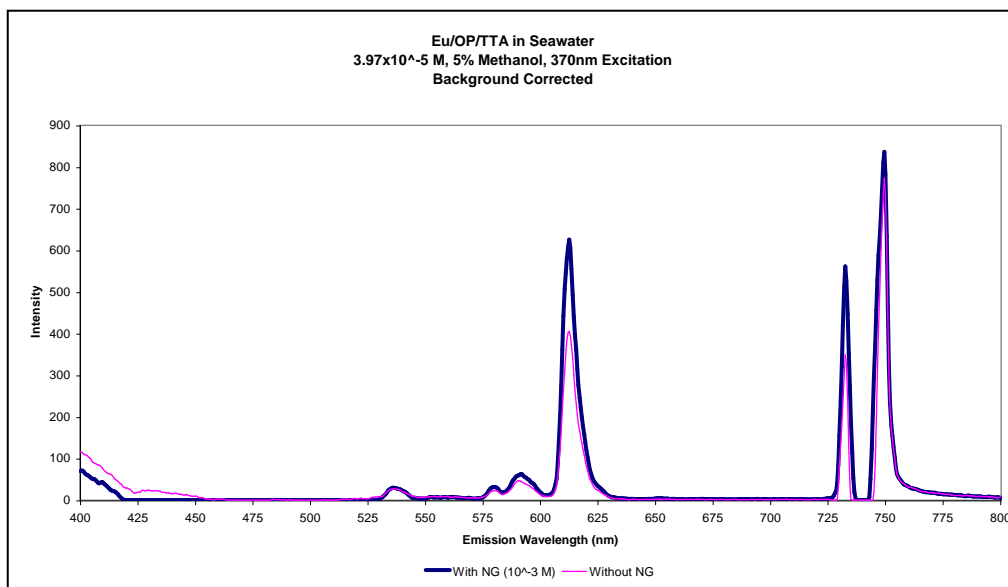


Figure 84 – Eu/OP/TTA  $3.97 \times 10^{-5}$  M Emission in Seawater Under 370 nm Excitation, With and Without Nitroglycerin, 5% Methanol

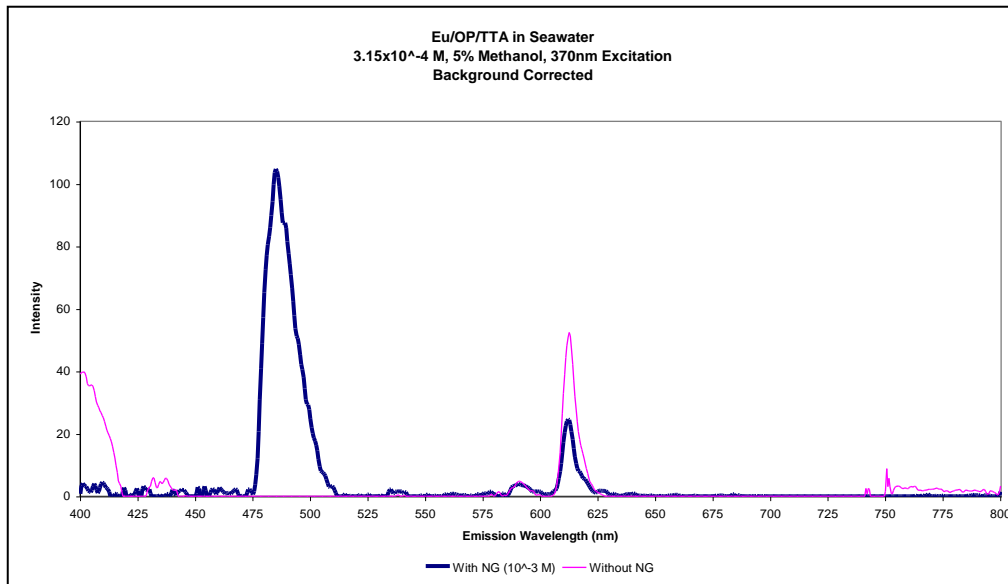


Figure 85 – Eu/OP/TTA  $3.15 \times 10^{-5}$  M Emission in Seawater Under 370 nm Excitation, With and Without Nitroglycerin, 5% Methanol

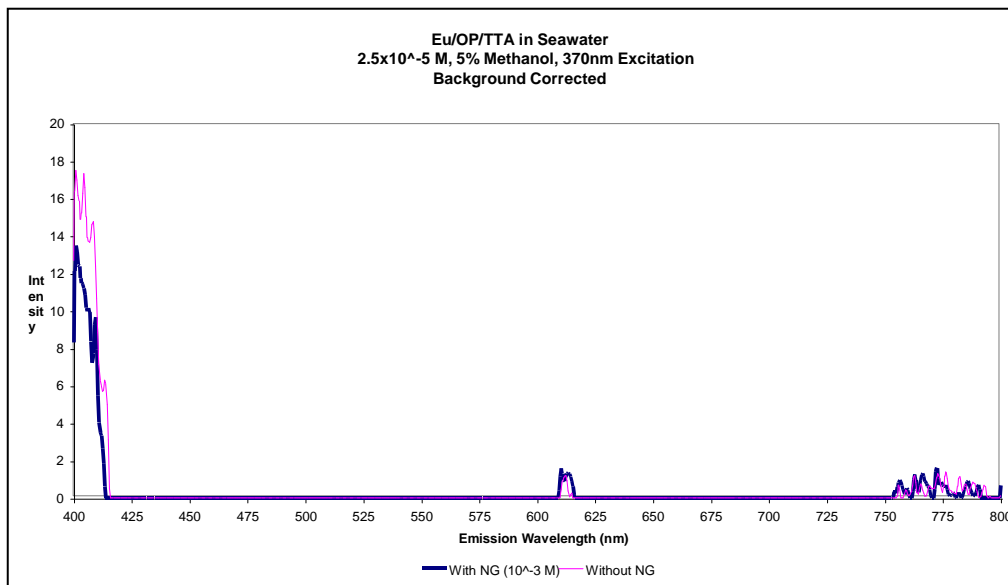


Figure 86 – Eu/OP/TTA  $2.5 \times 10^{-5}$  M Emission in Seawater Under 370 nm Excitation, With and Without Nitroglycerin, 5% Methanol

## A1-2 Ideal Excitation of Eu/TTA

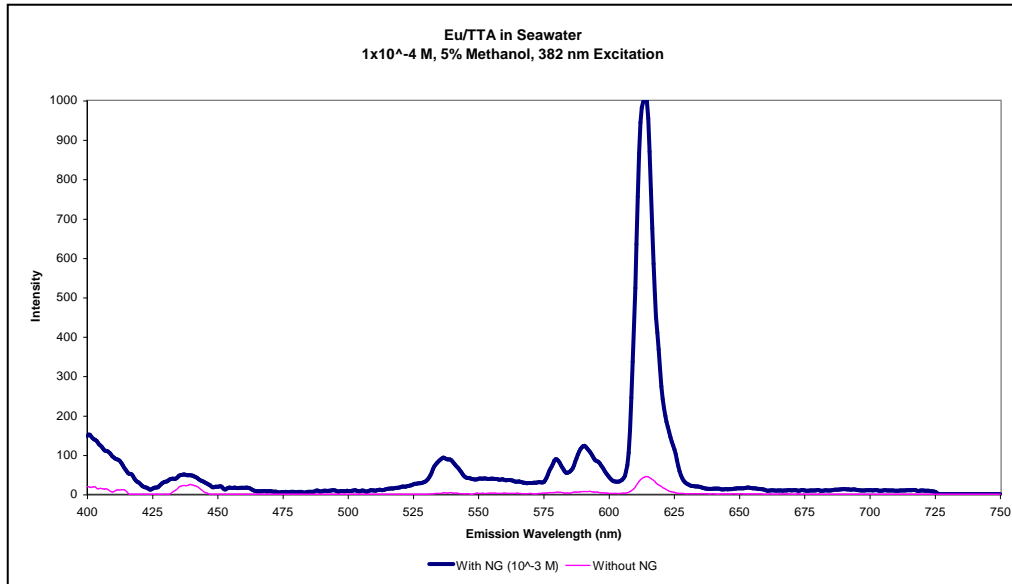


Figure 87 – Eu/TTA  $1 \times 10^{-4}$  M Emission in Seawater Under 382 nm Excitation, With and Without Nitroglycerin, 5% Methanol

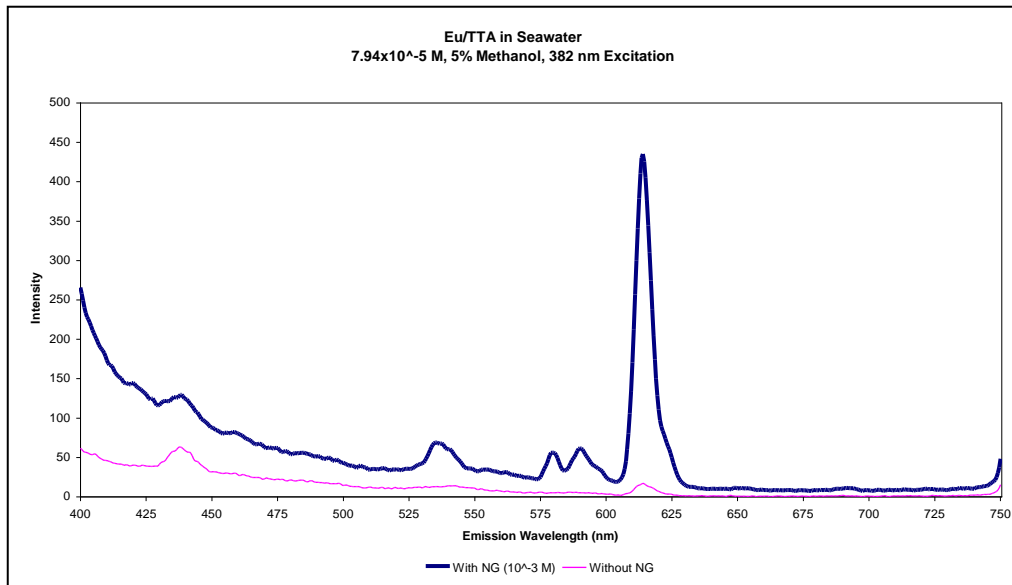


Figure 88 – Eu/TTA  $7.94 \times 10^{-5}$  M Emission in Seawater Under 382 nm Excitation, With and Without Nitroglycerin, 5% Methanol

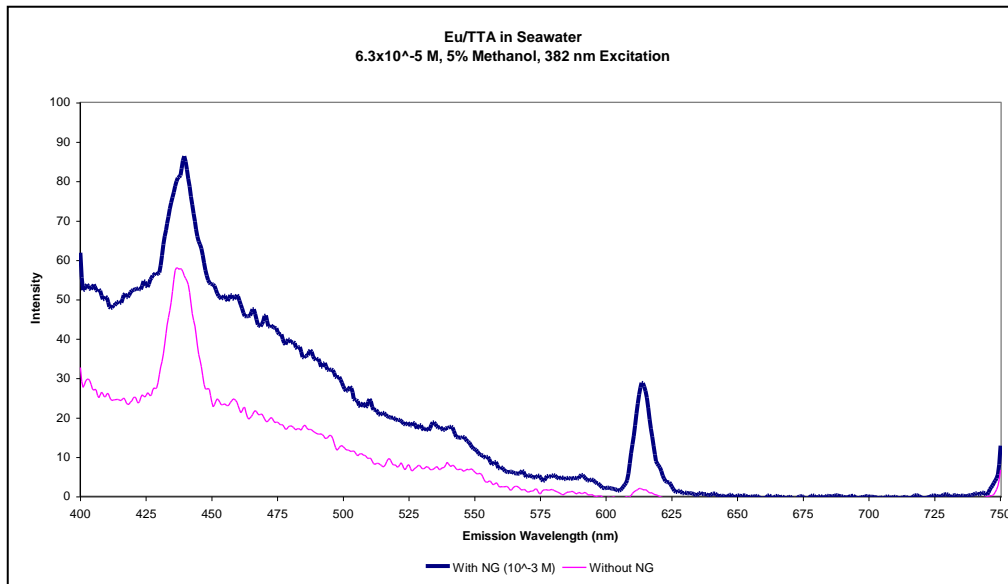


Figure 89 – Eu/TTA 6.3x10<sup>-5</sup> M Emission in Seawater Under 382 nm Excitation, With and Without Nitroglycerin, 5% Methanol

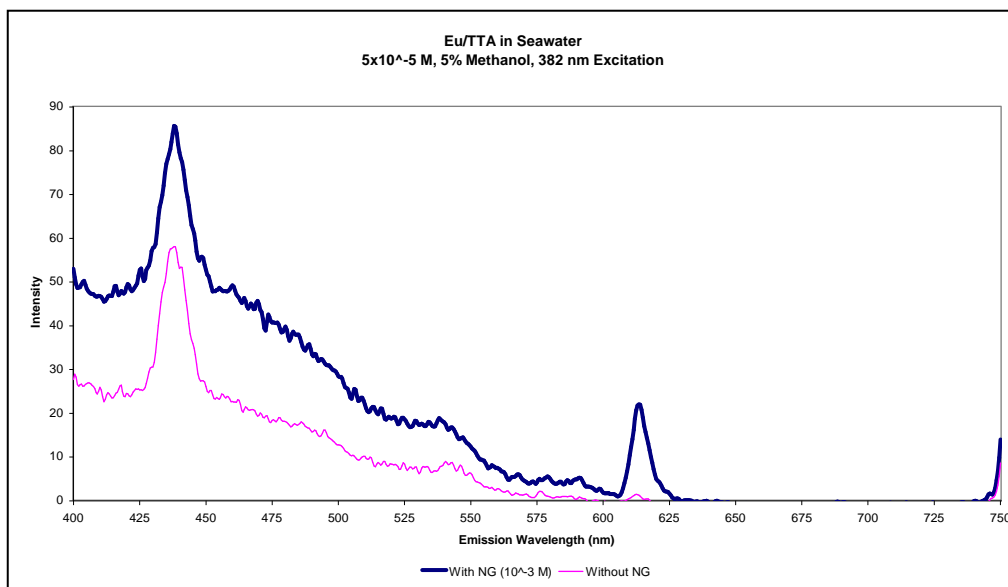


Figure 90 – Eu/TTA 5x10<sup>-5</sup> M Emission in Seawater Under 382 nm Excitation, With and Without Nitroglycerin, 5% Methanol

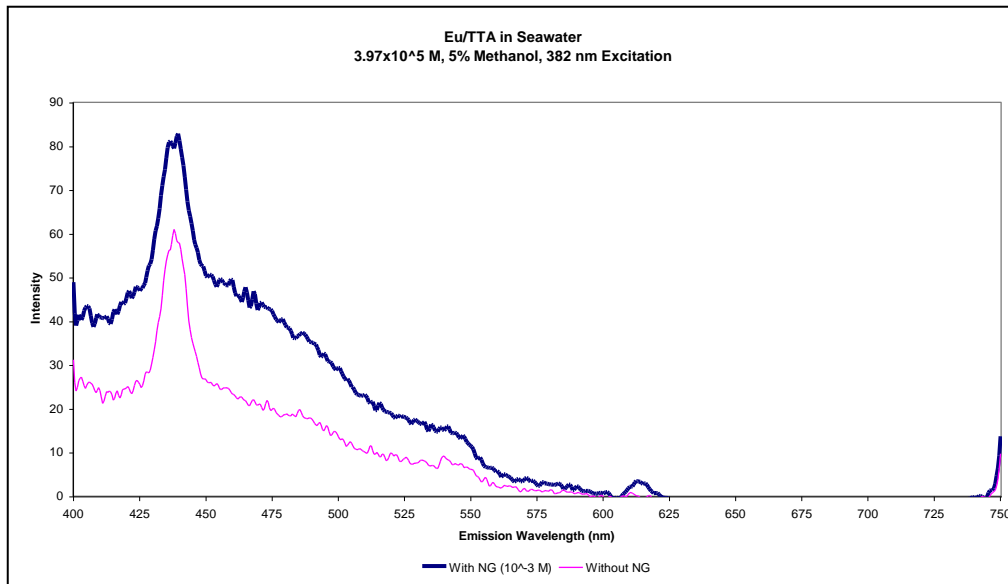


Figure 91 – Eu/TTA  $3.97 \times 10^{-5}$  M Emission in Seawater Under 382 nm Excitation, With and Without Nitroglycerin, 5% Methanol

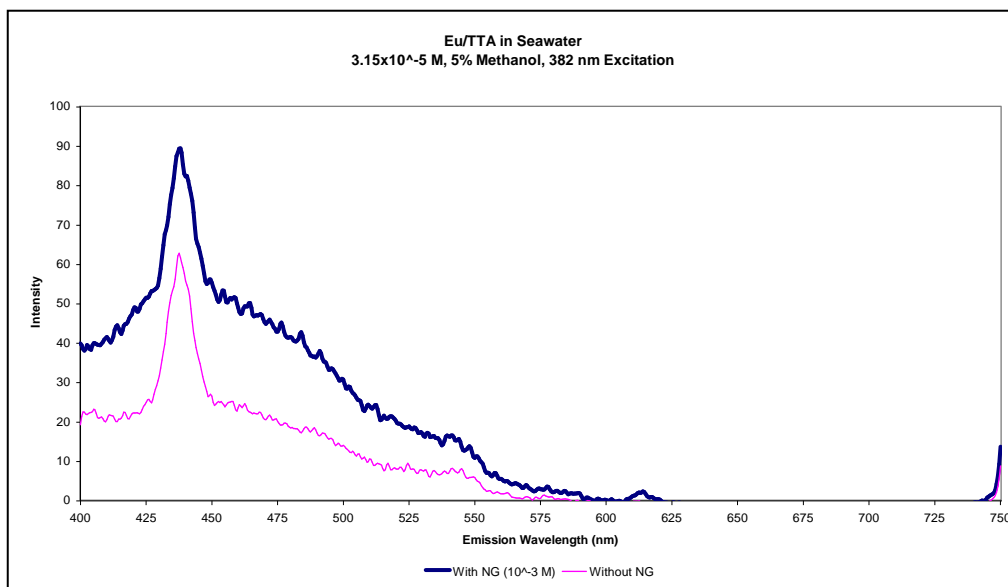


Figure 92 – Eu/TTA  $3.15 \times 10^{-5}$  M Emission in Seawater Under 382 nm Excitation, With and Without Nitroglycerin, 5% Methanol



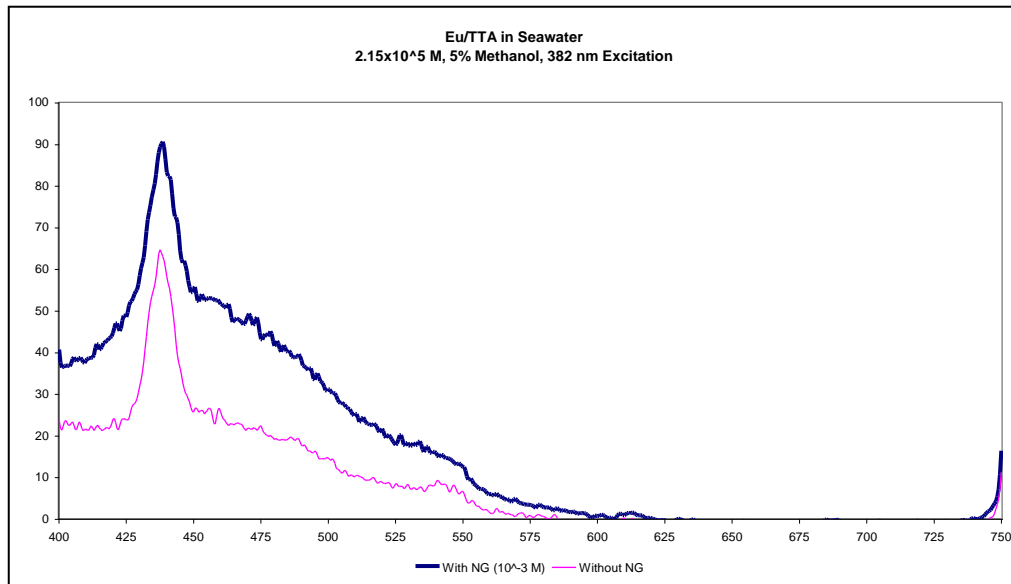


Figure 93 – Eu/TTA 2.15x10<sup>-5</sup> M Emission in Seawater Under 382 nm Excitation, With and Without Nitroglycerin, 5% Methanol

### A1-3 Methanol Effect

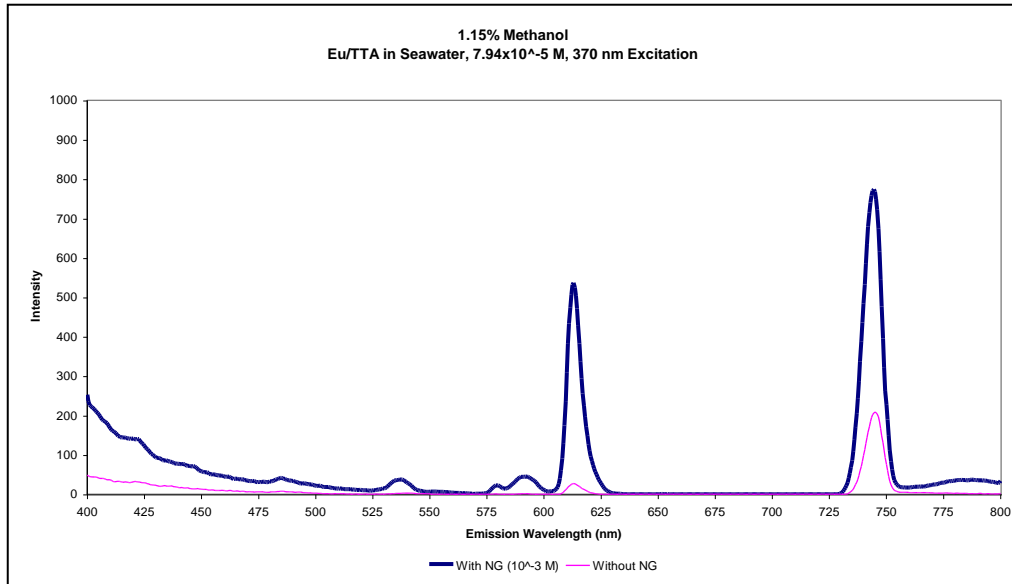


Figure 94 – Eu/TTA  $7.94 \times 10^{-5}$  M Emission in Seawater Under 370 nm Excitation, With and Without Nitroglycerin, 1.15% Methanol

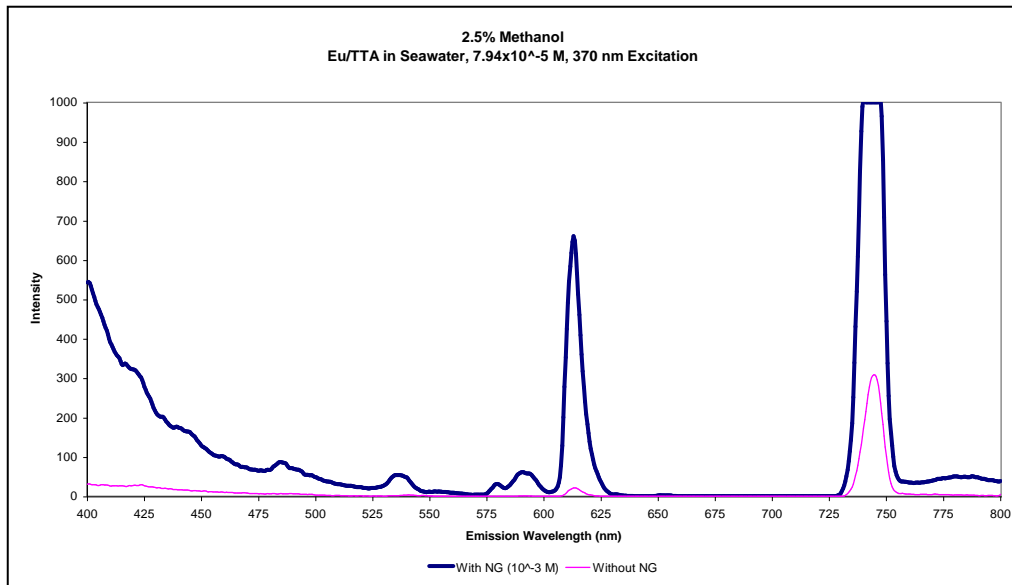


Figure 95 – Eu/TTA  $7.94 \times 10^{-5}$  M Emission in Seawater Under 370 nm Excitation, With and Without Nitroglycerin, 2.5% Methanol

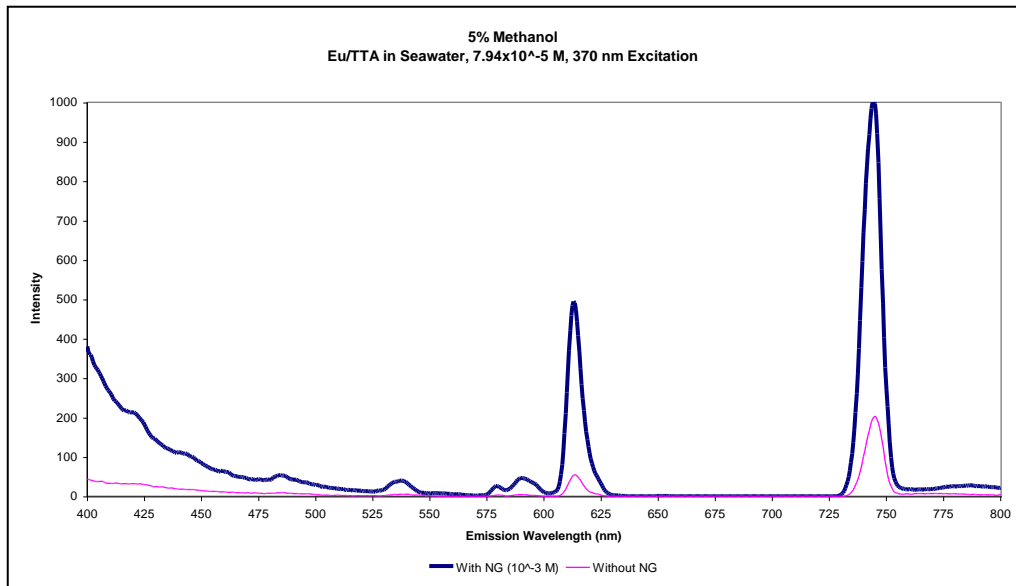


Figure 96 – Eu/TTA  $7.94 \times 10^{-5}$  M Emission in Seawater Under 370 nm Excitation, With and Without Nitroglycerin, 5% Methanol

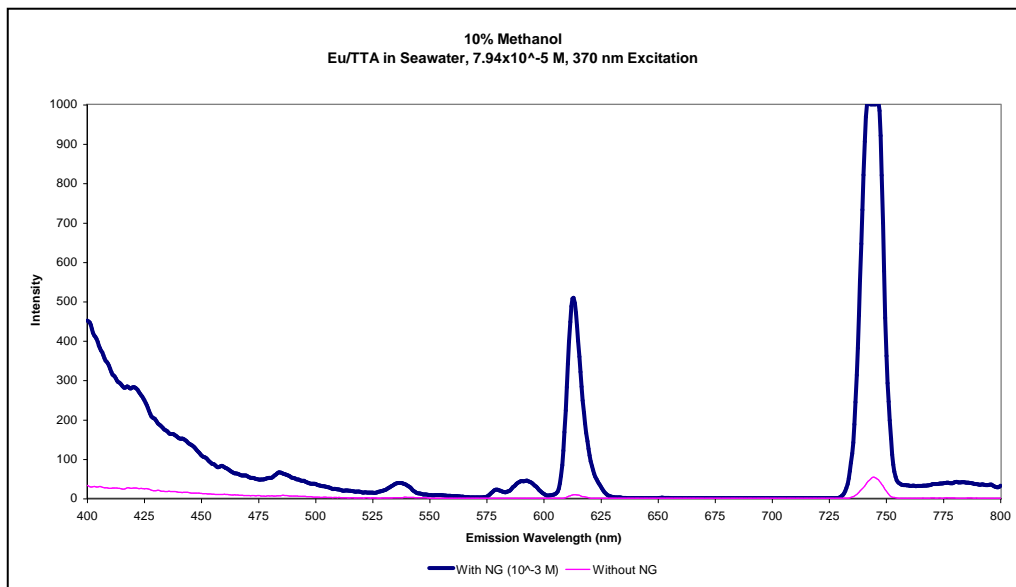


Figure 97 – Eu/TTA  $7.94 \times 10^{-5}$  M Emission in Seawater Under 370 nm Excitation, With and Without Nitroglycerin, 10% Methanol

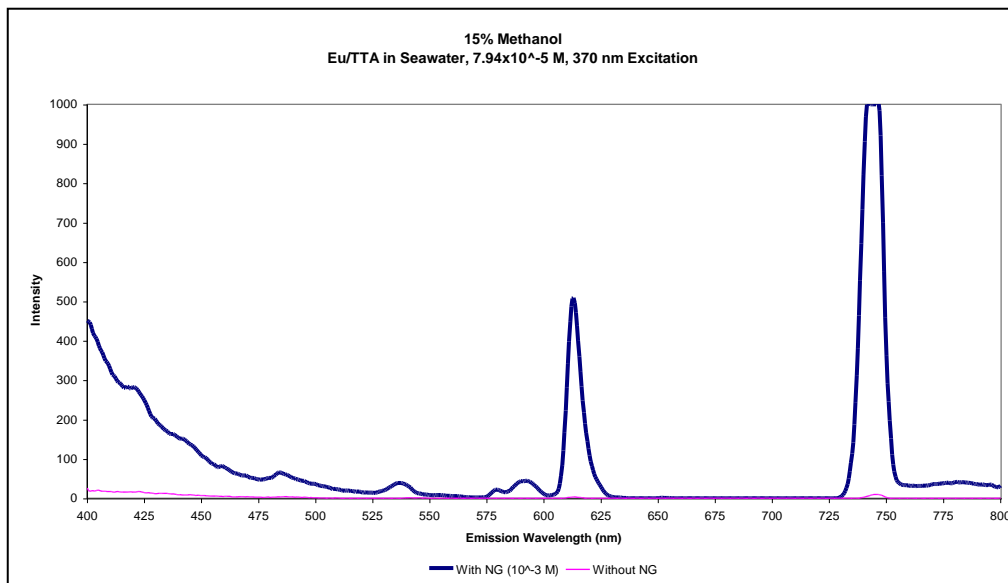


Figure 98 – Eu/TTA  $7.94 \times 10^{-5}$  M Emission in Seawater Under 370 nm Excitation, With and Without Nitroglycerin, 15% Methanol

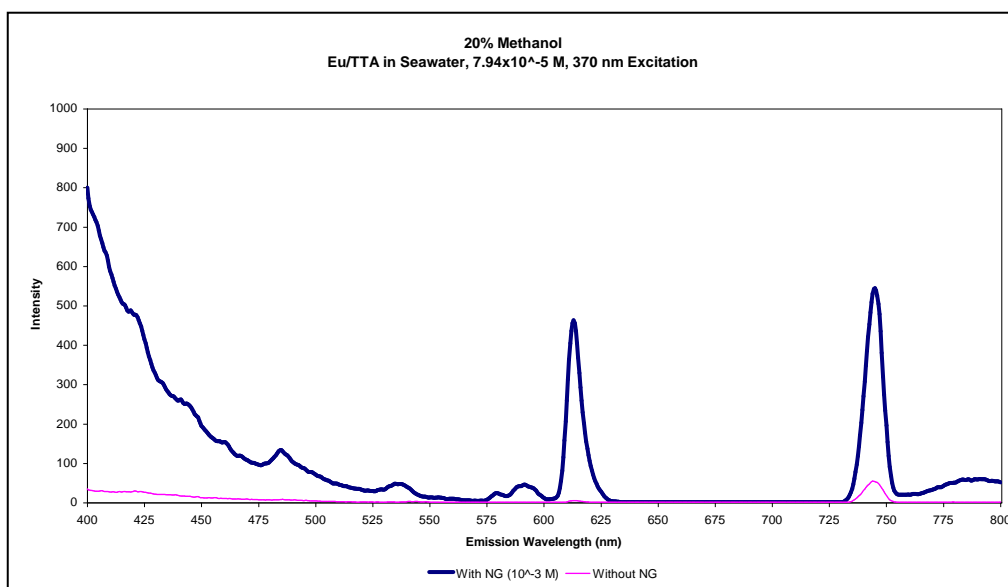


Figure 99 – Eu/TTA  $7.94 \times 10^{-5}$  M Emission in Seawater Under 370 nm Excitation, With and Without Nitroglycerin, 20% Methanol

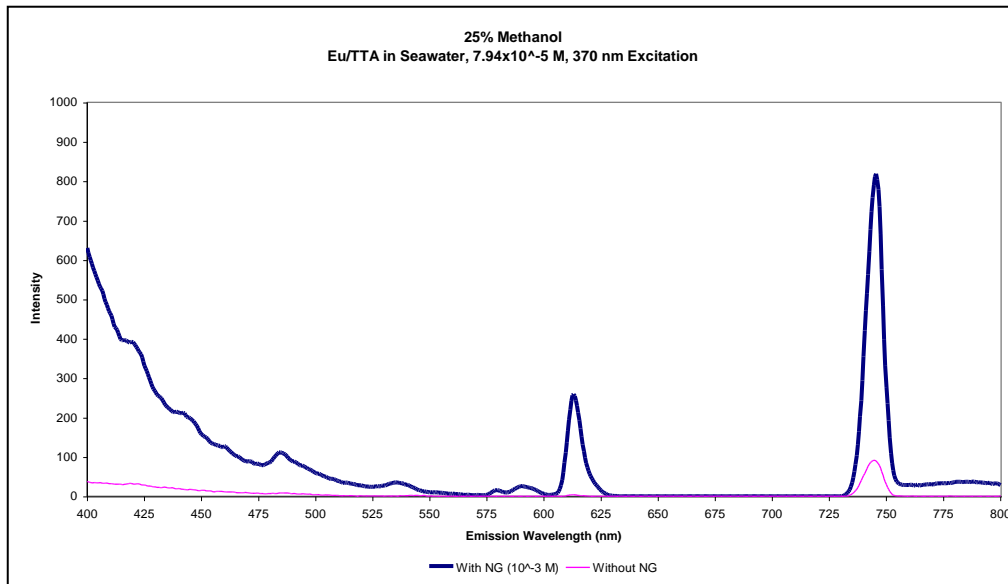


Figure 100 – Eu/TTA  $7.94 \times 10^{-5}$  M Emission in Seawater Under 370 nm Excitation, With and Without Nitroglycerin, 25% Methanol

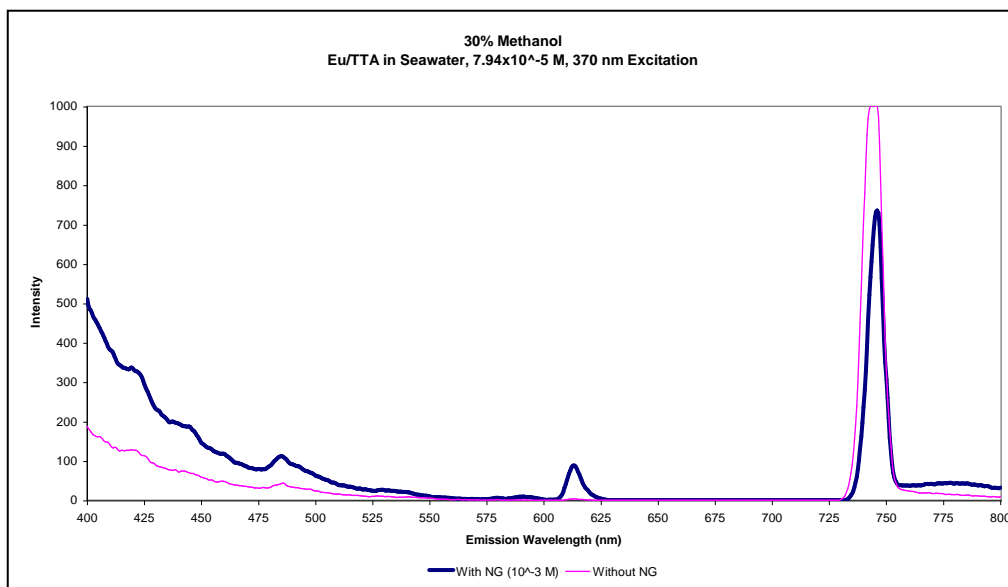


Figure 101 – Eu/TTA  $7.94 \times 10^{-5}$  M Emission in Seawater Under 370 nm Excitation, With and Without Nitroglycerin, 30% Methanol

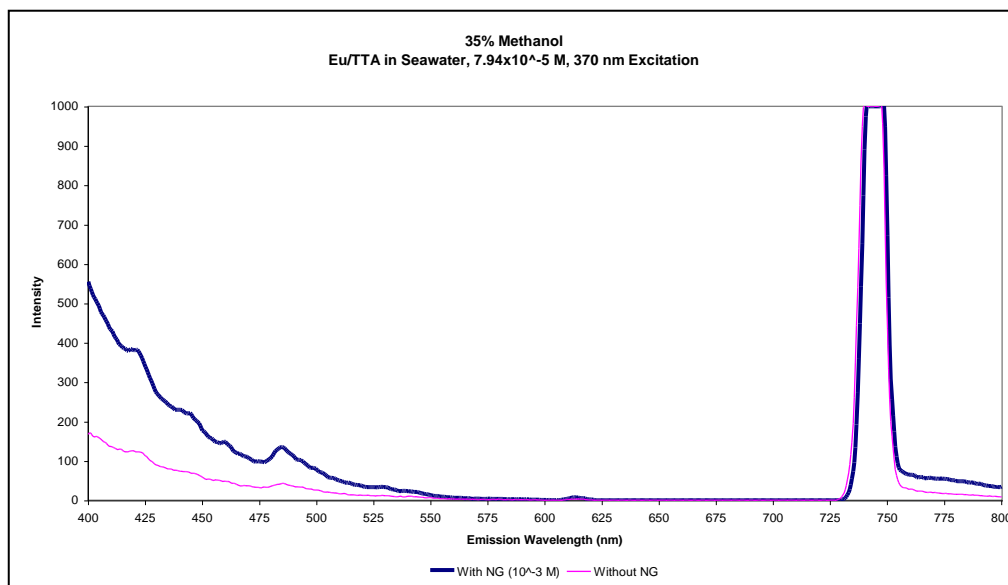


Figure 102 – Eu/TTA  $7.94 \times 10^{-5}$  M Emission in Seawater Under 370 nm Excitation, With and Without Nitroglycerin, 35% Methanol

## A1-4 Nitroglycerin Detection Limit

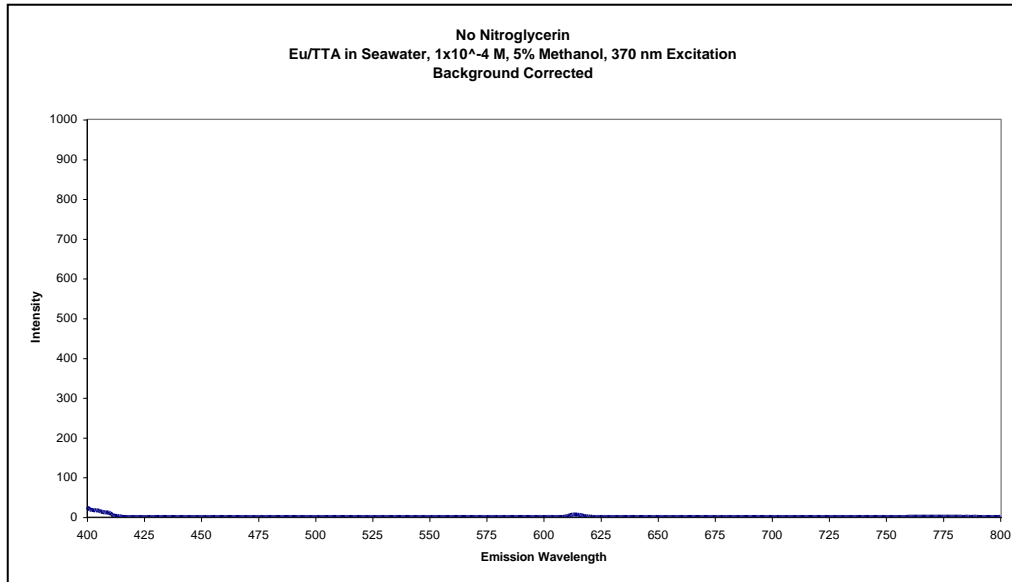


Figure 103 – Eu/TTA  $1 \times 10^{-4}$  M Emission in Seawater Under 370 nm Excitation, 5% Methanol, No Nitroglycerin

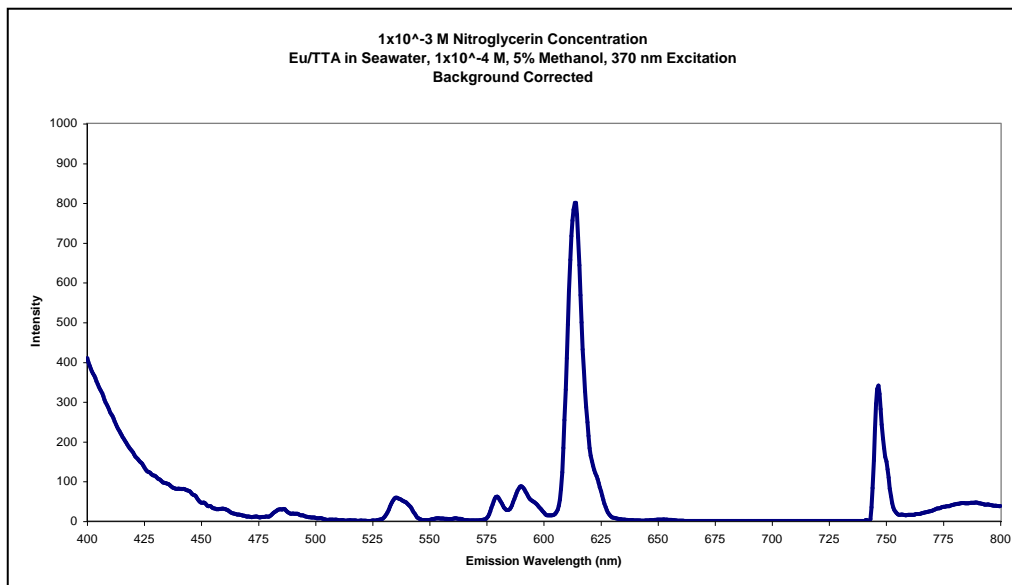


Figure 104 – Eu/TTA  $1 \times 10^{-4}$  M Emission in Seawater Under 370 nm Excitation, 5% Methanol,  $1 \times 10^{-3}$  M Nitroglycerin

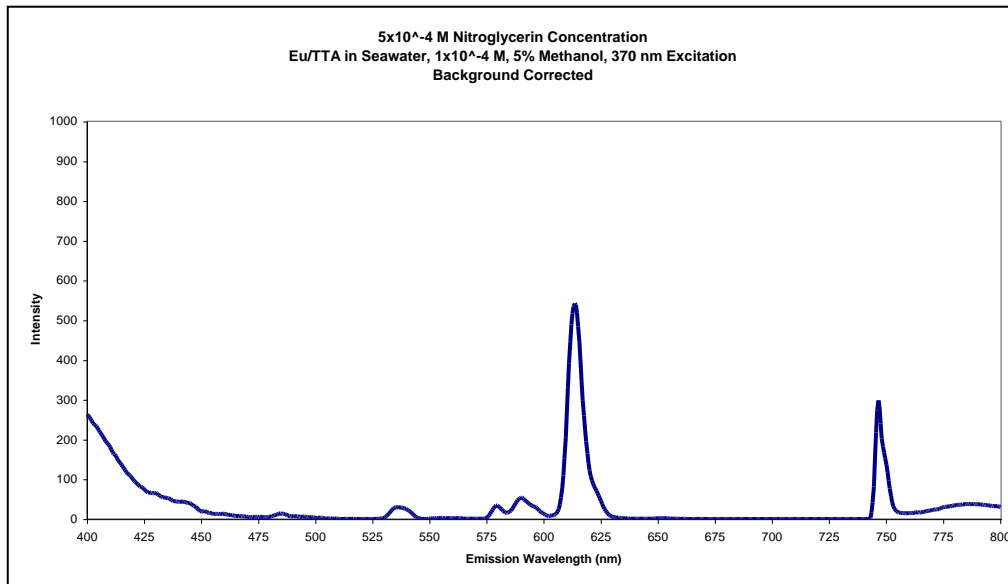


Figure 105 – Eu/TTA 1x10<sup>-4</sup> M Emission in Seawater Under 370 nm Excitation, 5% Methanol, 5x10<sup>-4</sup> M Nitroglycerin

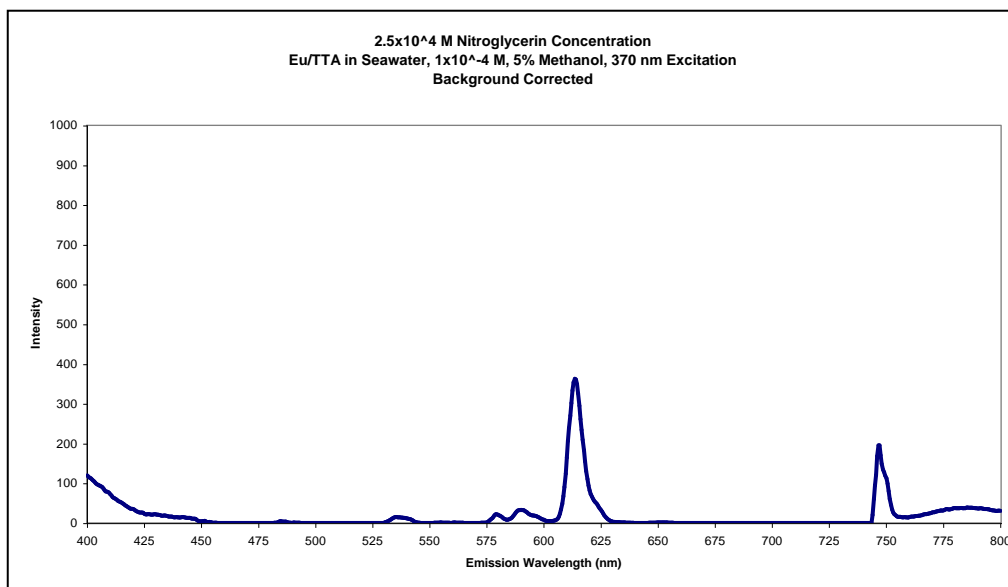


Figure 106 – Eu/TTA 1x10<sup>-4</sup> M Emission in Seawater Under 370 nm Excitation, 5% Methanol, 2.5x10<sup>-4</sup> M Nitroglycerin



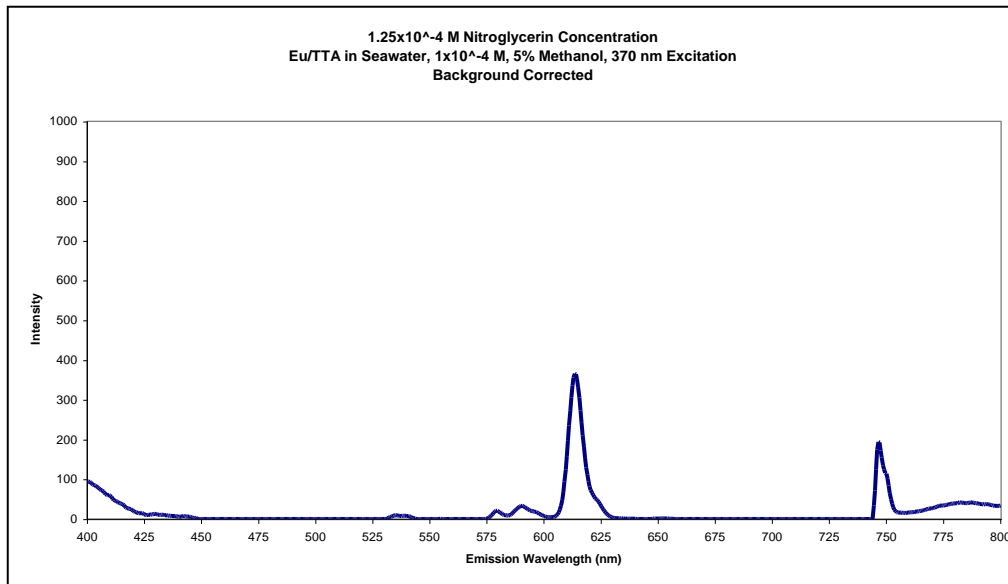


Figure 107 – Eu/TTA 1x10<sup>-4</sup> M Emission in Seawater Under 370 nm Excitation, 5% Methanol, 1.25x10<sup>-4</sup> M Nitroglycerin

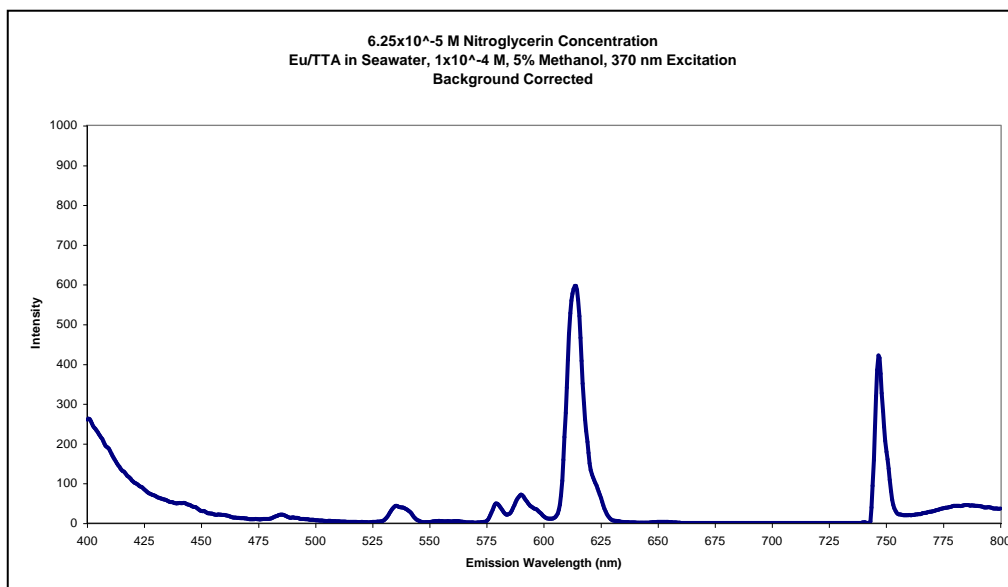


Figure 108 – Eu/TTA 1x10<sup>-4</sup> M Emission in Seawater Under 370 nm Excitation, 5% Methanol, 6.25x10<sup>-5</sup> M Nitroglycerin

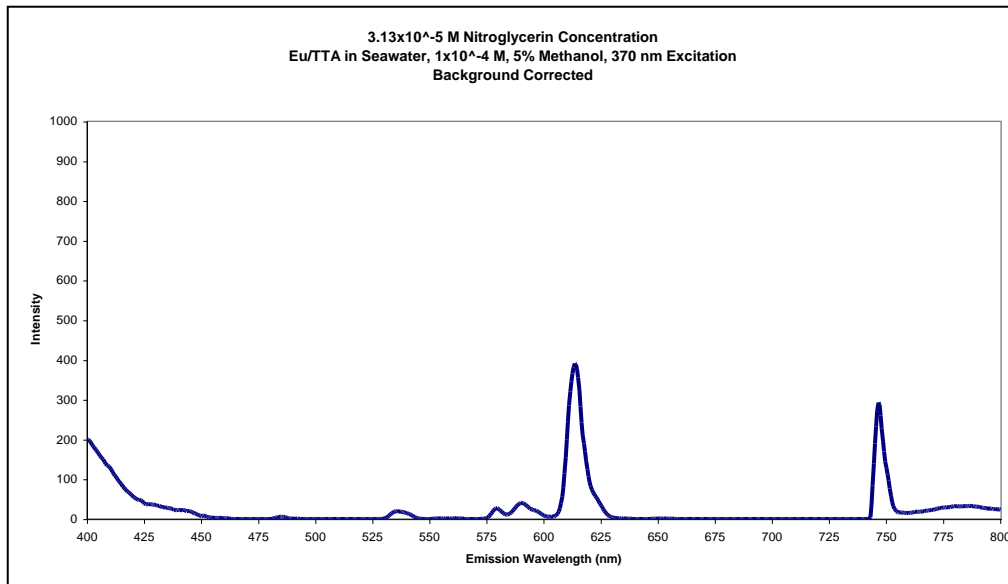


Figure 109 – Eu/TTA 1x10<sup>-4</sup> M Emission in Seawater Under 370 nm Excitation, 5% Methanol, 3.13x10<sup>-5</sup> M Nitroglycerin

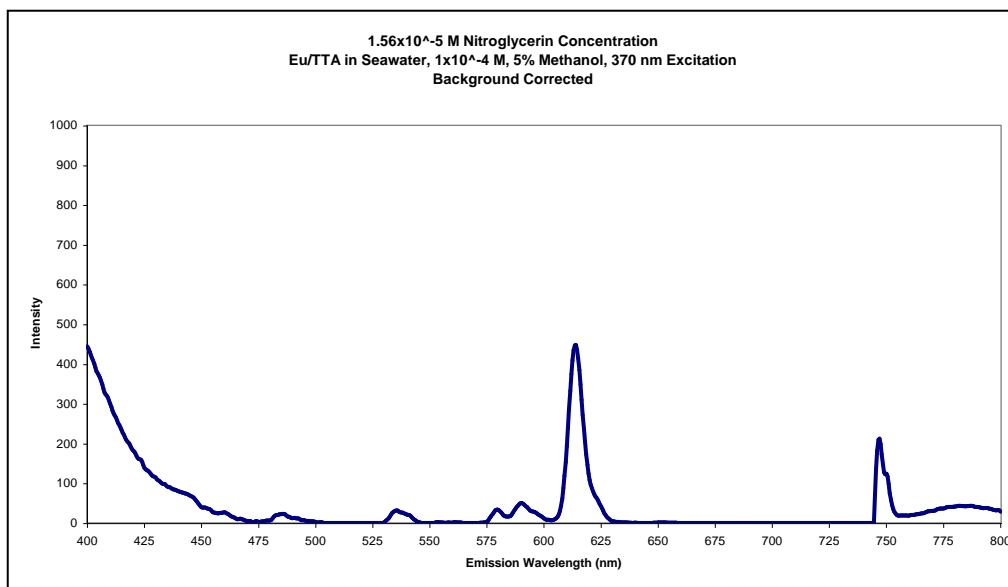


Figure 110 – Eu/TTA 1x10<sup>-4</sup> M Emission in Seawater Under 370 nm Excitation, 5% Methanol, 1.56x10<sup>-5</sup> M Nitroglycerin

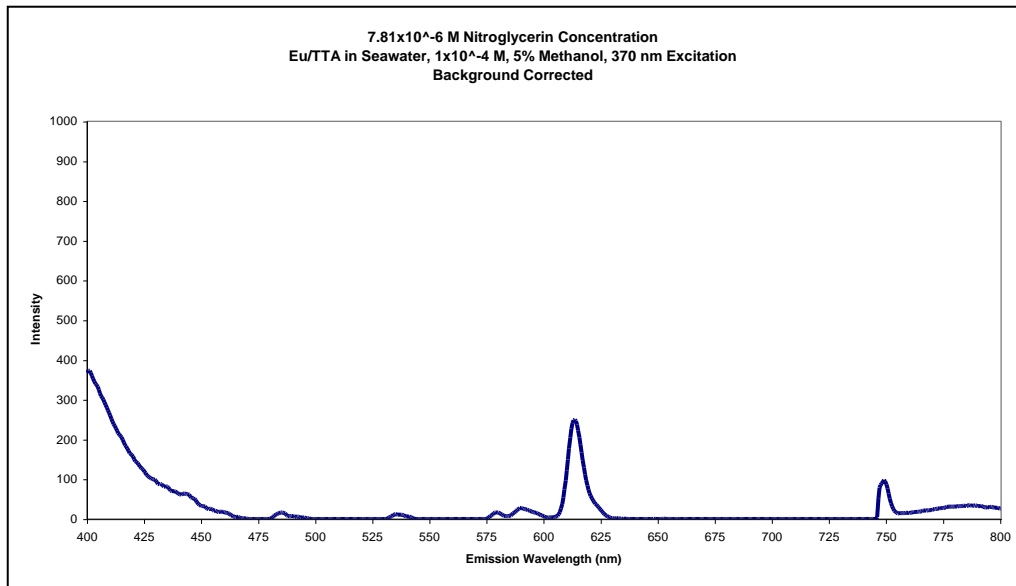


Figure 111 – Eu/TTA 1x10<sup>-4</sup> M Emission in Seawater Under 370 nm Excitation, 5% Methanol, 7.81x10<sup>-6</sup> M Nitroglycerin

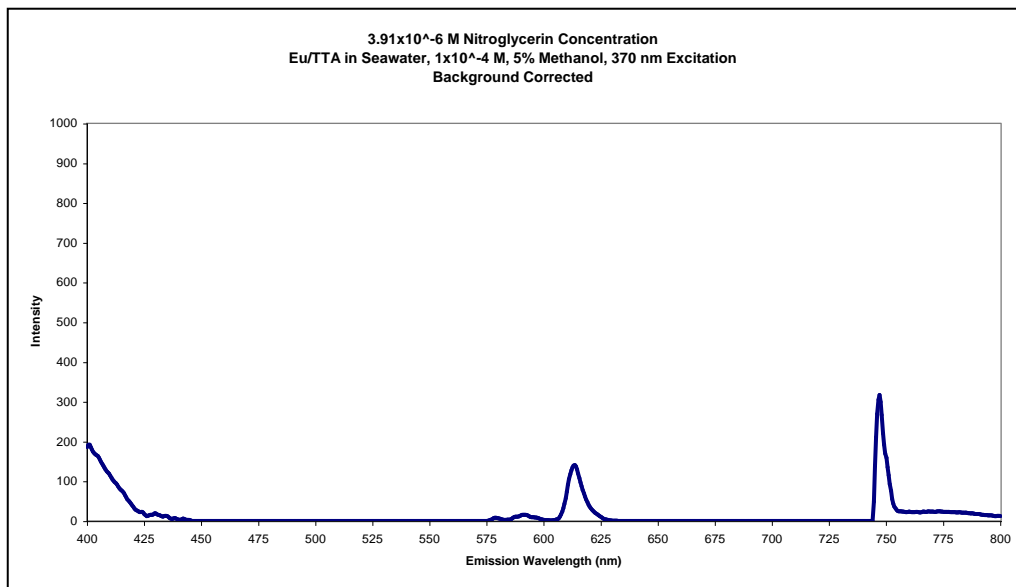


Figure 112 – Eu/TTA 1x10<sup>-4</sup> M Emission in Seawater Under 370 nm Excitation. 5% Methanol. 3.91x10<sup>-6</sup> M Nitroglycerin

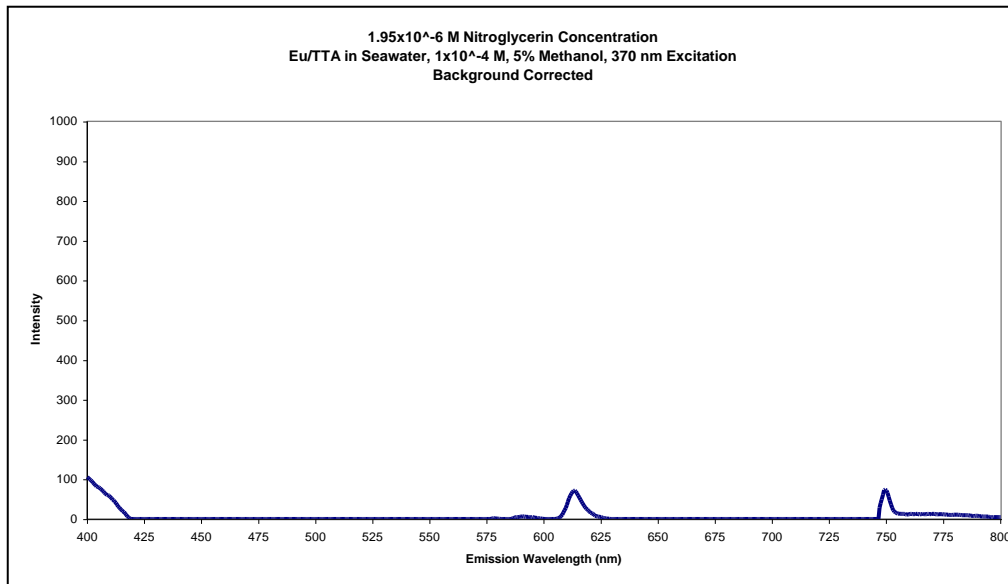


Figure 113 – Eu/TTA 1x10<sup>-4</sup> M Emission in Seawater Under 370 nm Excitation, 5% Methanol, 1.95x10<sup>-6</sup> M Nitroglycerin

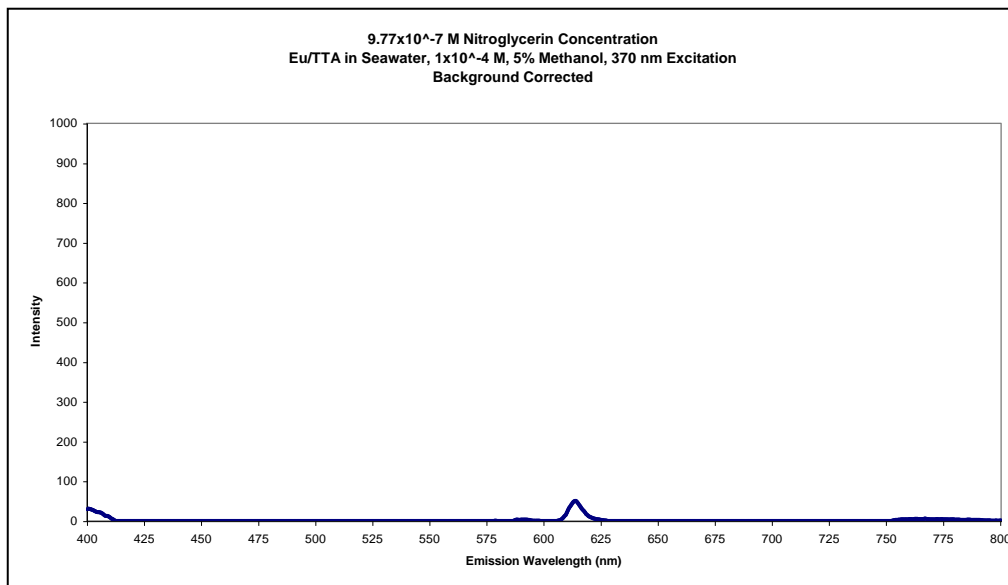


Figure 114 – Eu/TTA 1x10<sup>-4</sup> M Emission in Seawater Under 370 nm Excitation, 5% Methanol, 9.77x10<sup>-7</sup> M Nitroglycerin

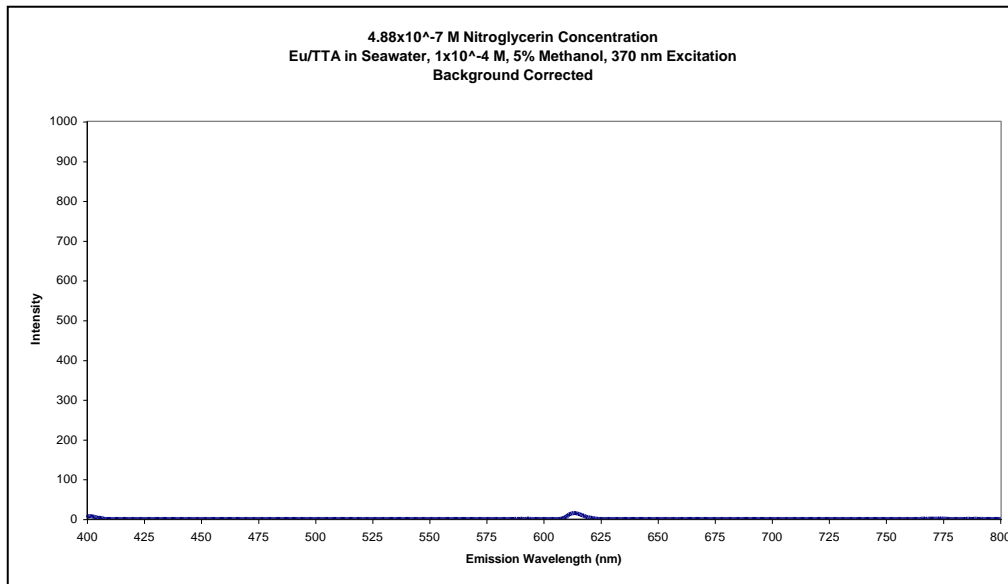


Figure 115 – Eu/TTA 1x10<sup>-4</sup> M Emission in Seawater Under 370 nm Excitation, 5% Methanol, 4.88x10<sup>-7</sup> M Nitroglycerin

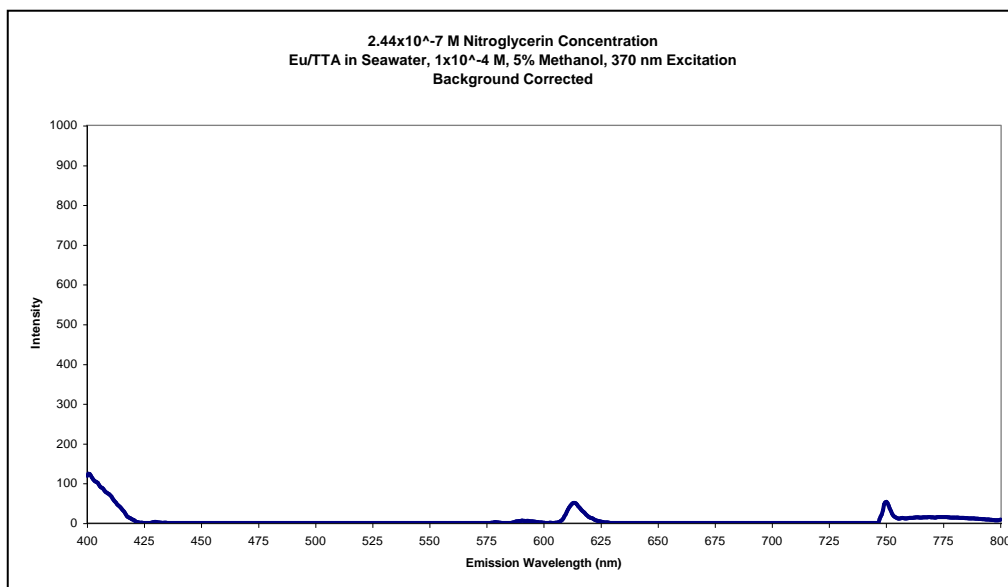


Figure 116 – Eu/TTA 1x10<sup>-4</sup> M Emission in Seawater Under 370 nm Excitation, 5% Methanol, 2.44x10<sup>-7</sup> M Nitroglycerin

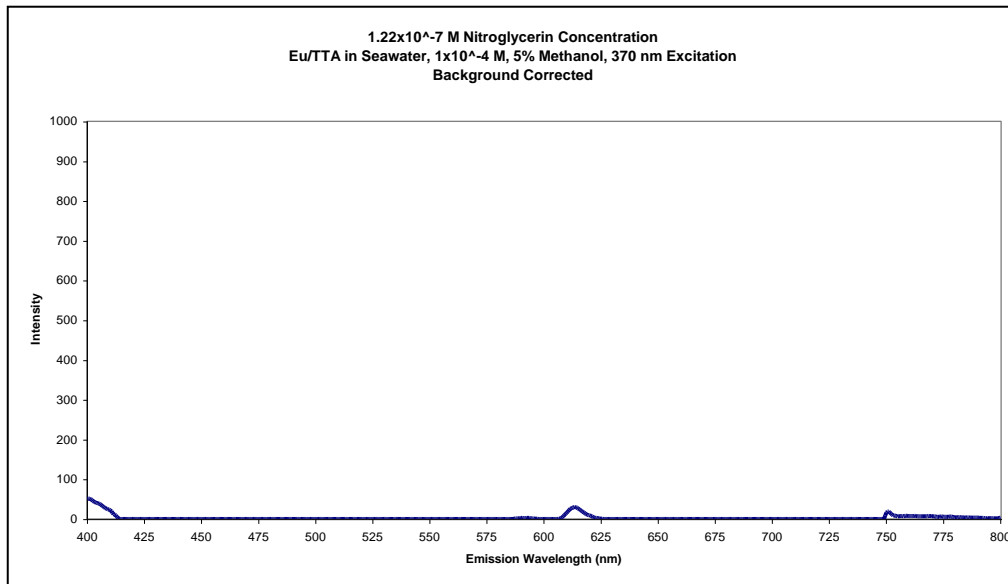


Figure 117 – Eu/TTA 1x10<sup>-4</sup> M Emission in Seawater Under 370 nm Excitation. 5% Methanol. 1.22x10<sup>-7</sup> M Nitroglycerin

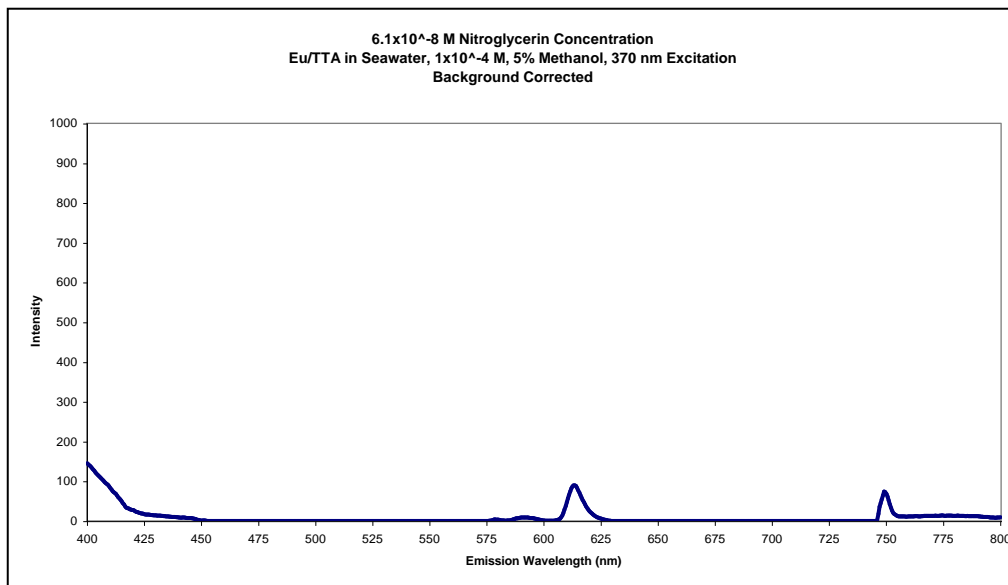


Figure 118 – Eu/TTA 1x10<sup>-4</sup> M Emission in Seawater Under 370 nm Excitation, 5% Methanol, 6.1x10<sup>-8</sup> M Nitroglycerin

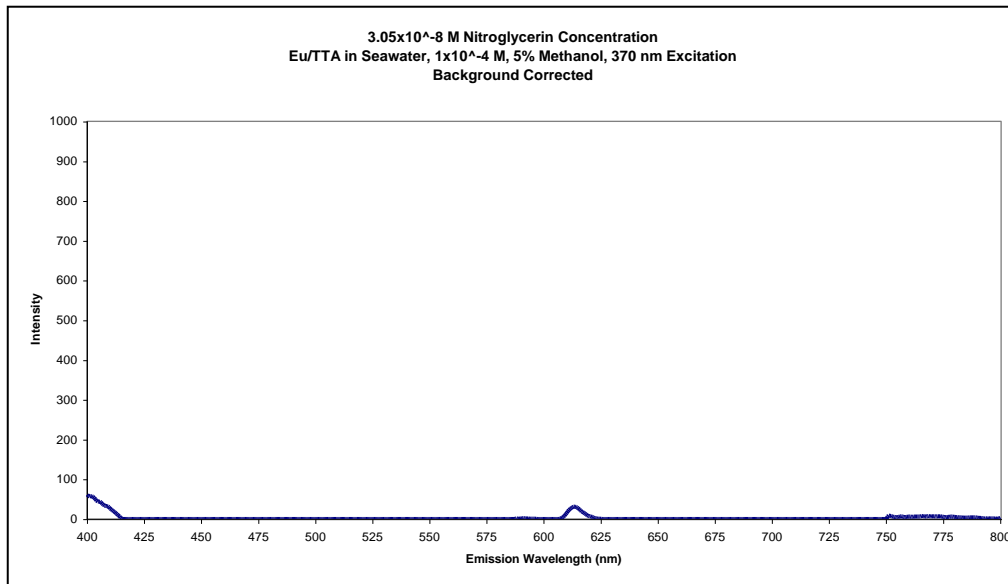


Figure 119 – Eu/TTA 1x10<sup>-4</sup> M Emission in Seawater Under 370 nm Excitation, 5% Methanol, 3.05x10<sup>-8</sup> M Nitroglycerin

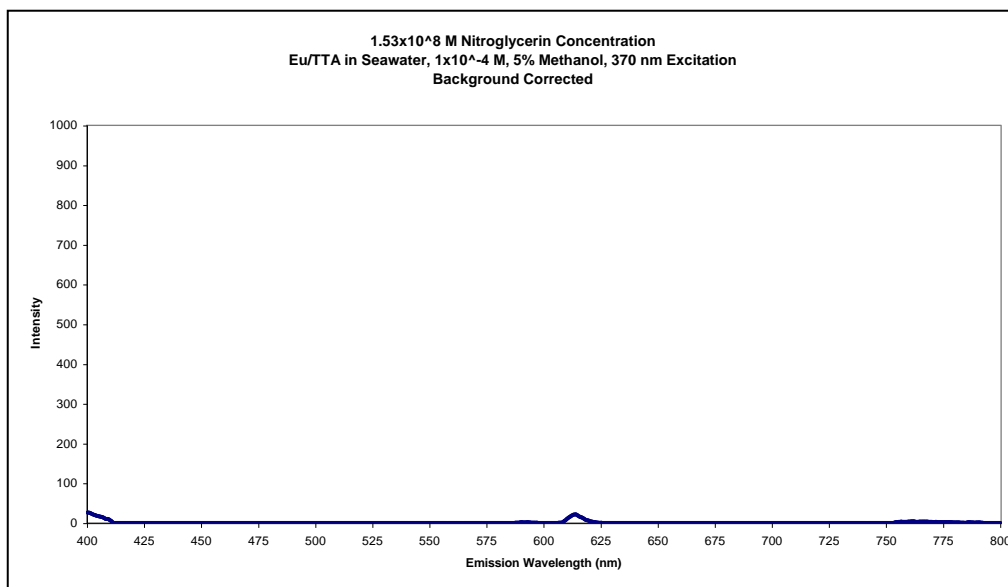


Figure 120 – Eu/TTA 1x10<sup>-4</sup> M Emission in Seawater Under 370 nm Excitation, 5% Methanol, 1.53x10<sup>-8</sup> M Nitroglycerin

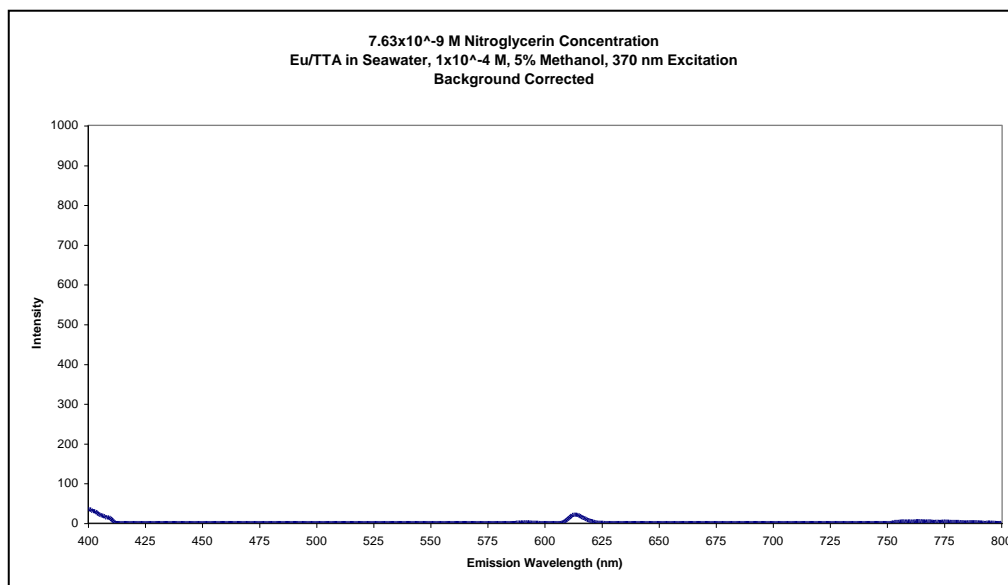


Figure 121 – Eu/TTA 1x10<sup>-4</sup> M Emission in Seawater Under 370 nm Excitation, 5% Methanol, 7.63x10<sup>-9</sup> M Nitroglycerin



## A1-5 Fresh Water Testing

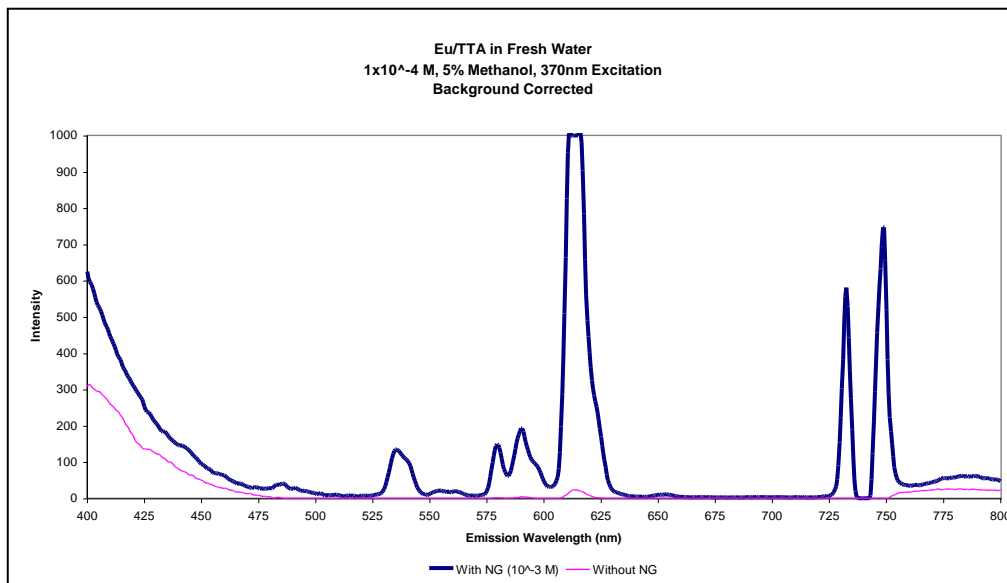


Figure 122 – Eu/TTA  $1 \times 10^{-4}$  M Emission in Fresh Water Under 370 nm Excitation, 5% Methanol, With and Without Nitroglycerin

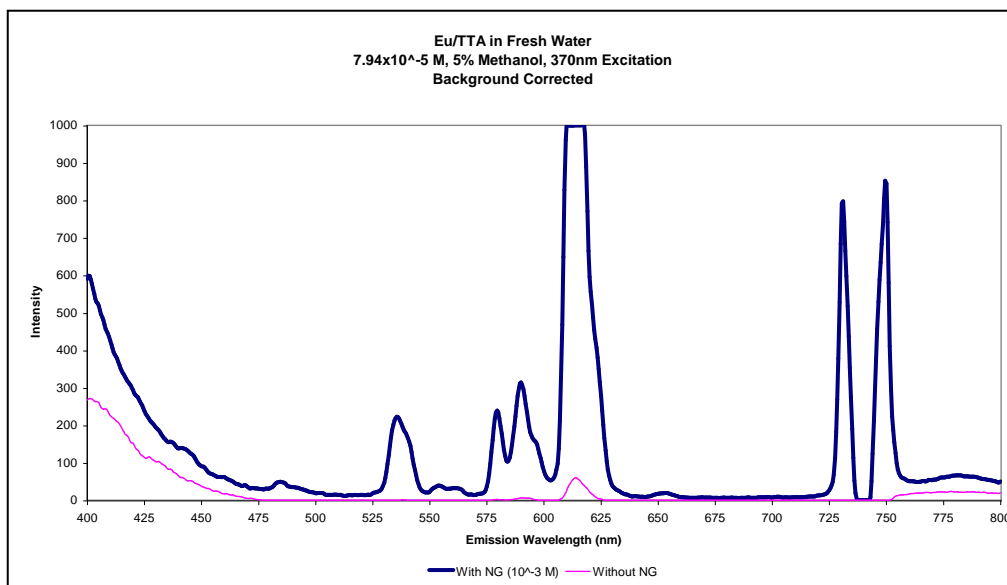


Figure 123 – Eu/TTA  $7.94 \times 10^{-5}$  M Emission in Fresh Water Under 370 nm Excitation, 5% Methanol, With and Without Nitroglycerin

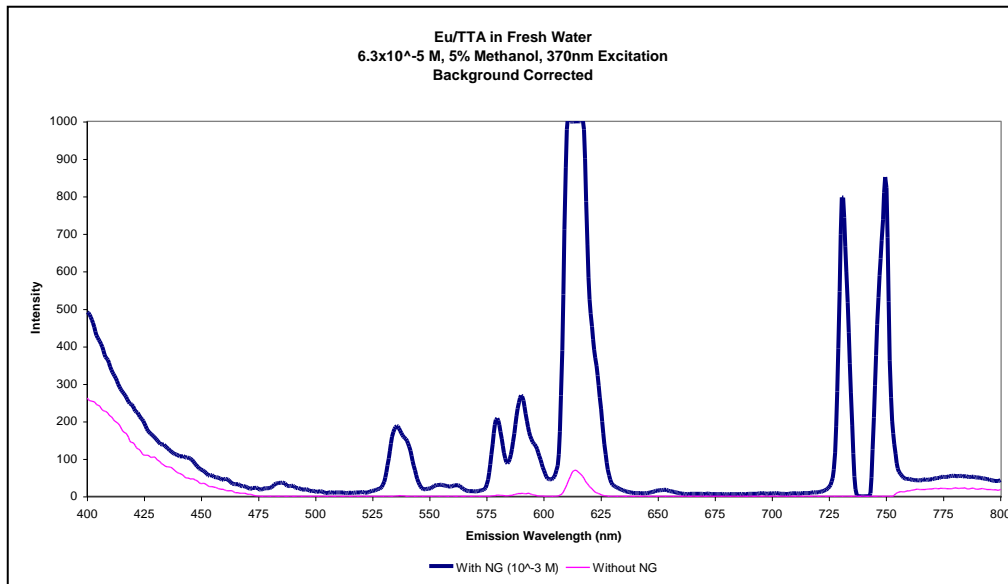


Figure 124 – Eu/TTA 6.3x10<sup>-5</sup> M Emission in Fresh Water Under 370 nm Excitation, 5% Methanol, With and Without Nitroglycerin

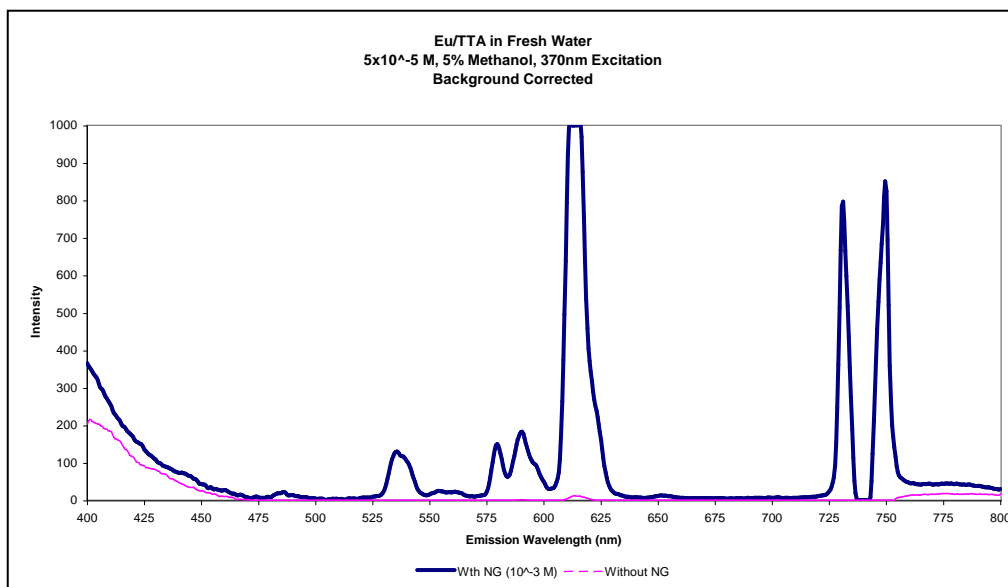


Figure 125 – Eu/TTA 5x10<sup>-5</sup> M Emission in Fresh Water Under 370 nm Excitation, 5% Methanol, With and Without Nitroglycerin

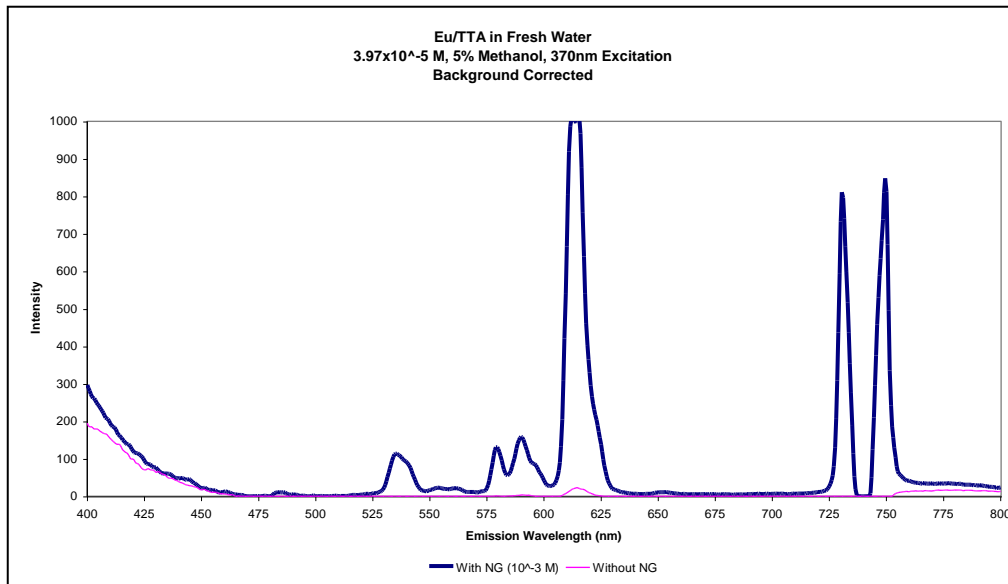


Figure 126 – Eu/TTA  $3.97 \times 10^{-5}$  M Emission in Fresh Water Under 370 nm Excitation, 5% Methanol, With and Without Nitroglycerin

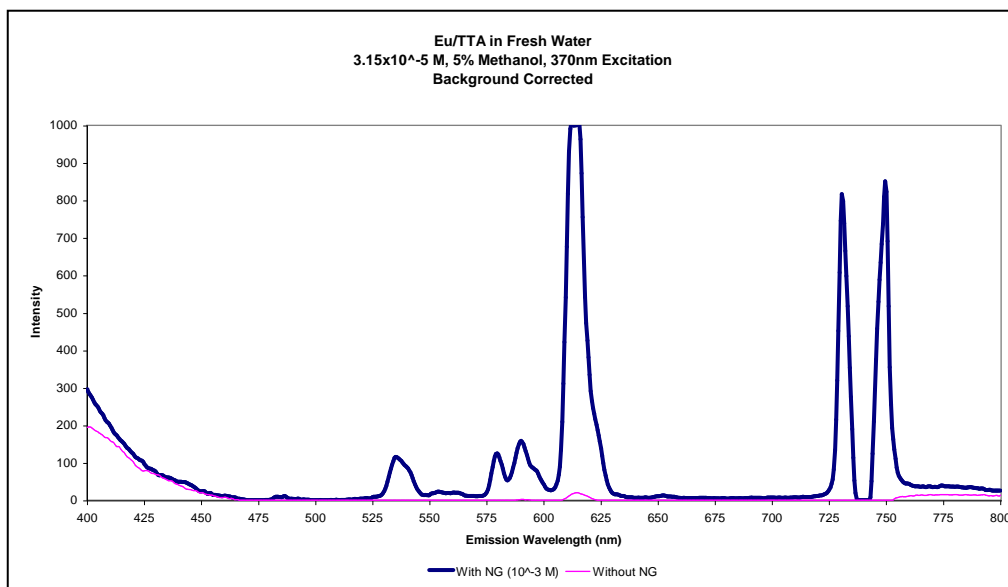


Figure 127 – Eu/TTA  $3.15 \times 10^{-5}$  M Emission in Fresh Water Under 370 nm Excitation, 5% Methanol, With and Without Nitroglycerin

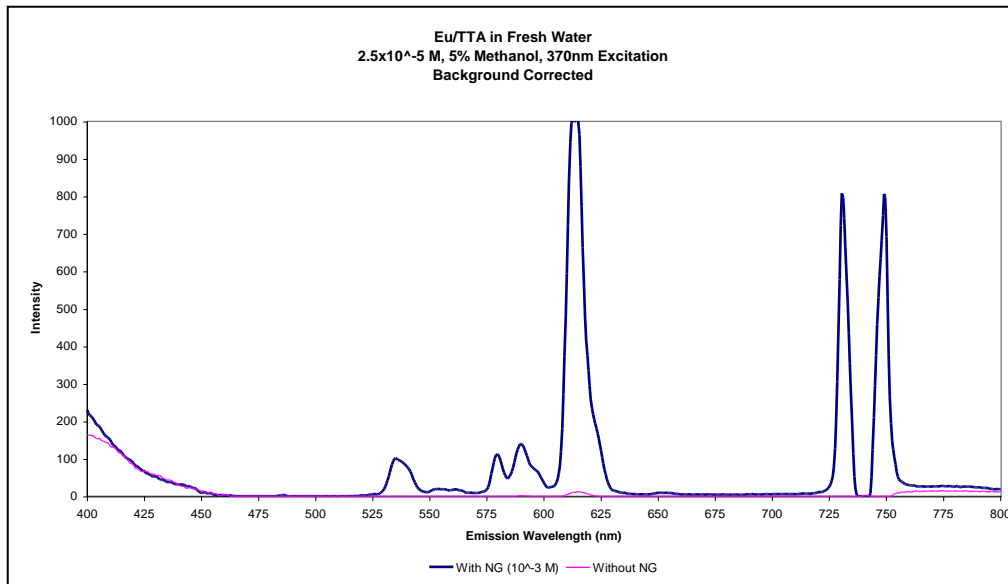


Figure 128 – Eu/TTA  $2.5 \times 10^{-5}$  M Emission in Fresh Water Under 370 nm Excitation, 5% Methanol, With and Without Nitroglycerin

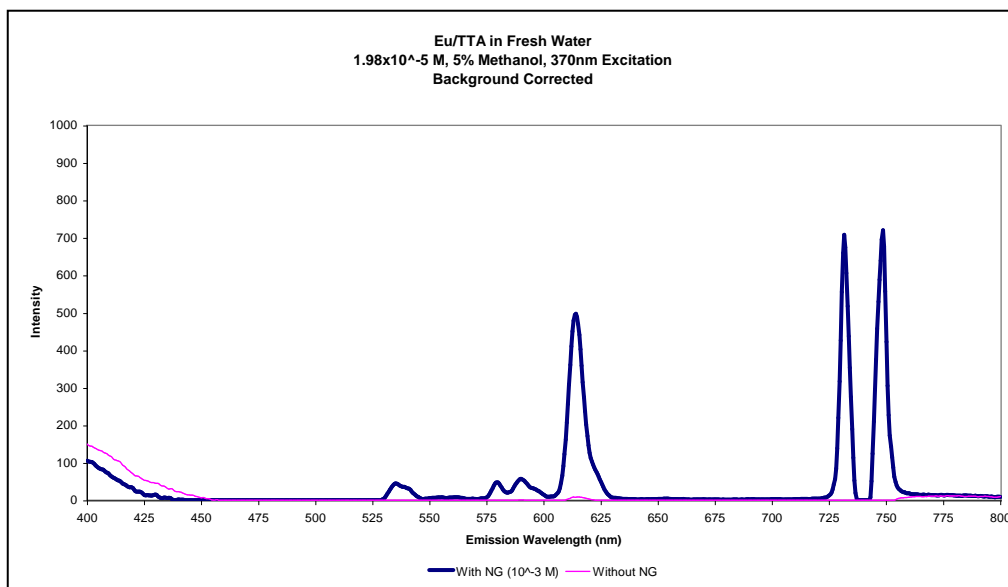


Figure 129 – Eu/TTA  $1.98 \times 10^{-5}$  M Emission in Fresh Water Under 370 nm Excitation, 5% Methanol, With and Without Nitroglycerin

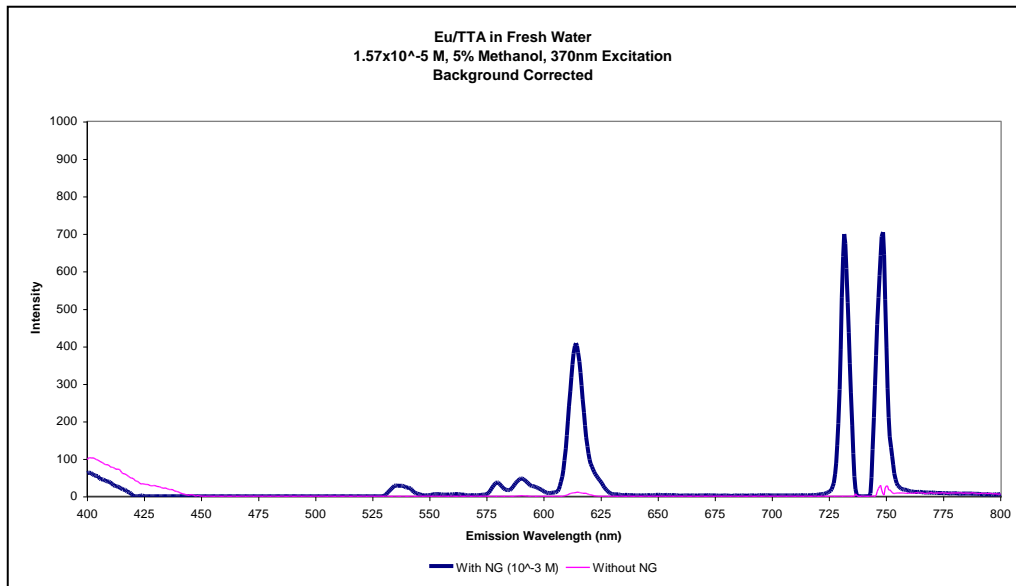


Figure 130 – Eu/TTA  $1.57 \times 10^{-5}$  M Emission in Fresh Water Under 370 nm Excitation, 5% Methanol, With and Without Nitroglycerin

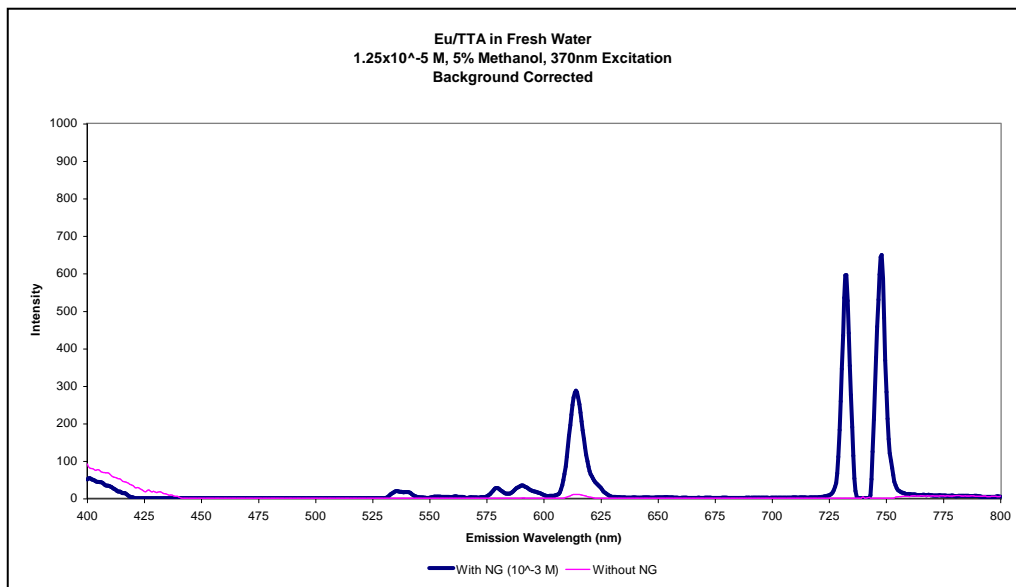


Figure 131 – Eu/TTA  $1.25 \times 10^{-5}$  M Emission in Fresh Water Under 370 nm Excitation, 5% Methanol, With and Without Nitroglycerin

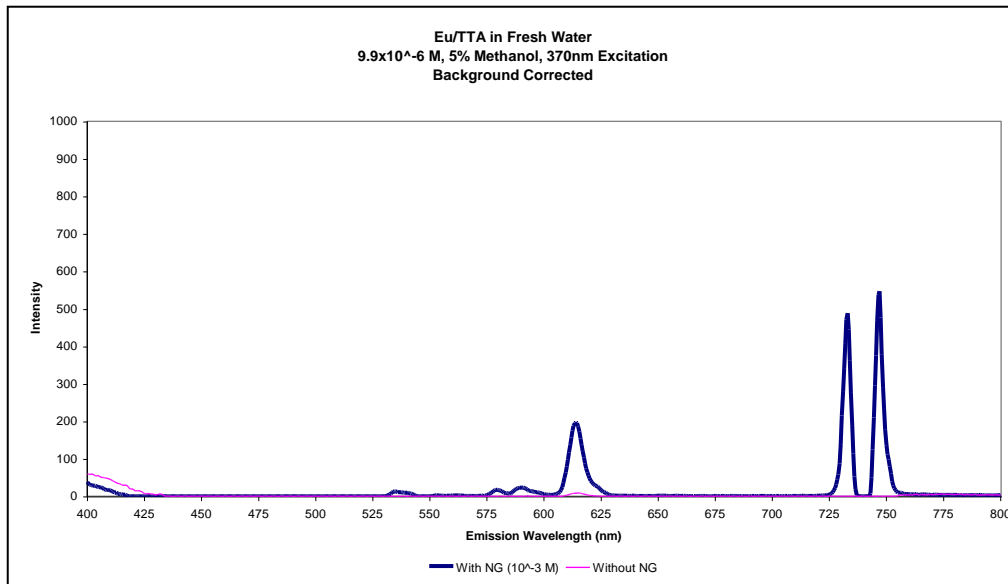


Figure 132 – Eu/TTA 9.9x10<sup>-6</sup> M Emission in Fresh Water Under 370 nm Excitation, 5% Methanol, With and Without Nitroglycerin

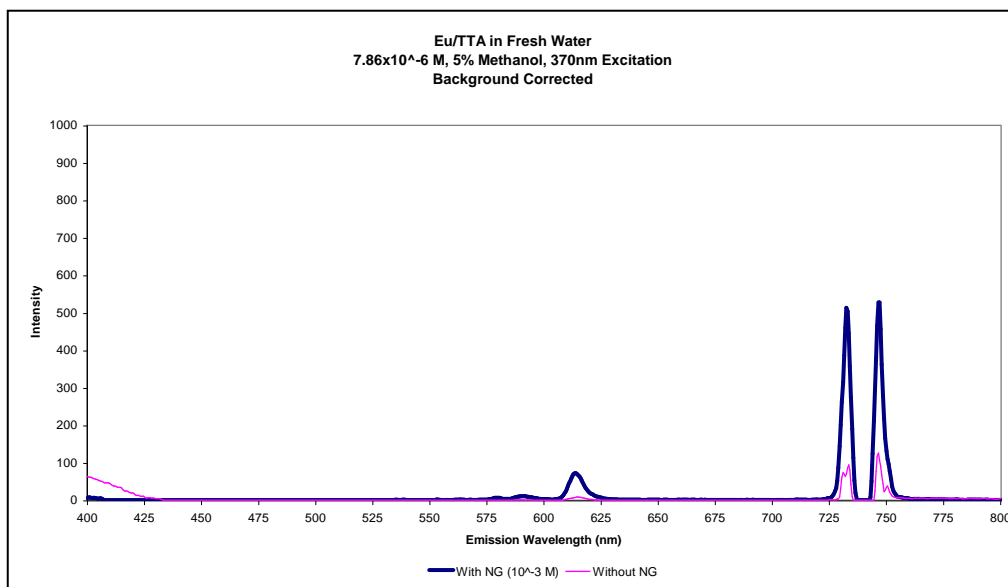


Figure 133 – Eu/TTA 7.86x10<sup>-6</sup> M Emission in Fresh Water Under 370 nm Excitation, 5% Methanol, With and Without Nitroglycerin

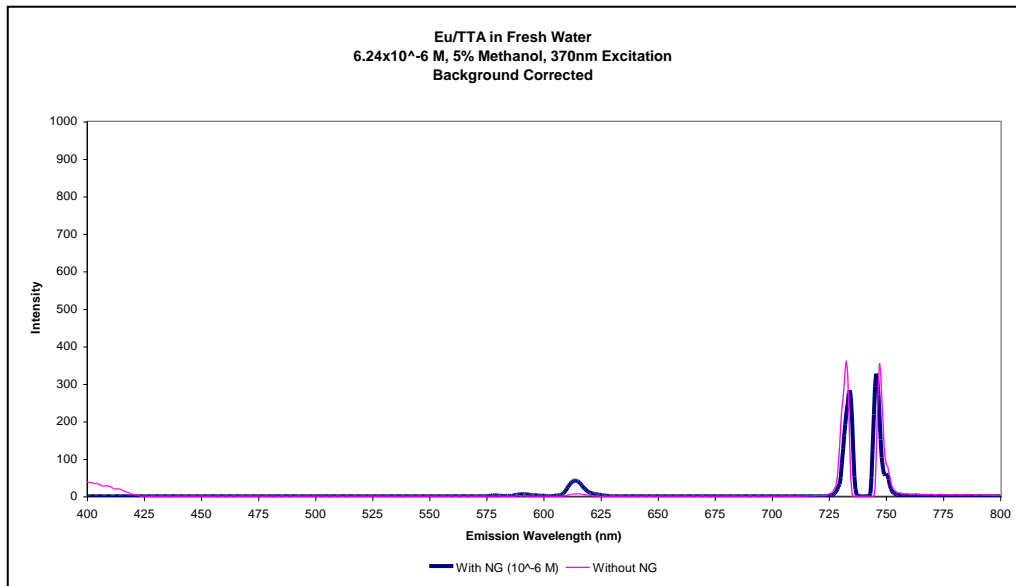


Figure 134 – Eu/TTA 6.24x10<sup>-6</sup> M Emission in Fresh Water Under 370 nm Excitation, 5% Methanol, With and Without Nitroglycerin

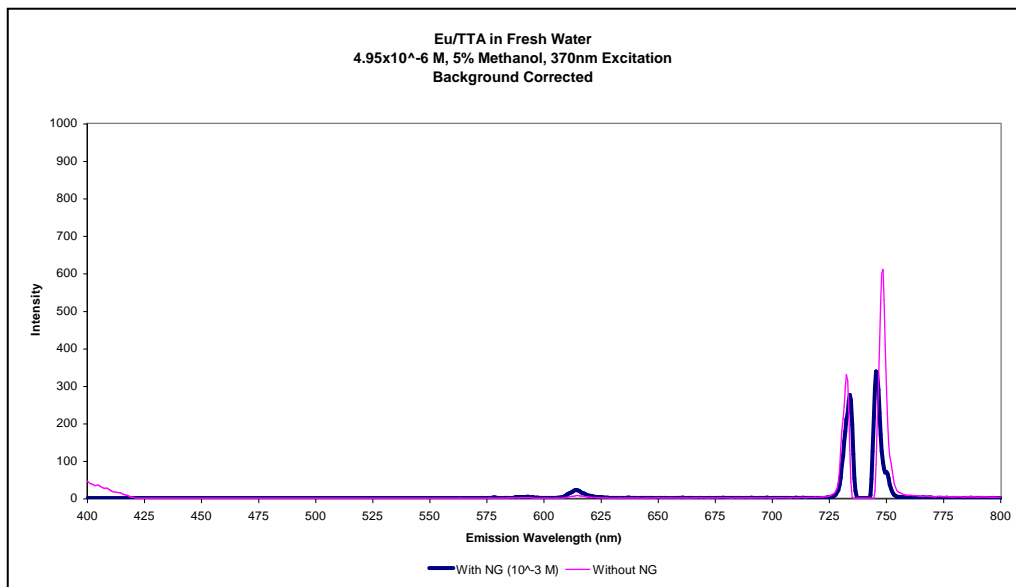


Figure 135 – Eu/TTA 4.95x10<sup>-6</sup> M Emission in Fresh Water Under 370 nm Excitation, 5% Methanol, With and Without Nitroglycerin

## A1-6 Acid and Metal Ion Tests

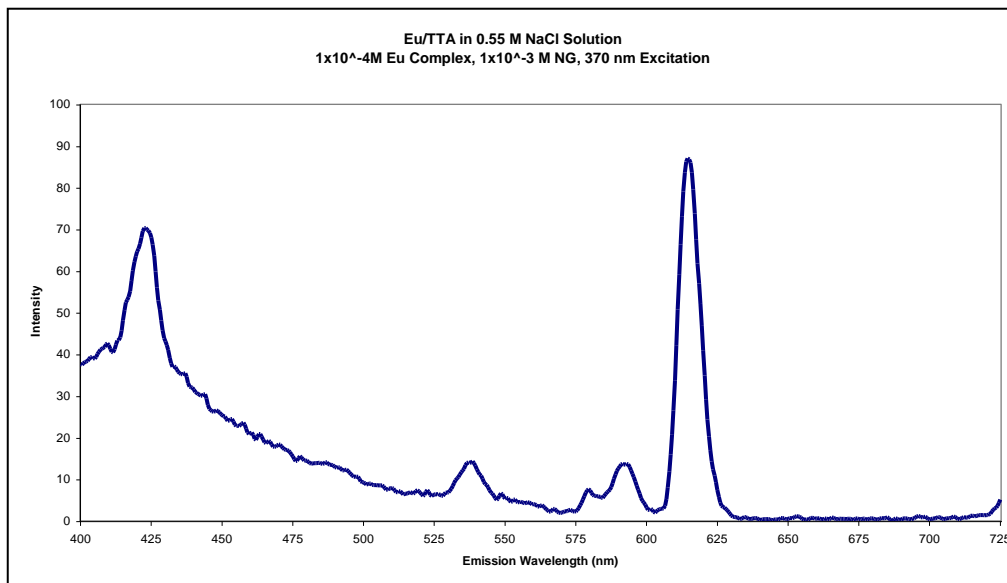


Figure 136 – Eu/TTA  $1 \times 10^{-4}$  M Emission in 0.55 M NaCl Solution Under 370 nm Excitation, 5% Methanol,  $1 \times 10^{-3}$  M Nitroglycerin

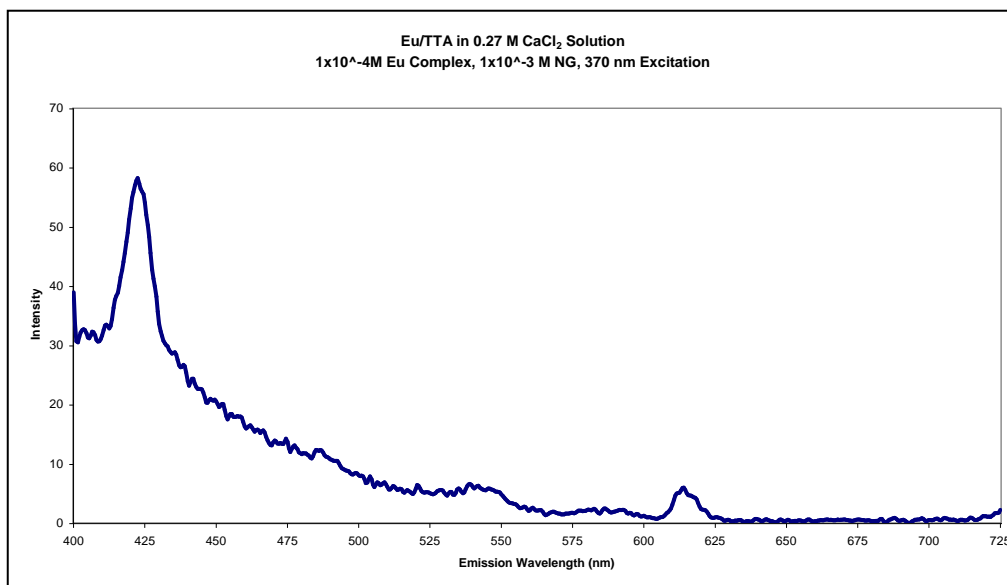


Figure 137 – Eu/TTA  $1 \times 10^{-4}$  M Emission in 0.27 M CaCl<sub>2</sub> Solution Under 370 nm Excitation, 5% Methanol,  $1 \times 10^{-3}$  M Nitroglycerin



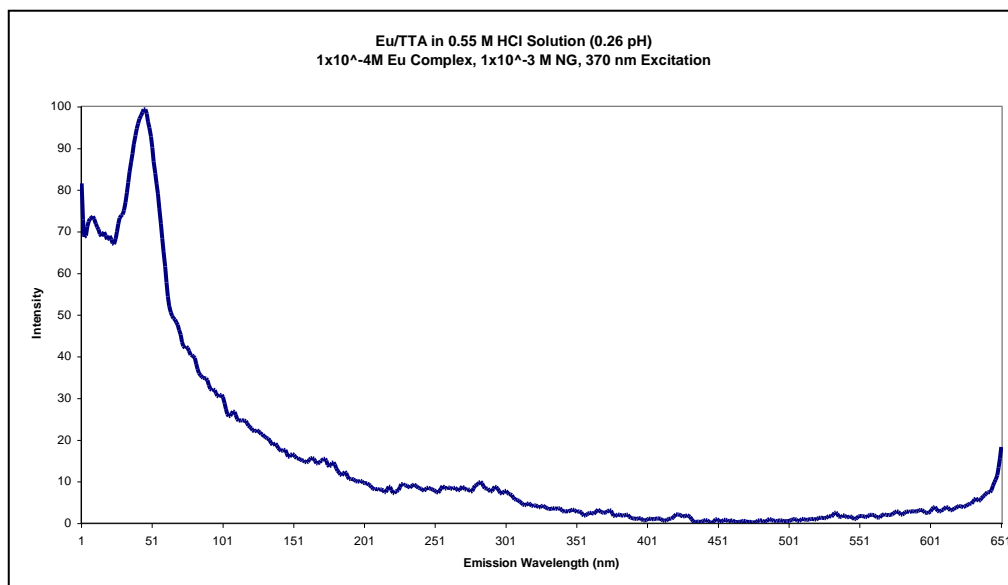


Figure 138 – Eu/TTA 1x10<sup>-4</sup> M Emission in 0.55 M HCl Solution Under 370 nm Excitation, 5% Methanol, 1x10<sup>-3</sup> M Nitroglycerin

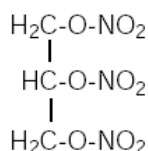
## A2 Nitroglycerin Sublingual Tablets Information Sheet

### NitroQuick® (Nitroglycerin Sublingual Tablets, USP)

#### Rx Only

**DESCRIPTION** NitroQuick® tablets are stabilized sublingual nitroglycerin tablets manufactured with a technology designed to stabilize the formulation. (This stabilized formulation has been shown to be more stable and more uniform than conventional molded tablets.) NitroQuick® tablets contain 0.3 mg (1/200 grain), 0.4 mg (1/150 grain) and 0.6 mg (1/100 grain) nitroglycerin. Also contains corn starch, crospovidone, lactose, magnesium stearate, and povidone.

Nitroglycerin, an organic nitrate, is a vasodilating agent. The chemical name for nitroglycerin is 1,2,3 propanetriol trinitrate and the chemical structure is:



$\text{C}_3\text{H}_5\text{N}_3\text{O}_9$

MOL WT 227.09

**ACTIONS/CLINICAL PHARMACOLOGY** Relaxation of vascular smooth muscle is the principal pharmacologic action of nitroglycerin. The mechanism by which nitroglycerin produces relaxation of smooth muscle is unknown. Although venous effects predominate, nitroglycerin produces, in a dose-related manner, dilation of both arterial and venous beds. Dilation of the postcapillary vessels, including large veins, promotes peripheral pooling of blood and decreases venous return to the heart, reducing left ventricular end-diastolic pressure (preload). Arteriolar relaxation reduces systemic vascular resistance and arterial pressure (afterload). Myocardial oxygen consumption or demand (as measured by the pressure-rate product, tension-time index and stroke-work index) is decreased by both the arterial and venous effects of nitroglycerin, and a more favorable supply-demand ratio can be achieved.

Nitroglycerin also dilates large epicardial coronary arteries; however, the extent to which this effect contributes to the relief of exertional angina is unclear.

Therapeutic doses of nitroglycerin may reduce systolic, diastolic and mean arterial blood pressure. Effective coronary perfusion pressure is usually maintained, but can be compromised if blood pressure falls excessively or

increased heart rate decreases diastolic filling time.

Elevated central venous and pulmonary capillary wedge pressures, pulmonary vascular resistance and systemic vascular resistance are also reduced by nitroglycerin therapy. Heart rate is usually slightly increased, presumably a reflex response to the fall in blood pressure. Cardiac index may be increased, decreased, or unchanged. Patients with elevated left ventricular filling pressure and systemic vascular resistance values in conjunction with a depressed cardiac index are likely to experience an improvement in cardiac index. On the other hand, when filling pressures and cardiac index are normal, cardiac index may be slightly reduced by intravenous nitroglycerin.

**Mechanism Of Action** Nitroglycerin forms free radical nitric oxide (NO) which activates guanylate cyclase, resulting in an increase of guanosine 3'5' monophosphate (cyclic GMP) in smooth muscle and other tissues. This eventually leads to dephosphorylation of the light chain of myosin, which regulates the contractile state in smooth muscle, resulting in vasodilation.

**Pharmacokinetics And Metabolism** Nitroglycerin is rapidly absorbed following sublingual administration. Its onset of action is approximately one to three minutes. Significant pharmacologic effects are present for 30 to 60 minutes following administration by the above route.

Nitroglycerin is rapidly metabolized to dinitrates and mononitrates, with a short half-life, estimated at 1 to 4 minutes. A liver reductase enzyme is of primary importance in the metabolism of nitroglycerin to glycerol nitrate metabolites and organic nitrate. Two active major metabolites 1,2- and 1,3-dinitroglycerols are less potent vasodilators and have longer half-lives than the parent compound. Dinitrates are metabolized to mononitrates and ultimately glycerol. The monohydrate is not considered biologically active with respect to cardiovascular effects.

At plasma concentrations of between 50 and 500 ng/mL, the binding of nitroglycerin to plasma proteins is approximately 60%, while that of 1,2 dinitroglycerin and 1,3 dinitroglycerin is 60% and 30%, respectively. The activity and half-life of 1,2 dinitroglycerin and 1,3 dinitroglycerin are not well characterized. The mononitrate is not active.

**INDICATIONS AND USAGE** Nitroglycerin is indicated for the acute relief of an attack or prophylaxis of angina pectoris due to coronary artery disease.

**CONTRAINDICATIONS** Sublingual nitroglycerin therapy is contraindicated in patients with early myocardial infarct-

tion, severe anemia, increased intracranial pressure, and those with a known hypersensitivity to nitroglycerin.

**WARNINGS** The use of nitroglycerin during the early course of acute myocardial infarction requires particular attention to hemodynamic monitoring and clinical status.

#### **PRECAUTIONS**

**General** Only the smallest dose required for effective relief of the acute anginal attack should be used. Excessive use may lead to the development of tolerance. NitroQuick® tablets are intended for sublingual or buccal administration and should not be swallowed.

Severe hypotension, particularly with upright posture, may occur even with small doses of nitroglycerin. The drug should be used cautiously in patients with volume depletion or low systolic blood pressure.

Paradoxical bradycardia and increased angina pectoris may accompany nitroglycerin-induced hypotension.

Nitrate therapy may aggravate angina caused by hypertrophic cardiomyopathy.

Tolerance to the vascular and antianginal effects of nitroglycerin and cross-tolerance to other nitrates and nitrites may occur.

The drug should be discontinued if blurring of vision or drying of the mouth occurs. Excessive dosage of nitroglycerin may produce severe headaches.

**Information For Patients** If possible, patients should sit down when taking NitroQuick® tablets. This eliminates the possibility of falling due to lightheadedness or dizziness.

Nitroglycerin may produce a burning or tingling sensation when administered sublingually; however, the ability to produce a burning or tingling sensation should not be considered a reliable method for determining the potency of the tablets.

Nitroglycerin should be kept in the original glass container, tightly capped.

**Drug Interactions** Concomitant use of nitrates and alcohol may cause hypotension. Patients receiving antihypertensive drugs, beta-adrenergic blockers, or phenothiazines and nitrates should be observed for possible additive hypotensive effects. Marked orthostatic hypotension has been reported when calcium channel blockers and organic nitrates were used concomitantly. Dose adjustment of either class of agent may be necessary.

Aspirin may decrease the clearance and enhance the hemodynamic effects of sublingual nitroglycerin.

A decrease in the therapeutic effect of sublingual nitroglycerin may result from use of long-acting nitrates.

**Drug/Laboratory Test Interactions** Nitrates may interfere with the Zlatkis-Zak color reaction causing a false report of decreased serum cholesterol.

**Carcinogenesis, Mutagenesis, Impairment Of Fertility** No long-term studies in animals were performed to evaluate the carcinogenic potential of nitroglycerin.

**Pregnancy Teratogenic Effects. Pregnancy category C** Animal reproduction studies have not been conducted with nitroglycerin. It is also not known whether nitroglycerin can cause fetal harm when administered to a pregnant woman or can affect reproduction capacity. Nitroglycerin should be given to a pregnant woman only if clearly needed.

**Nursing Mothers** It is not known whether nitroglycerin is excreted in human milk. Because many drugs are excreted in human milk, caution should be exercised when intravenous nitroglycerin is administered to a nursing woman.

**Pediatric Use** The safety and effectiveness of nitroglycerin in pediatric patients have not been established.

**Geriatric Use** Clinical studies on this product have not been performed in sufficient numbers of subjects aged 65 and over to determine whether they respond differently from younger subjects. Other reported clinical experience has not identified differences in responses between the elderly and younger patients. In general, dose selection for an elderly patient should be cautious, usually starting at the low end of the dosing range, reflecting the greater frequency of decreased hepatic, renal, or cardiac function, and of concomitant disease or other drug therapy.

**ADVERSE REACTIONS** Headache which may be severe and persistent may occur immediately after use. Vertigo, weakness, palpitation, and other manifestations of postural hypotension may develop occasionally, particularly in erect, immobile patients. Marked sensitivity to the hypotensive effects of nitrates (manifested by nausea, vomiting, weakness, diaphoresis, pallor and collapse) may occur at therapeutic doses. Syncope due to nitrate vasodilation has been reported. Flushing, drug rash, and exfoliative dermatitis have been reported in patients receiving nitrate therapy.

**OVERDOSAGE** Nitrate overdose may result in: severe hypotension, tachycardia, bradycardia, heart block, palpitation, death due to circulatory collapse, syncope, persistent throbbing headache, vertigo, visual disturbance, increased intracranial pressure, paralysis and coma followed by convulsions, flushing and diaphoresis, nausea and vomiting, colic and diarrhea, dyspnea and methemoglobinemia.

Since hypotension from nitroglycerin overdosage results from venodilation and arterial hypovolemia, therapy should be directed toward central volume expansion. Elevation of extremities may be sufficient, but intravenous infusion may also be necessary. Use of arterial vasoconstrictors may do more harm than good. Management of nitroglycerin overdose in patients with renal disease or congestive heart failure may require invasive monitoring.

If methemoglobinemia is present, intravenous administration of methylene blue 1-2 mg/kg of body weight may be required.

**DOSAGE AND ADMINISTRATION** One tablet should be dissolved under the tongue or in the buccal pouch at the first sign of an acute anginal attack. The dose may be repeated approximately every five minutes, until relief is obtained. If the pain persists after a total of 3 tablets in a 15-minute period, prompt medical attention is recommended. NitroQuick® may be used prophylactically 5 to 10 minutes prior to engaging in activities which might precipitate an acute attack.

During administration the patient should rest, preferably in the sitting position.

No dosage adjustment is required in patients with renal failure.

**HOW SUPPLIED**

NitroQuick® is supplied in three strengths in bottles containing 100 tablets each, with color-coded labels, and in Patient Convenience Packages of four bottles of 25 tablets each.

- 0.3 mg (1/200 grain): NDC 58177-323-04  
Bottle of 100 tablets
- 0.4 mg (1/150 grain): NDC 58177-324-18  
Convenience Package  
NDC 58177-324-04  
Bottle of 100 tablets
- 0.6 mg (1/100 grain): NDC 58177-325-04  
Bottle of 100 tablets

**Store at controlled room temperature 15°-30°C (59°-86°F).  
Protect from moisture.**

Manufactured by  
KV Pharmaceutical Co. for  
**ETHEX Corporation**  
St. Louis, MO 63043-2413

Revised: 02/02

P3033-2



A3 Wet Labs Inc. WETStar Chlorophyll Fluorometer



Fluorometer

**WETStar**

- Chlorophyll
- CDOM
- Uranine
- Rhodamine
- Phycoerythrin

The highly successful WETStar fluorometer family is growing! These miniature, low cost, low power optical instruments provide comparable performance to other available fluorometers at a fraction of their cost, power requirements, and size. The unit employs a novel optical flow tube design that lends itself to both pump-through and flow-through operation. It is easily mated with existing CTD packages and is available with optional digital output.



**Specifications**

Mechanical		Electrical	
Diameter	2.7 in (6.9 cm)	Response time	0.17 sec (analog); 0.125 sec (digital)
Length	6.7 in (17.1 cm)	Input	7-15 VDC
Weight in air	1.7 lbs (0.8 kg)	Current draw	< 40 mA (analog); < 80 mA (digital)
Weight in water	0.25 lbs (0.1 kg)	Linearity	≥ 99% R <sup>2</sup>
Environmental		Output	0-5 VDC (analog); 0-4095 counts (digital)
Temperature range	0-30 deg C	<i>Specifications subject to change without notice.</i>	
Depth rating	600 m		

**Chlorophyll**—an indicator of viable phytoplankton biomass and chlorophyll concentrations in water.  
 EX: 460 nm • EM: 666 nm • Sensitivity: ≥ 0.03 µg/l • Dynamic range: 0.03-75 µg/l (std)

**CDOM**—Created from decayed biomass, CDOM contributes to coloration of both fresh and marine waters.  
 EX: 370 nm • EM: 460 nm • Sensitivity: 0.100 ppb QSD • Dynamic range: 100, 250, or 1000 ppb

**Uranine**—Used as a dye to study hydraulic connections and water transport mechanisms.  
 EX: 485 nm • EM: 532 nm • Sensitivity: 1 µg/l • Dynamic range: 1-4000 µg/l uranine

**Rhodamine**—Used as a dye similar to uranine.  
 EX: 470 nm • EM: 570 nm

**New!** **Phycoerythrin**—Allows measurement of the red pigment in cyanobacteria.  
 EX: 525 nm • EM: 575 nm

WET Labs, Inc.      01-641-828-6860 FAX -828-6277      www.wetlabs.com

Rev G 1/11/05



# WETStar

## Specifications Sheet

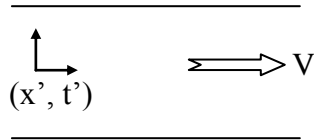
Revision History

Revision	Date	Revision Description	Originator
A	12/01/99	Begin revision control	H. Van Zee
B	01/03/00	Change depth rating; add excitation and emission	D. Harkins
C	12/12/00	Change sensitivity range	D. Harkins
D	11/26/01	Revise ex and em values (DCR 164)	J. Kitchen
E	04/10/02	Add digital capabilities (DCR 213)	H. Van Zee
F	6/8/04	Update format (DCR 402)	H. Van Zee
G	1/11/05	Combine fluorometer specs (DCR435)	M. Everett

Rev G 1/11/05

## A4 Convection - Diffusion Equation Derivation and Calculations

### A4-1 Forward Direction Diffusion – Convection Solution



1-D Diffusion Equation:

$$\frac{\partial C}{\partial t'} = k \frac{\partial^2 C}{\partial x'^2}$$

Initial Condition:

$$C(x, 0) = 0$$

Boundary Conditions:

$$C(0, t) = C_0$$

$$C(\infty, t) = 0$$

Use a moving coordinate system that moves with the speed of the average fluid velocity:

$$x = x' + Vt', \quad t = t'$$

Relate the moving coordinate system to the fixed coordinate system with the chain rule:

For  $C = C(x(x', t'), t(x', t'))$ ,

$$\frac{\partial C}{\partial t'} = \frac{\partial C}{\partial t} \frac{\partial t}{\partial t'} + \frac{\partial C}{\partial x} \frac{\partial x}{\partial t'} = \frac{\partial C}{\partial t} + V \frac{\partial C}{\partial x}$$

$$1 \quad \frac{\partial x}{\partial t'} = \frac{\partial}{\partial t'}(x' + Vt')$$

$$\frac{\partial C}{\partial x'} = \frac{\partial C}{\partial t} \frac{\partial t}{\partial x'} + \frac{\partial C}{\partial x} \frac{\partial x}{\partial x'} = \frac{\partial C}{\partial x}$$

$t = t'$ , not a  
function of  $x$       1

The diffusion equation in the moving coordinate system becomes:

$$\frac{\partial C}{\partial t} + V \frac{\partial C}{\partial x} = k \frac{\partial^2 C}{\partial x^2}$$

Solve by Laplace Transform with respect to time:

$$L\{C(x,t)\} = \int_0^{\infty} e^{-st} C(x,t) dt = \bar{C}(x,s)$$

$$L\left\{\frac{\partial C(x,t)}{\partial t}\right\} = \int_0^{\infty} e^{-st} \frac{\partial C(x,t)}{\partial t} dt$$

Integration by parts:

$$\begin{aligned} u &= e^{-st} & v &= C \\ du &= -se^{-st} dt & dv &= \frac{\partial C}{\partial t} dt \\ &= e^{-st} C + s \int_0^{\infty} C e^{-st} dt = C e^{-st} \Big|_{t=0}^{\infty} + s \bar{C} \\ &= C \Big|_{t=\infty} e^{-s\infty} - C \Big|_{t=0} e^{-0} + s \bar{C}(x,s) \end{aligned}$$

Approaches 0      0 from initial  
as  $t \rightarrow \infty$       condition

$$L\left\{\frac{\partial C(x,t)}{\partial t}\right\} = s \bar{C}(x,s)$$

$$L\left\{\frac{\partial C(x,t)}{\partial x}\right\} = \frac{\partial \bar{C}(x,s)}{\partial x}$$

$$L\left\{\frac{\partial^2 C(x,t)}{\partial x^2}\right\} = \frac{\partial^2 \bar{C}(x,s)}{\partial x^2}$$

The transformed moving diffusion equation can be expressed as:

$$\frac{\partial^2 \bar{C}}{\partial x^2} - \frac{V}{k} \frac{\partial \bar{C}}{\partial x} - \frac{s}{k} \bar{C} = 0$$



The boundary conditions in the s domain:

$$\bar{C}(0, s) = \int_0^{\infty} e^{-st} C_o dt = \frac{C_o}{s}$$

$$\bar{C}(\infty, s) = L\{0\} = 0$$

The initial condition does not change:

$$\bar{C}(x, 0) = 0$$

Solve for  $\bar{C}(x, s)$ :

Find the roots of the characteristic equation:

$$r^2 - \frac{V}{k}r - \frac{s}{k} = 0$$

$$r = \frac{\frac{V}{k} \pm \sqrt{\frac{V^2}{k^2} + 4\frac{s}{k}}}{2} = \frac{V}{2k} \pm \frac{1}{2} \sqrt{\frac{V^2}{k^2} + 4\frac{s}{k}}$$

Assume solution of the form:

$$\bar{C}(x, s) = Ae^{-r_1x} + Be^{r_2x} = A \exp\left[\frac{V}{2k} + \frac{1}{2} \sqrt{\frac{V^2}{k^2} + 4\frac{s}{k}}\right] + B \exp\left[\frac{V}{2k} - \frac{1}{2} \sqrt{\frac{V^2}{k^2} + 4\frac{s}{k}}\right]$$

Approaches  $\infty$   
as  $t \rightarrow \infty$

$$= B \exp\left[\frac{V}{2k} - \frac{1}{2} \sqrt{\frac{V^2}{k^2} + 4\frac{s}{k}}\right]$$

Apply boundary conditions to solve for B:

Boundary Condition 1

$$\bar{C}(0, s) = \frac{C_o}{s}$$

$$\frac{C_o}{s} = Be^0 \Rightarrow B = \frac{C_o}{s}$$

Boundary Condition 2

$$\bar{C}(\infty, s) = 0 = 0 \Rightarrow \exp\left[\frac{V}{2k} - \sqrt{\frac{V^2}{4k^2} + \frac{s}{k}}\right]x \rightarrow 0 \text{ as } x \rightarrow \infty$$

Therefore:

$$\bar{C}(x, s) = \frac{C_o}{s} \exp\left[\frac{V}{2k} - \sqrt{\frac{V^2}{4k^2} + \frac{s}{k}}\right]x$$

Use the inverse Laplace transform to find the answer as a function of time:

$$C(x, t) = \frac{1}{2\pi i} \int_{c-i\infty}^{c+i\infty} e^{st} \bar{C}(x, s) ds = \frac{1}{2\pi i} \int_{c-i\infty}^{c+i\infty} e^{st} \frac{C_o}{s} e^{\frac{Vx}{2k}} e^{-x\sqrt{\frac{V^2}{4k^2} + \frac{s}{k}}} ds$$

A branch point will result from the  $e^{-x\sqrt{\frac{V^2}{4k^2} + \frac{s}{k}}}$  term. Make a substitution in the term to help identify the branch point.

$$p = s + \frac{V^2}{4k} \Rightarrow s = p - \frac{V^2}{4k}$$

$$C(x, t) = \frac{C_o e^{\frac{Vx}{2k}}}{2\pi i} \int_{c-i\infty}^{c+i\infty} \frac{e^{\left(p - \frac{V^2}{4k}\right)t}}{p - \frac{V^2}{4k}} e^{-\left(\frac{p}{k}\right)^{\frac{1}{2}}x} dp = \frac{C_o e^{\frac{Vx}{2k} - \frac{V^2 t}{4k}}}{2\pi i} \int_{c-i\infty}^{c+i\infty} \frac{e^{pt} e^{-\left(\frac{p}{k}\right)^{\frac{1}{2}}x}}{p - \frac{V^2}{4k}} dp$$

Identify the singularities:

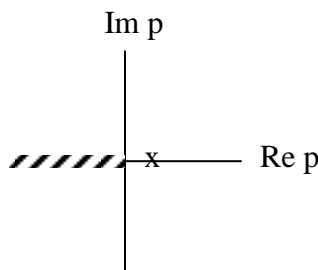
$$\text{Pole: } p = \frac{V^2}{4k}$$

Branch point:  $p = 0$ , because  $e^{-\left(\frac{p}{k}\right)^{\frac{1}{2}}x} = e^{-\left(\frac{\text{Re}(\theta+2\pi m)}{k}\right)^{\frac{1}{2}}x} = e^{-\sqrt{\frac{R}{k}} e^{i\frac{\theta}{2}} e^{im}} = e^{-\sqrt{\frac{R}{k}} e^{i\frac{\theta}{2}} e^{im}}$ . This is multivalued. For  $n$  even:  $e^{im} = 1$ . For  $n$  odd:  $e^{im} = -1$ .

Using the inverse Laplace Transform,  $c$  must be to the right of all the singularities. Thus,  $c$  must be shifted after the above substitution:

$$C(x,t) = \frac{C_0 e^{\frac{Vx - V^2 t}{4k}}}{2\pi i} \int_{c + \frac{V^2}{4k} - i\infty}^{c + \frac{V^2}{4k} + i\infty} \frac{e^{pt} e^{-\left(\frac{p}{k}\right)^2 x}}{p - \frac{V^2}{4k}} dp$$

Since there is a branch point at  $p = 0$ , make a branch cut along the negative real axis:



$$p = \rho e^{i\theta}$$

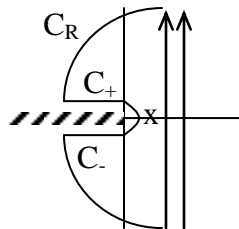
$$-\pi < \theta \leq \pi$$

A contour integral is used, and Jordan's Lemma is relied upon to show that the arc approaches 0 as  $R$  approaches infinity.

$$\text{Jordan's Lemma has the form: } \lim_{R \rightarrow \infty} \int_{C_R} f(z) e^{mz} dz = 0$$

$$\text{In this case: } \lim_{R \rightarrow \infty} \int_{C_R} f(p) e^{tp} dp = 0$$

To match the required form of Jordan's Lemma,  $t$  must be positive ( $t > 0$ ) and the semi-circular arc must be drawn in the left hand plane:



The contour integral is as follows:

$$\frac{1}{2\pi i} \int_{c+\frac{V^2}{4k}-i\infty}^{c+\frac{V^2}{4k}+i\infty} \frac{e^{pt} e^{-\left(\frac{p}{k}\right)^{\frac{1}{2}} x}}{p - \frac{V^2}{4k}} dp = \frac{1}{2\pi i} \left\{ \int_{c+\frac{V^2}{4k}-i\infty}^{c+\frac{V^2}{4k}+i\infty} + \int_{C_R} + \int_{C_+} + \int_{C_-} \right\} \frac{e^{pt} e^{-\left(\frac{p}{k}\right)^{\frac{1}{2}} x}}{p - \frac{V^2}{4k}} dp$$

To satisfy Jordan's Lemma,  $f(p)$  must be analytic in the region  $\text{Re } p \leq 0$ , except at poles and  $|f(z)| \rightarrow 0$  as  $R \rightarrow \infty$ .

$$\text{From the above integral, } f(p) = \frac{e^{-\left(\frac{p}{k}\right)^{\frac{1}{2}} x}}{p - \frac{V^2}{4k}} = \frac{e^{-\left(\frac{R}{k}\right)^{\frac{1}{2}} e^{i\frac{\theta}{2}} x}}{\text{Re } i\theta - \frac{V^2}{4k}}$$

Clearly, the  $\frac{1}{R}$  term and the  $e^{-(R)^{\frac{1}{2}}}$  terms both drive  $|f(z)| \rightarrow 0$  as  $R \rightarrow \infty$ .

$f(p)$  satisfies the Cauchy-Riemann conditions and is analytic.

Evaluate the contour integral.  
By Cauchy's residue theorem:

$$\oint_C f(p) dp = 2\pi i b$$

$b = \text{residue} = \text{coefficient of } 1/(p-a) \text{ term.}$

$$2\pi i b = 2\pi i \left( \frac{1}{2\pi i} \frac{e^{pt} e^{-\left(\frac{p}{k}\right)^{\frac{1}{2}} x}}{p - \frac{V^2}{4k}} \right) \Bigg|_{p=\frac{V^2}{4k}}$$

Therefore:

$$\oint \frac{e^{pt} e^{-\left(\frac{p}{k}\right)^{\frac{1}{2}} x}}{p - \frac{V^2}{4k}} dp = e^{\frac{V^2 t}{4k} - \frac{Vx}{2k}}$$

The time solution:

$$C(x,t) = \frac{e^{\frac{Vx}{2k} - \frac{V^2 t}{4k}}}{2\pi i} \int_{c + \frac{V^2}{4k} - i\infty}^{c + \frac{V^2}{4k} + i\infty} \frac{e^{pt} e^{-\left(\frac{p}{k}\right)^{\frac{1}{2}} x}}{p - \frac{V^2}{4k}} dp$$

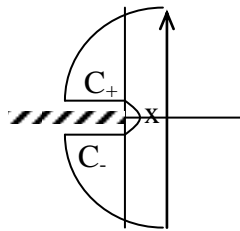
$$\frac{C(x,t)}{C_0} = \frac{e^{\frac{Vx}{2k} - \frac{V^2 t}{4k}}}{2\pi i} \left( \int_{c + \frac{V^2}{4k} - i\infty}^{c + \frac{V^2}{4k} + i\infty} \frac{e^{pt} e^{-\left(\frac{p}{k}\right)^{\frac{1}{2}} x}}{p - \frac{V^2}{4k}} dp - \left( \int_{C_+} + \int_{C_-} \right) \frac{e^{pt} e^{-\left(\frac{p}{k}\right)^{\frac{1}{2}} x}}{p - \frac{V^2}{4k}} dp \right)$$

$$= e^{\frac{Vx}{2k} - \frac{V^2 t}{4k}} \left( e^{\frac{V^2 t}{4k} - \frac{Vx}{2k}} - \left( \int_{C_+} + \int_{C_-} \right) \frac{e^{pt} e^{-\left(\frac{p}{k}\right)^{\frac{1}{2}} x}}{p - \frac{V^2}{4k}} dp \right)$$

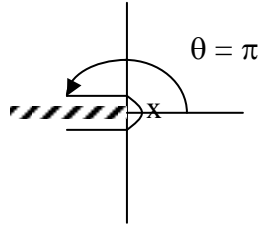
$$= 1 - e^{\frac{Vx}{2k} - \frac{V^2 t}{4k}} \left( \left( \int_{C_+} + \int_{C_-} \right) \frac{e^{pt} e^{-\left(\frac{p}{k}\right)^{\frac{1}{2}} x}}{p - \frac{V^2}{4k}} dp \right)$$

$$= 1 - e^{\frac{Vx}{2k} - \frac{V^2 t}{4k}} (J)$$

$$J = C_+ + C_-$$



$C_+$



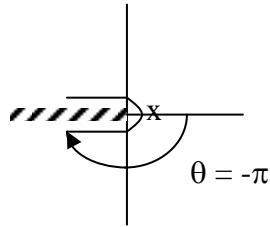
$$p = \rho e^{i\pi}, e^{i\pi} = -1$$

$$\frac{1}{2\pi i} \int_{C_+} = \frac{1}{2\pi i} \int_{-\infty}^0 \frac{e^{\rho t} e^{-\left(\frac{\rho}{k}\right)^{\frac{1}{2}} x}}{p - \frac{V^2}{4k}} d\rho = -\frac{1}{2\pi i} \int_{-\infty}^0 \frac{e^{\rho(-1)t} e^{-\left(\frac{\rho(-1)}{k}\right)^{\frac{1}{2}} x}}{\rho(-1) - \frac{V^2}{4k}} d\rho = -\frac{1}{2\pi i} \int_{-\infty}^0 \frac{e^{-\rho t} e^{-i\left(\frac{\rho}{k}\right)^{\frac{1}{2}} x}}{\left(\rho + \frac{V^2}{4k}\right)} d\rho$$

flip integral:

$$= -\frac{1}{2\pi i} \int_0^{\infty} \frac{e^{-\rho t} e^{-i\left(\frac{\rho}{k}\right)^{\frac{1}{2}} x}}{\rho + \frac{V^2}{4k}} d\rho$$

$C_-$



$$\frac{1}{2\pi i} \int_{C_-} = -\frac{1}{2\pi i} \int_0^{\infty} \frac{e^{-\rho t} e^{i\left(\frac{\rho}{k}\right)^{\frac{1}{2}} x}}{\left(\rho + \frac{V^2}{4k}\right)} d\rho = \frac{1}{2\pi i} \int_0^{\infty} \frac{e^{-\rho t} e^{i\left(\frac{\rho}{k}\right)^{\frac{1}{2}} x}}{\rho + \frac{V^2}{4k}} d\rho$$

Sum  $J = C_+ + C_-$ .

$$J = \frac{1}{2\pi i} \{C_+ + C_-\} = \frac{1}{2\pi i} \left\{ \int_0^\infty \left( \frac{e^{-\rho} e^{-i\left(\frac{\rho}{k}\right)^{\frac{1}{2}} x} + e^{-\rho} e^{i\left(\frac{\rho}{k}\right)^{\frac{1}{2}} x}}{\rho + \frac{V^2}{4k}} \right) d\rho \right\} = \frac{1}{2\pi i} \int_0^\infty \left( \frac{e^{-\rho}}{\rho + \frac{V^2}{4k}} \right) \left( e^{-i\left(\frac{\rho}{k}\right)^{\frac{1}{2}} x} + e^{i\left(\frac{\rho}{k}\right)^{\frac{1}{2}} x} \right) d\rho$$

$$\sin A = \frac{e^{iA} - e^{-iA}}{2i}$$

$$J = \frac{1}{\pi} \int_0^\infty \left( \frac{e^{-\rho}}{\rho + \frac{V^2}{4k}} \right) \sin \left( \left( \frac{\rho}{k} \right)^{\frac{1}{2}} x \right) d\rho$$

Integrate  $J$

Change variables

$$\sqrt{\rho} = u, \text{ therefore } \rho = u^2 \text{ and } d\rho = 2u du$$

$$\text{Therefore, } J = \frac{2}{\pi} \int_0^\infty \left( \frac{ue^{-u^2}}{u^2 + \frac{V^2}{4k}} \right) \sin \left( \frac{u}{\sqrt{k}} x \right) du$$

Multiplying by two is the same as doubling the integration range:

$$J = \frac{1}{\pi} \int_{-\infty}^\infty \left( \frac{ue^{-u^2}}{u^2 + \frac{V^2}{4k}} \right) \sin \left( \frac{u}{\sqrt{k}} x \right) du$$

The range  $-\infty$  to  $\infty$  is an even range. Therefore, any cosine terms will sub to zero. Thus,

we can replace  $u \sin \frac{u}{\sqrt{k}} x$  with  $iue^{-\frac{u}{\sqrt{k}} x}$ , knowing that the cosine portion of Euler's

formula equals zero.

$$J = \frac{1}{\pi} \int_{-\infty}^\infty \left( \frac{iue^{-u^2} e^{-i\frac{u}{\sqrt{k}} x}}{u^2 + \frac{V^2}{4k}} \right) du$$

Move  $i$  to the denominator:

$$J = -\frac{1}{\pi i} \int_{-\infty}^{\infty} \left( \frac{ue^{-u^2 t} e^{-i\frac{u}{\sqrt{k}}x}}{u^2 + \frac{V^2}{4k}} \right) du$$

Multiplying by  $2/2$ ,  $\frac{2u}{u^2 + \frac{V^2}{4k}}$  can be factored to equal  $\left( \frac{1}{u + \frac{iV}{2\sqrt{k}}} + \frac{1}{u - \frac{iV}{2\sqrt{k}}} \right)$

$$J = -\frac{1}{2\pi i} \int_{-\infty}^{\infty} e^{-\left(u^2 t + \frac{iux}{\sqrt{k}}\right)} \left( \frac{1}{u + \frac{iV}{2\sqrt{k}}} + \frac{1}{u - \frac{iV}{2\sqrt{k}}} \right) du$$

Complete the square in the exponential term to obtain an expression of the form  $e^{(\quad)}$ :

The exponential term is  $e^{-\left(u^2 t + \frac{iux}{\sqrt{k}}\right)}$ .

Define  $\sigma = u\sqrt{t} + \frac{ix}{2\sqrt{kt}}$

Complete the squares by allowing  $u^2 t = \frac{iux}{\sqrt{k}} = \sigma^2 + \frac{x^2}{4kt}$

Check to make sure both expressions are equal:

$$\sigma^2 + \frac{x^2}{4kt} = \left(u\sqrt{t} + \frac{ix}{2\sqrt{kt}}\right) \left(u\sqrt{t} + \frac{ix}{2\sqrt{kt}}\right) + \frac{x^2}{4kt} = u^2 t + \frac{2iux}{2\sqrt{k}} - \frac{x^2}{4kt} + \frac{x^2}{4kt} = u^2 t = \frac{iux}{\sqrt{k}}$$

Therefore:

$$J = -\frac{1}{2\pi i} \int_{-\infty}^{\infty} e^{-\left(\sigma^2 t + \frac{x^2}{4kt}\right)} \left( \frac{1}{u + \frac{iV}{2\sqrt{k}}} + \frac{1}{u - \frac{iV}{2\sqrt{k}}} \right) du$$

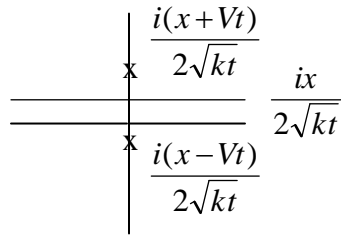


Put integral in terms of  $\sigma$ , instead of  $u$ :

$$u = \frac{\sigma}{\sqrt{t}} - \frac{ix}{2\sqrt{kt}}$$

$$\begin{aligned} J &= -\frac{e^{-\left(\frac{x^2}{4kt}\right)}}{2\pi i} \int_{-\infty}^{\infty} e^{-(\sigma^2)} \left( \frac{1}{\sigma - \frac{ik\sqrt{t}}{2\sqrt{kt}} + \frac{iV\sqrt{t}}{2\sqrt{kt}}} + \frac{1}{\sigma - \frac{ik\sqrt{t}}{2\sqrt{kt}} - \frac{iV\sqrt{t}}{2\sqrt{kt}}} \right) d\sigma \\ &= -\frac{e^{-\left(\frac{x^2}{4kt}\right)}}{2\pi i} \int_{-\infty}^{\infty} e^{-(\sigma^2)} \left( \frac{1}{\sigma - \frac{i(x-Vt)}{2\sqrt{kt}}} + \frac{1}{\sigma - \frac{i(x+Vt)}{2\sqrt{kt}}} \right) d\sigma \end{aligned}$$

Poles exist at  $\sigma = \frac{i(x-Vt)}{2\sqrt{kt}}$  and  $\frac{i(x+Vt)}{2\sqrt{kt}}$  in the complex  $\sigma$  plane:



The path of integration in the  $\sigma$  plane will be between the poles at the imaginary height  $\frac{ix}{2\sqrt{kt}}$ . Because the path of integration is not on the real axis, the  $J$  integral must be shifted by this imaginary amount:

$$J = -\frac{e^{-\left(\frac{x^2}{4kt}\right)}}{2\pi i} \int_{-\infty + \frac{ix}{2\sqrt{kt}}}^{\infty + \frac{ix}{2\sqrt{kt}}} e^{-(\sigma^2)} \left( \frac{1}{\sigma - \frac{i(x-Vt)}{2\sqrt{kt}}} + \frac{1}{\sigma - \frac{i(x+Vt)}{2\sqrt{kt}}} \right) d\sigma$$

Substitute variables. Call  $\xi = \frac{x}{2\sqrt{kt}}$ , and  $\xi_{\pm} = \frac{x \pm Vt}{2\sqrt{kt}}$

The J integral becomes:

$$J = -\frac{e^{-\left(\frac{x^2}{4kt}\right)}}{2\pi i} \int_{-\infty+\xi}^{\infty+\xi} e^{-(\sigma^2)} \left( \frac{1}{\sigma - i\xi_-} + \frac{1}{\sigma - i\xi_+} \right) d\sigma = -\frac{e^{-\left(\frac{x^2}{4kt}\right)}}{2\pi i} \int_{-\infty+\xi}^{\infty+\xi} \left( \frac{e^{-(\sigma^2)}}{\sigma - i\xi_-} d\sigma + \frac{e^{-(\sigma^2)}}{\sigma - i\xi_+} d\sigma \right)$$

Each of these integrals is in the form:

$$I = \int_{-\infty+\xi}^{\infty+\xi} \frac{e^{-(\sigma^2)}}{\sigma - i\gamma} d\sigma$$

The solution to this integral is given in exercise 9.7 of “Mathematical Analysis in Engineering” by C. C. Mei, and is shown as follows:

$$I = -i\pi e^{\gamma^2} (1 + \operatorname{erfc}\gamma) = i\pi e^{\gamma^2} (-2 + \operatorname{erfc}\gamma), \xi > \gamma. \text{ This applies for } \xi_-.$$

$$I = i\pi e^{\gamma^2} (1 - \operatorname{erfc}\gamma) = i\pi e^{\gamma^2} \operatorname{erfc}\gamma, \xi < \gamma. \text{ This applies for } \xi_+.$$

$$I = -i\pi e^{\xi_-^2} (-2 + \operatorname{erfc}\xi_-) = i\pi e^{\frac{(x-Vt)^2}{4kt}} (-2 + \operatorname{erfc}\left(\frac{x-Vt}{2\sqrt{kt}}\right)), \xi > \gamma.$$

$$I = i\pi e^{\frac{(x+Vt)^2}{4kt}} (-2 + \operatorname{erfc}\left(\frac{x+Vt}{2\sqrt{kt}}\right)), \xi < \gamma.$$

The total solution for concentration becomes:

$$\frac{C(x,t)}{C_o} = 1 - \left( e^{\frac{Vx}{2k} - \frac{V^2t}{4k}} \right) J$$

$$= 1 + \frac{e^{\frac{Vx}{2k}} e^{-\frac{V^2t}{4k}} e^{-\frac{x^2}{4kt}}}{2\pi i} \left\{ i\pi e^{-\frac{(x-Vt)^2}{4kt}} (-2 + \operatorname{erfc}\left(\frac{x-Vt}{2\sqrt{kt}}\right)) + i\pi e^{-\frac{(x-Vt)^2}{4kt}} (-2 + \operatorname{erfc}\left(\frac{x+Vt}{2\sqrt{kt}}\right)) \right\}$$

$$(x - Vt)^2 = x^2 - 2Vtx + V^2t^2, \quad (x + Vt)^2 = x^2 + 2Vtx + V^2t^2$$

$$= 1 + \frac{e^{\frac{Vx}{2k}} e^{-\frac{V^2t}{4k}} e^{-\frac{x^2}{4kt}}}{2\pi i} \left\{ e^{\frac{V^2t^2}{4kt}} e^{-\frac{2Vtx}{4kt}} e^{-\frac{x^2}{4kt}} (-2) + e^{\frac{V^2t^2}{4kt}} e^{-\frac{2Vtx}{4kt}} e^{-\frac{x^2}{4kt}} \operatorname{erfc}\left(\frac{x-Vt}{2\sqrt{kt}}\right) + e^{\frac{V^2t^2}{4kt}} e^{-\frac{2Vtx}{4kt}} e^{-\frac{x^2}{4kt}} \operatorname{erfc}\left(\frac{x+Vt}{2\sqrt{kt}}\right) \right\}$$

$$= 1 - 1 + \frac{1}{2} \operatorname{erfc}\left(\frac{x-Vt}{2\sqrt{kt}}\right) + \frac{1}{2} e^{\frac{Vx}{k}} \operatorname{erfc}\left(\frac{x+Vt}{2\sqrt{kt}}\right)$$

And finally, the total solution:

$$C(x,t) = \frac{C_o}{2} \left\{ \operatorname{erfc} \left( \frac{x-Vt}{2\sqrt{kt}} \right) + e^{\frac{Vx}{k}} \operatorname{erfc} \left( \frac{x+Vt}{2\sqrt{kt}} \right) \right\}$$

## A4-2 Matlab Code for Forward Direction Diffusion-Convection Calculation

```
Co = 1*10^-4;

x1 = .3048; %m
x2 = 3.048; %m

V = .1105; %m/s

K = 1.5*(10^-9); %m^2/s

t=[.001:.001:30];

for i=1:30000

    z1 = (x1-V*t(i))/(2*sqrt(K*t(i)));
    z2 = (x2-V*t(i))/(2*sqrt(K*t(i)));

    z1out(i) = z1;
    z2out(i) = z2;

end

%C = (Co/2)*(erfc(z1out)+(exp(V*x/K)*erfc(z2out)));
%C = .5*(1+erf(-z1out))
C1 = (Co/2)*erfc(z1out)
```

$$C2 = (C_0/2) * \text{erfc}(z2_{\text{out}})$$

```
subplot(2,1,1);
```

```
plot(t,C1);
```

```
Title('Distance = 1 ft.');
```

```
xlabel('time (s)');
```

```
ylabel('Concentration (M)');
```

```
subplot(2,1,2);
```

```
plot(t,C2);
```

```
Title('Distance = 10 ft.');
```

```
xlabel('time (s)');
```

```
ylabel('Concentration (M)');
```

### A4-3 Matlab Code for Cross-Channel Diffusion Calculation

```
Co = 1%*10^-4;

r = .25/39.37; %m

K = .5*(10^-9); %m^2/s

h=[0:.25:50];
t=h*3600;

%for i=1:10000

% P = exp(-(r^2/(4*K*t(i))))/((4*pi*K*t(i)));

% Pout(i) = P;

%end

Pout = erfc(r./(2*sqrt(2*K*t)*sqrt(2)))

plot(h,Pout);

Title('Cross-Channel Diffusion v. Time');

xlabel('time (h)');

ylabel('Error Function');

Ylim([0,(1)]);
```